Okinawa Institute of Science and Technology

Graduate University

Thesis submitted for the degree

Doctor of Philosophy

Functional Analysis of CCR4-NOT Complex in Pancreatic β Cell

by

Dina Mostafa

Under the Supervision of:

Prof. Dr. Tadashi Yamamoto

February 2020
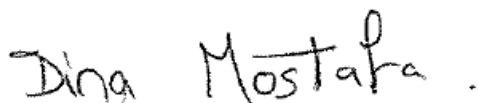
Declaration of Original and Sole Authorship

I, Dina Mostafa Abdel Azim Mostafa, declare that this thesis entitled "**Functional analysis of CCR4-NOT complex in pancreatic β cell**" and the data presented in it are original and my own work.

I confirm that:

- This work was done solely while a candidate for the research degree at the Okinawa Institute of Science and Technology Graduate University, Japan.

- No part of this work has previously been submitted for a degree at this or any other university.

- References to the work of others have been clearly attributed. Quotations from the work of others have been clearly indicated and attributed to them.

- In cases where others have contributed to part of this work, such contribution has been clearly acknowledged and distinguished from my own work.

- None of this work has been previously published elsewhere with the exception of the following:

Dina Mostafa, Akinori Takahashi, Akiko Yanagiya, Tomokazu Yamaguchi, Takaya Abe, Taku Kureha, Keiji Kuba, Yumi Kanegae, Yasuhide Furuta, Tadashi Yamamoto and Toru Suzuki. Essential functions of the CNOT7/8 catalytic subunits of the CCR4-NOT complex in mRNA regulation and cell viability. RNA Biology. 2020;17(3):403-16.

Signature:

Dina Mostafa.

Date: 6th February, 2020

Abstract

Functional analysis of CCR4-NOT complex in pancreatic β cell

Pancreatic β cells are responsible for production and secretion of insulin in response to increasing blood glucose levels. Therefore, defects in pancreatic β cell function lead to hyperglycemia and diabetes mellitus. While extensive research has focused on signaling, transcriptional, and epigenetic regulation in β cells, how post-transcriptional mechanisms influence the β cell gene expression program is largely unknown. The carbon catabolite repression 4 (CCR4)–negative on TATA-less (NOT) complex (CCR4-NOT complex), a major deadenylase conserved in eukaryotes, catalyzes mRNA deadenylation which is the rate limiting step in mRNA decay pathway. The CCR4-NOT complex has been implicated in the development of metabolic diseases. However, whether the CCR4-NOT complex affects β cell function is not addressed. In this thesis, I aim to understand the importance of post-transcriptional regulation in β cells by generating mice lacking the *Cnot3* gene, which encodes an essential CCR4-NOT complex subunit, in β cells. Suppression of CNOT3 in β cells caused β cell dysfunction and diabetes. This was associated with the decreased expression of β cell-specific genes and increased expression of genes specifically repressed in β cells, called "β cell disallowed genes". By combining whole transcriptome and proteome analyses and subsequent validations using quantitative PCR (qPCR) and immunoblot analyses, I found that mRNA and protein expression patterns were largely different from normal β cells upon CNOT3 suppression, which was clearly relevant to the observed phenotypes. I also found that some β cell disallowed genes were stabilized in the absence of CNOT3, suggesting that their expression was maintained at low levels under the control of the CCR4-NOT complex. Together, this study uncovered mRNA deadenylation by CCR4-NOT complex as a novel molecular mechanism by which β cell identity and function are regulated.

Acknowledgements

List of Abbreviations

Act. D	Actinomycin D
Ago	Argonaute
Aldob	Aldolase B
ARE	AU-rich element
BCA	Bicinchoninic acid
BSA	Bovine serum albumin
CCR4	Carbon catabolite repression 4
CN	Catalytic negative
*Cnot3*βKO	β cell-specific *Cnot3* knockout
Cpe	Carboxypeptidase E
DE	Differentially expressed
dKO	Double knockout
DN	Dominant negative
EEP	Exonuclease-endonuclease-phosphatase
FBS	Fetal bovine serum
FC	Fold change
FDR	False discovery rate
Gck	Glucokinase
GLUC	Glucagon
Glut2/ Slc2a2	Glucose Transporter 2/ Solute Carrier Family 2 Member 2
GO	Gene Ontology
GSEA	Gene set enrichment analysis
GSIS	Glucose-stimulated insulin secretion
H & E	Hematoxylin and Eosin
HBSS	Hank's buffered salt solution
Het	heterozygous
HFD	high-fat diet
HRP	horseradish peroxidase
IP	Immunoprecipitates
Ins1	insulin gene, isoform 1
Ins2	insulin gene, isoform 2

KO	knockout
KRB	Krebs Ringer buffer
LC/MS	Liquid Chromatography/Mass Spectrometry
Ldha	Lactate dehydrogenase A
lncRNAs	long non-coding RNAs
LRR	leucine rich repeat
MEF	mouse embryonic fibroblast
mG	membrane localized EGFP
MIN6	Mouse insulinoma-6
miRISC	miRNA-induced silencing complex
MS	Mass spectrometry
mT	membrane localized tdTomato
ND	normal diet
Ngn3	Neurogenin 3
NOT	negative on TATA-less
PABP	poly(A) binding protein
PBS	phosphate-buffered saline
PC	Prohormone convertase
Pcsk	Proprotein Convertase Subtilisin/Kexin
PDVF	polyvinylidene fluoride
PFA	Paraformaldehyde
PI	Propidium iodide
PPT	Pancreatic polypeptide
Pre-miRNA	Precursor miRNA
qPCR	quantitative PCR
RBPs	RNA binding proteins
RIP	RNA immunoprecipitation
RNA-seq	RNA sequencing
SDS-PAGE	SDS-polyacrylamide gel electrophoresis
S.E.M	Standard error of the mean
SST	Somatostatin
SYP	Synaptophysin
T1D	Type 1 diabetes

T2D	Type 2 diabetes
TCA	Tricarboxylic acid
TEM	Transmission electron microscopy
TTP	tristetrapolin
TUNEL	Terminal deoxynucleotidyl transferase dUTP nick end labeling
Ucn3	Urocortin 3
UTR	untranslated region
WT	wild-type

Table of contents

List of Figures

List of Tables

1 Chapter 1: General Introduction

1.1 Introduction to Diabetes

Diabetes is one of the largest global health emergencies in the 21st Century. The latest global trends show 463 million people have diabetes and this is predicted to rise by 51% by the year 2045 (IDF Diabetes Atlas ninth edition, 2019). Diabetes is characterized by hyperglycemia due to defective insulin secretion by pancreatic β cells, defective insulin action (termed insulin resistance) or both. Thus, diabetes is widely defined by two forms: type 1 diabetes (T1D) that develops due to an autoimmune response against pancreatic β cells; and type 2 diabetes (T2D) which is more common in adults and is associated initially with insulin resistance that progresses to loss of β cell mass and function (Butler et al., 2003; Rosengren et al., 2012).

Type 2 diabetes is a complex metabolic disorder caused by a combination of genetic and environmental factors. Obesity is one of the main risk factors for the development of T2D. Obesity contributes to insulin resistance early before the onset of T2D. At this stage, β cell undergoes compensatory changes releasing more insulin to compensate for the increased metabolic demand due to insulin resistance. Notably, glucose and free fatty acids are important nutrients for the β cell that essentially regulate its function and proliferation. They regulate the expression of multiple genes involved in energy metabolism, insulin biosynthesis/ secretion, intracellular signaling and gene transcription (Schuit et al., 2002). However, chronic exposure to high blood glucose and these lipids causes β cell dysfunction associated with β cell apoptosis. How the nutrient environment modulates the β cell response during adaptation to such diabetogenic conditions is not completely understood (Blandino-Rosano et al., 2016). Possibly, this adaptation involves alterations in the expression of genes essential for β cell function. Not only the metabolic factors contribute to β cell dysfunction but also insulin resistance is accompanied by a state of chronic low-grade inflammation which adversely affects β cell function (Shoelson et al., 2006).

1.2 The islets of Langerhans and β cell origin

The pancreas is an important metabolic glandular organ that has both exocrine and endocrine functions (Edlund, 2002). The exocrine pancreas consists of acinar and ductal cells and is responsible for the production and release of digestive enzymes into the duodenum. The islets of Langerhans constitute its endocrine part. The islets consist of groups of specialized cells that produce and secrete hormones essential for maintaining glucose homeostasis. These cells

include β, α, δ, PP and ε cells that secrete the islet hormones insulin, glucagon (GLUC), somatostatin (SST), pancreatic polypeptide (PPT) and ghrelin respectively (Shih et al., 2013). The islets represent only ~1-2% of the total pancreas, the insulin-secreting β cells represent at least ~65-80% of the islet mass, which means β cells are the most abundant of the cell types within the islets (an illustration of the islet structure is shown in Figure 1.1) (MacDonald and Rorsman, 2006).
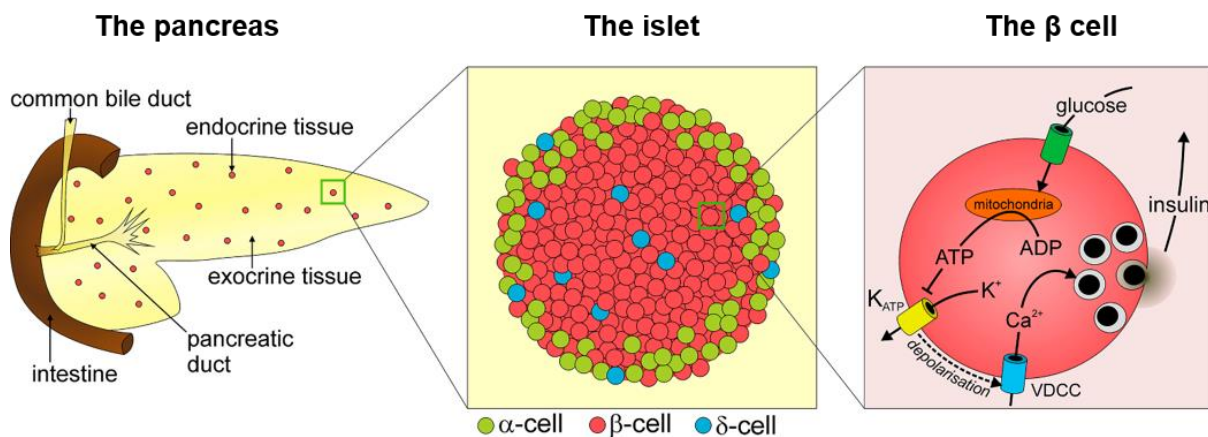
Figure 1.1 An overview of the pancreas anatomy and the islet architecture
The figure shows the architecture of the mouse islet with centrally located β cells and other islet cells located on the periphery (MacDonald and Rorsman, 2006).

Paracrine signaling between these different cell types is essential to regulate β cell function (Halban et al., 1982). During development, these different cell types originate from a progenitor cell that expresses *Neurogenin3* (*Ngn3*), a transcription factor required for endocrine cell differentiation in the pancreas (Edlund, 2002). Eventually, transcription factors such as Pdx1, Pax4, Nkx2.2, Nkx6.1, MafA, and Foxo1 maintain the β cell identity (Ziv et al., 2013). However, the existence of β cell progenitors in the adult pancreas remains controversial and unclear. Current evidence suggests that the primary mechanism of adult β cells proliferation/expansion is self-replication of pre-existing cells rather than differentiation from stem cells (Georgia and Bhushan, 2004; Meier et al., 2008). Yet there are reports that multipotent cells exist within the adult pancreas and could differentiate into β cells (Xu et al., 2008). Interestingly, some studies also demonstrated that α and δ cells could transdifferentiate into β-like cells during conditions of extreme β cell loss in mice (Chera et al., 2014; Thorel et al., 2010). On the other hand, primary human β cells are capable of converting into α cells (Spijker et al., 2013). In addition, other studies demonstrated that the β cells can dedifferentiate into progenitor cells upon loss of any of the aforementioned β cell-specific transcription factors

during the development of diabetes (Nishimura et al., 2015; Wang et al., 2014). β cell dedifferentiation is now recognized as a mechanism of β cell loss in T2D (Talchai et al., 2012).

1.3   Insulin biosynthesis

Pancreatic β cells are essential for maintaining blood glucose homeostasis by producing and secreting insulin into circulation where insulin acts on insulin-sensitive tissues, including muscle, liver and adipocytes. The amount of insulin released is proportional to blood glucose levels. In addition to its stimulation of insulin release, glucose activates the transcription of the gene encoding preproinsulin (simply "the insulin gene"). Insulin gene expression is a highly regulated process that is dependent on the intricate balance between transcriptional activators and repressors acting upon the insulin promotor (Andrali et al., 2008). Transcriptional activators include Pdx1, MafA, NeuroD, Pax6, Nkx2.2 and Nkx6.1 (reviewed in (Cerf, 2006), while transcriptional repressors include Hes1, Insm1/A1, Sox6, Bhlhe22 and Crem (Melkman-Zehavi et al., 2011). Glucose is known to exert a pleiotropic role in insulin gene expression both transcriptionally and post-transcriptionally. During insulin transcription, glucose recruits transcriptional activators to the insulin promotor. Additionally, glucose stabilizes preproinsulin mRNA through binding of polypyrimidine tract-binding protein to pyrimidine-rich sequences in the 3'untranslated region (3'UTR) (Poitout et al., 2006).

Preproinsulin contains a signal peptide that is cleaved in the endoplasmic reticulum, yielding proinsulin. Proinsulin is then further processed by prohormone convertases (PC1/3 and PC2) and carboxypeptidase E (CPE) to active insulin as it is packaged in insulin secretory granules in the Golgi apparatus (Goodge and Hutton, 2000). Eventually, mature insulin resides in insulin granules as a reserve pool within the β cell, in which <1% of the granules are docked and primed at the plasma membrane (Olofsson et al., 2002). The release of insulin from primed granules corresponds to 1st phase insulin secretion while its release from granules within the larger reserve pool represents the 2nd phase insulin secretion (Eliasson et al., 2008).

1.4   Glucose-stimulated insulin secretion

Glucose-stimulated insulin secretion (GSIS) is a pivotal process in the β cell that controls glucose homeostasis (Ashcroft and Rorsman, 2004). This process is highly dynamic and is primarily regulated by the levels of extracellular glucose. Other regulators involve hormonal factors such as gastrointestinal hormones incretins i.e., glucagon-like peptide 1 (GLP-1) and

glucose-dependent insulinotropic polypeptide (GIP) and neural factors. Any dysregulation of this process results in hyperglycemia and T2D development (Weir and Bonner-Weir, 2004).

Glucose-stimulated insulin secretion starts with the uptake of glucose by glucose transporter-2 (GLUT2) on the cell membrane. Then glucose is rapidly phosphorylated by glucokinase (Gck) to begin the glycolytic process. Glycolysis ends with the production of pyruvate, that enters the tricarboxylic acid (TCA) cycle in the mitochondria and gets converted to acetyl CoA. Acetyl CoA is ultimately oxidized to carbon dioxide. The electrons produced in the TCA cycle are used to generate ATP by oxidative phosphorylation in the mitochondria. The increased ATP/ADP ratio causes the closure of ATP-sensitive potassium channels leading to depolarization of plasma membrane which allows the opening of voltage-dependent calcium channels and the influx of calcium. Increased intracellular calcium causes the fusion of insulin granules to the plasma membrane and insulin exocytosis. While most studies focused on the dynamics of GSIS, it is worth investigating its underlying molecular mechanisms (reviewed in (Seino et al., 2011)).

1.5   β cell maturation

Newly differentiated fetal β cells are immature and have deficient physiological responses to glucose. These immature cells become functionally mature postnatally in the first 4 weeks after birth in rodents (Blum et al., 2012; Stolovich-Rain et al., 2015). During maturation, β cells undergo a number of metabolic and molecular changes. These changes define the β cell identity and β cell acquires GSIS feature.

This transition from immature to mature β cell involves the increased expression of β cell-specific markers such as MafA, Urocortin3 (Ucn3), Gck and many other components that couple the metabolism of glucose to the insulin exocytotic machinery. MafA is recognized as a driver of β cell maturation where it specifically improves GSIS in immature β cells, likely through transcriptional regulation of a number of genes related to insulin secretion (Wang et al., 2007; Zhang et al., 2005). The others only serve as markers of β cell maturation such as Ucn3, a secreted protein in the corticotropin-releasing factor hormone family that is highly expressed in adult mouse and human β cells (Blum et al., 2012; van der Meulen et al., 2012). *Ucn3* increases during maturation of mouse β cells as well as over the maturation of human stem cell-derived insulin-expressing cells (Blum et al., 2012; van der Meulen and Huising,

2014). Ucn3 injections enhance plasma levels of insulin in rats, but treatment with Ucn3 does not promote maturation of stem cell-derived insulin-expressing cells (Blum et al., 2012).

Mature β cells are defined by not only the presence of maturity genes (described above) but also the repression of specific genes. Among these genes are the genes for high-affinity hexokinase 1 (HK1), monocarboxylate transporter 1 (MCT1) and lactate dehydrogenase A (LDHA). HK1 has high affinity for glucose and thus allows insulin secretion in response to low glucose and is replaced by the low affinity Gck during maturation, allowing only insulin secretion in response to higher glucose. MCT1 is a pyruvate transporter that feeds into the TCA cycle. Since lactate and pyruvate can be produced by other tissues such as muscle during exercise, repression of *Mct1* (also named *Slc16a1*) in mature β cells prevents such metabolic interference that could otherwise promote insulin secretion in the absence of glucose (Pullen et al., 2012). *Ldha* repression further prevents conversion of exogenous lactate into pyruvate, which could similarly dysregulate insulin secretion (reviewed in (Liu and Hebrok, 2017). β cell maturation is illustrated in Figure 1.2. The molecular mechanisms that drive β cell maturation are not completely understood.
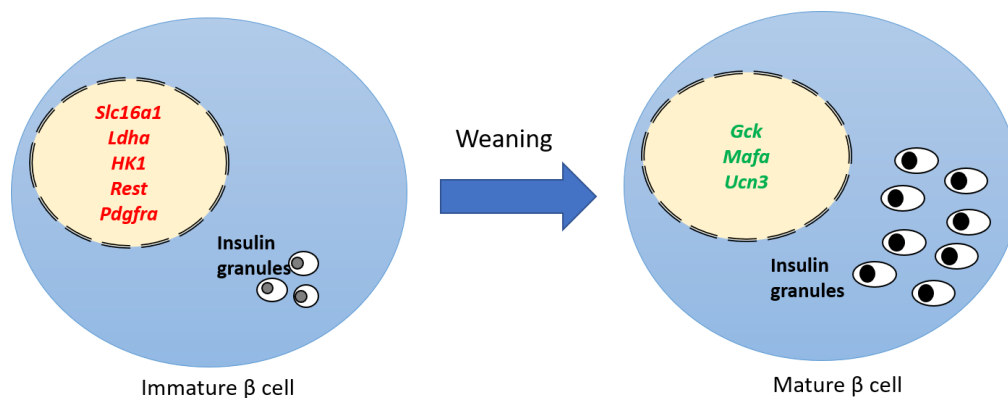
Figure 1.2 Cartoon of β cell maturation

Transition from immature to mature β cell involves the upregulation of: *Mafa*, *Gck* and *Ucn3*; and the down regulation of *Slc16a1*, *Ldha*, *Hk1*, *Rest* and *Pdgfra*. The number of insulin granules are increased too.

1.6 Post-transcriptional regulation of β cell function

In the past decade, miRNAs have attracted a great deal of research attention for post-transcriptional regulation of gene expression in pancreatic β cells. miRNAs have been shown to regulate β cell development, differentiation, insulin biosynthesis, exocytosis and compensatory β cell expansion (Ozcan, 2015).

miRNAs are endogenously produced, short RNAs of 21–25 nucleotides (Bartel, 2009). miRNA synthesis starts initially by transcription of DNA by RNA polymerase II to relatively long primary transcripts with multiple hairpin loop structures called pri-miRNAs. These pri-miRNAs are then processed by the RNase III enzyme "Drosha" to precursor miRNAs (pre-miRNAs) of ~61 nucleotides. Finally, pre-miRNAs are exported to the cytoplasm where they are further processed into mature miRNA duplexes ~21-25 nucleotides in length by the type III RNase enzyme, Dicer. Dicer then transfers a single mature miRNA strand to the miRNA-induced silencing complex (miRISC) that typically comprises Argonaute (Ago) family proteins (Kim et al., 2009). miRNA binds to the 3'UTR of its target gene through complementary base pairing. Ago2, a member of the Ago protein family interacts with an mRNA-binding protein, GW182, causing miRNA-induced mRNA gene silencing through translation repression and mRNA degradation (Braun et al., 2013; Fabian et al., 2011).

Studies on mice revealed many miRNAs that are enriched in the β cell and play critical roles in modulating its physiology (Poy et al., 2004; Tattikota et al., 2015). Studies with β cell specific deletions of *Dicer* and *Ago2* in mice demonstrated the important regulatory function of miRNAs in β cell function. Such studies spanned from investigating their role in the development of endocrine pancreas to the adult differentiated β cell. Dicer is found to be essential for the development of the endocrine pancreas and insulin biosynthesis and exocytosis in the adult β cell (Lynn et al., 2007; Martinez-Sanchez et al., 2015; Melkman-Zehavi et al., 2011). miRNA inactivation by *Dicer* deletion in adult pancreatic β cells resulted in a striking diabetic phenotype in mice due to diminished insulin synthesis. Mechanistically, miRNAs in the adult β cell are found to be important for insulin expression through down regulating insulin transcriptional repressors such as Bhlhe22 and Sox6 (Melkman-Zehavi et al., 2011). However, Martinez-Sanchez et al. (2015) further showed that *Dicer* deletion caused β cell death following a decrease in GSIS was due to the upregulation of three disallowed genes that are direct targets for miRNAs. β cell disallowed genes are a group of genes that are normally abundantly expressed in most tissues and selectively repressed in β cells (Lemaire et al., 2016; Pullen and Rutter, 2013). The miRNA regulatory network is found to be equally important in another aspect of adult β cell function - compensatory β cell expansion. miRNA-184 is down regulated in the β cells of obese mice leading to upregulation of *Ago2*. Ago2 is shown to be required for insulin secretion and β cell compensatory expansion (Tattikota et al., 2014; Tattikota et al., 2013). Tattikota et al. (2014) have shown that miRNA-184 is a unique miRNA that is down regulated during insulin resistance. This causes the upregulation of its target *Ago2*. Ago2, a

critical player in miRISC, causes silencing of the targets of another miRNA, miRNA-375, leading to compensatory β cell expansion. Further studies have implicated specific miRNAs in affecting insulin production (Setyowati Karolina et al., 2013; Zhang et al., 2011), exocytosis (Lovis et al., 2008a; Tattikota et al., 2015), or β cell apoptosis (Lovis et al., 2008b; Ruan et al., 2011).

Understanding post-transcriptional control of gene expression by miRNAs is complicated because a single miRNA can have several target mRNAs, and several miRNAs can work synergistically to affect the translation of a single mRNA. Deregulated expression of some miRNAs is involved in β cell dysfunction and the development of diabetes. Moreover, the expression of some miRNAs changes in response to metabolic demand as a compensatory response to allow for β cell proliferation and enhancement of insulin secretion (Guay and Regazzi, 2015; Nesca et al., 2013; van de Bunt et al., 2013).

1.7   The CCR4-NOT complex: Definition, Structure and function

Maintaining correct levels of mRNA expression requires the balance between mRNA synthesis and decay. Deregulation of mRNA decay can lead to the aberrant accumulation of mRNAs and the proteins they encode. mRNA decay begins with shortening of the poly(A) tail. Deadenylation is considered the rate limiting step of mRNA decay and is catalyzed by two main deadenylase complexes: the poly(A)-nuclease deadenylation complex (PAN2/3) and the CCR4-NOT complex (Chen and Shyu, 2011).

The CCR4-NOT complex is a multi-meric complex of more than 2MDa size that is highly conserved in eukaryotes. Deadenylation activity of the CCR4-NOT complex was first identified in yeast (Tucker et al., 2001). In yeast, it consists of nine subunits (Ccr4, Caf1, Caf40, Caf130, Not1-5), and in mammals it consists of eight subunits (CNOT1, CNOT2, CNOT3, either CNOT7 or CNOT8, either CNOT6 or CNOT6L, CNOT9, CNOT10 and CNOT11) (Bartlam and Yamamoto, 2010; Collart, 2016; Collart and Panasenko, 2012). Although it is particularly highlighted as a major deadenylase that is essential for mRNA decay, CCR4-NOT is rather multifunctional and has been implicated in different aspects of RNA and protein expression which places CCR4-NOT as a core molecule in regulation of gene expression (Villanyi and Collart, 2015). Its diverse functions include regulation of transcription, transcription elongation, mRNA export, translational repression, chromatin modification, ubiquitination and protein modification (Collart, 2016; Collart and Panasenko, 2012; Miller

and Reese, 2012). Subunits of the CCR4–NOT complex have been found in both the nucleus and cytoplasm (Shi and Nelson, 2005; Tucker et al., 2002), which supports the involvement of the complex in both nuclear and cytoplasmic functions. However, it has not been determined whether the CCR4–NOT complex as an entity exists in both cellular compartments. The structure and function of CCR4-NOT complex are illustrated in Figure 1.3.
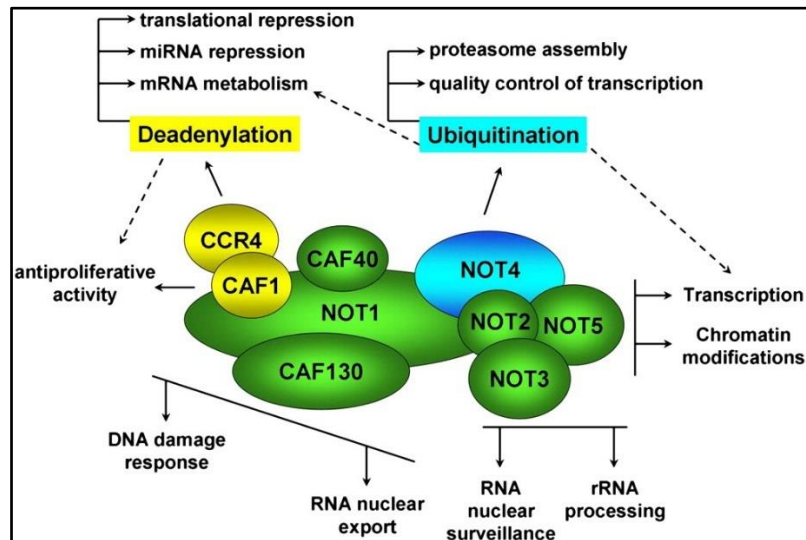
Figure 1.3 Schematic representation of the CCR4-NOT complex structure and function

(Collart and Panasenko, 2012)

Mammalian CCR4-NOT complex subunits are classified as four catalytic and at least six non-catalytic subunits. The catalytic subunits comprise two exonuclease-endonuclease-phosphatase (EEP) family proteins (CNOT6 and CNOT6L), and two DEDD (Asp-Glu-Asp-Asp) family proteins (CNOT7 and CNOT8) which are orthologs of yeast Ccr4 and Caf1, respectively, while the non-catalytic subunits include CNOT1, CNOT2, CNOT3, CNOT9, CNOT10 and CNOT11 (Bawankar et al., 2013; Boland et al., 2013; Lau et al., 2009; Raisch et al., 2019). Mammalian CNOT3 was suggested to be the functional homologue of the yeast Not5 (Collart, 2016). The mammalian CCR4-NOT complex subunits and their corresponding yeast CCR4-NOT complex subunits are summarized in Table 1.

Table 1: Yeast and mammalian CCR4-NOT complex subunits

Yeast CCR4-NOT complex	Mammalian CCR4-NOT complex
Not1	CNOT1
Not2	CNOT2
Not3	
Not4	CNOT4 (not stably associated with the complex (Lau et al., 2009))
Not5	CNOT3
Ccr4	CNOT6/6L
Caf1	CNOT7/8
Caf40	CNOT9
Caf130	
	CNOT10
	CNOT11

Despite the association of all of the subunits in a single complex, each subunit has a very specific role in gene expression (Azzouz et al., 2009). Regarding deadenylation function, only the catalytic subunits clearly contribute to mRNA deadenylation, but various different other subunits act as modulators of deadenylase activity and are important for recruitment of the CCR4-NOT complex to specific mRNAs (Bawankar et al., 2013; Boland et al., 2013; Chen et al., 2014; Ito et al., 2011a; Ito et al., 2011b; Morita et al., 2011; Petit et al., 2012; Raisch et al., 2019). Of note, CCR4-NOT is more active and selective for poly(A) than the isolated catalytic subunits. The catalytic subunits require at least two out of three conserved non-catalytic modules (CNOT9, CNOT10/CNOT11 or CNOT2/CNOT3) for full activity in CCR4-NOT complex (Raisch et al., 2019).

Structural analyses revealed that CNOT1 is the largest subunit and is responsible for the assembly of the complex components. The CNOT2-CNOT3 heterodimer binds to C-terminus of CNOT1 (Basquin et al., 2012; Boland et al., 2013; Petit et al., 2012). Although the four catalytic subunits are all associated with the CCR4-NOT complex, only one subunit of EEP family and one subunit of DEDD family deadenylase exist in a particular complex (Lau et al., 2009). While CNOT1 binds directly to CNOT7/8 through its MIF4G domain (Bartlam and Yamamoto, 2010; Basquin et al., 2012; Petit et al., 2012), CNOT7/8 subunits are important for the association of CNOT6/6L subunits to the complex through protein-protein interaction

of CNOT7/8 with leucine rich repeat (LRR) domain of CNOT6/6L (Clark et al., 2004). When CNOT1 is suppressed in HeLa cells, most other subunits also decrease, resulting in severe reduction of deadenylase activity (Ito et al., 2011b). Therefore, CNOT1 is critical not only for assembly, but also for maintenance of the CCR4–NOT complex subunits expression. Similarly, CNOT3 contributes to complex stability, activity and recruits CCR4-NOT to target genes (Boland et al., 2013; Chicoine et al., 2007). Thus, deficiency of CNOT3 in mice affects stability of some mRNAs due to poor recruitment of the CCR4-NOT complex to the mRNA 3'UTRs (Chicoine et al., 2007; Morita et al., 2011; Suzuki et al., 2019; Suzuki et al., 2015; Watanabe et al., 2014). Knockout (KO) of *Cnot3* is embryonically lethal in mice and causes necroptosis of mouse embryonic fibroblasts (MEFs) (Morita et al., 2011; Suzuki et al., 2015). These studies provide an evidence of the importance of CNOT3 in the CCR4-NOT complex deadenylase activity.

1.8   Role of the CCR4-NOT complex in post-transcriptional regulation

The main function of the CCR4-NOT complex is mRNA deadenylation. The deadenylation process occurs via two distinct steps (Chen and Shyu, 2011). In the first step, PAN2/3 catalyzes mRNA deadenylation and shortens poly(A) tail to approximately 110 nucleotides. This step doesn't trigger mRNA decay as cytoplasmic poly(A) adenylases can still bind and add adenosine residues, extending the tail. In the second phase, CCR4-NOT catalyzes shortening of the 3′ poly(A) tail to variable lengths of 20~110 nucleotides which reduces the binding of poly(A) tail binding proteins, leading to a reduction in the rate of translation. As a result, the Dcp1/Dcp2 decapping complex is recruited and removes the 5' cap structure of target mRNAs followed by rapid 5' to 3' degradation by the exoribonuclease, Xrn1. Alternatively, mRNAs are degraded from 3' to 5' by the exosome (Parker, 2012; Parker and Song, 2004). Both 3' to 5' and 5' to 3' decay processes can occur together on the same mRNA molecule. CCR4-NOT complex is directed to specific mRNAs through association with RNA-binding proteins (RBPs) that bind directly to the 3'UTR of target mRNAs (Inada and Makino, 2014; Lykke-Andersen and Wagner, 2005; Semotok et al., 2005) and by miRNAs (Fabian et al., 2009; Wahle and Winkler, 2013) (See further in Figure 1.4).

Several RBPs have been shown to mediate the interaction between CCR4-NOT complex subunits and particular target mRNAs. These RBPs recognize *cis*-acting elements within the mRNA 3'UTRs (Brennan and Steitz, 2001). AU-rich elements (ARE) in the 3'UTR are one of the well-characterized *cis*-acting elements that signals mRNA decay (Brennan and

Steitz, 2001). Tristetraprolin (TTP) family proteins such as BRF1 are among those RBPs, that recruit the CCR4-NOT complex, through interaction with ARE (Fabian et al., 2013; Takahashi et al., 2015; Wahle and Winkler, 2013). Other identified RBPs are: BTG/Tob family, Roquin, and Nanos2 (Bhandari et al., 2014; Leppek et al., 2013; Suzuki et al., 2010). CNOT1 is known to interact with TTP (Sandler et al., 2011). CNOT3 may also interact with Roquin thus recruiting CCR4-NOT complex to specific targets (Murakawa et al., 2015).
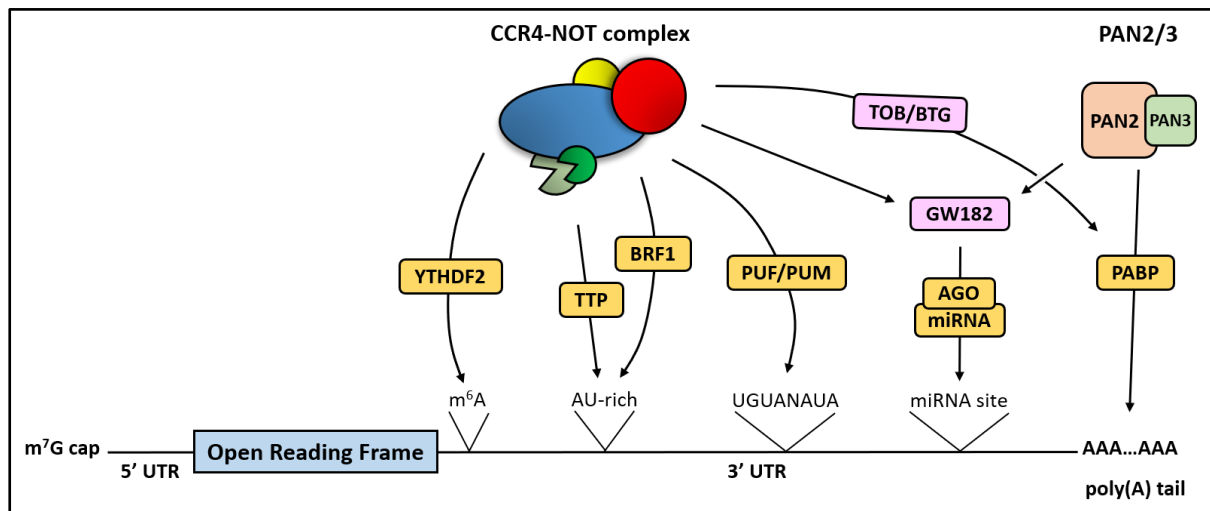
Figure 1.4 Schematic illustration of recruitment of CCR4-NOT complex to its target mRNAs

A complete description is provided in the main text (Figure adapted from (Ashworth et al., 2019)

Current evidence suggests that miRNA-mediated gene silencing requires direct interaction between GW182 and CCR4-NOT via CNOT1. Further structural studies showed the involvement of another subunit of CCR4-NOT complex, CNOT9, in inducing gene silencing by miRNA. CNOT9 attaches to a domain of unknown function (DUF3819) in CNOT1 resulting in a complex that provides binding sites for GW182. Furthermore, CNOT1 interacts with DDX6, a known translational inhibitor (Chen et al., 2014; Rouya et al., 2014). The role of the CCR4-NOT complex in miRNA-mediated gene repression is supported by an increasing number of studies. One study showed that miRNA-dependent deadenylation is suppressed in CNOT1-depleted *Drosophila melanogaster* cells (Behm-Ansmant et al., 2006) and another study showed that miRNA-induced deadenylation in mouse was slowed down in cells overexpressing a dominant negative (DN) CNOT7 (Chen et al., 2009). Additionally, it was demonstrated that about 60% of Ago targets in *Drosophila melanogaster* are regulated by CNOT1 and/or CNOT7, and that 45% require both, suggesting that deadenylation is a

widespread effect of miRNA regulation (Eulalio et al., 2009). More recently, CNOT2 was found necessary for miRNA-mediated gene silencing in *Drosophila* development (Knox et al., 2016). However, to what extent deadenylation contributes to miRNA-mediated repression is still under debate (Doidge et al., 2012).

1.9   Multifunctional roles of CCR4-NOT complex in mammals

The physiological significance of CCR4-NOT complex in mammals has been addressed by examining the phenotypes of conventional KO mice. Accumulating evidence suggests that each subunit, both catalytic and non-catalytic, plays an important physiological role (Shirai et al., 2014). The embryonic lethal phenotype occurring as a result of deletion of specific subunits (*Cnot1, Cnot3, Cnot8, Cnot9* and *Cnot10*) hampered the use of these mouse mutants for assessment of specific subunits functions in organs and tissues. To circumvent this obstacle, conditional KO of a specific subunit in a specific organ or tissue is valuable for functional analysis.

Although CCR4-NOT subunits are ubiquitously expressed (Chen et al., 2011a), it is evident that specific subunits regulate distinct biological processes. Targeted deletions of specific subunits of CCR4-NOT complex enabled the identification of their specific roles in the regulation of specific physiological processes. Thus, disruption of specific subunit could be relevant to specific disease (Doidge et al., 2012). Indeed, the CCR4–NOT complex has been implicated in the development of metabolic disorders. *Cnot3* heterozygous (het), *Cnot6l* KO and *Cnot7* KO mice are lean and display resistance to high-fat diet (HFD) induced obesity (Morita et al., 2011; Morita et al., 2019; Takahashi et al., 2015). Conditional *Cnot3* or *Cnot1* KO in mice adipose tissue is associated with lipodystrophy and hyperlipidemia (Li et al., 2017; Takahashi et al., 2019). *Cnot3* KO in heart is associated with autophagy and heart failure (Yamaguchi et al., 2018). *Cnot3* KO in liver is associated with inflammation and the increased expression immature genes expression (Suzuki et al., 2019). *Cnot7* KO mice have defects in spermatogenesis (Berthet et al., 2004). Accordingly, unraveling physiological roles of CCR4-NOT complex would be a novel approach to elucidate disease pathogenesis and develop new therapeutics.

1.10 Problem statement and thesis aims

Diabetes is one of the greatest healthcare challenges in the 21st Century. The number of diabetic patients continues to rise because how diabetes develops is not completely understood. Loss of β cell identity and dedifferentiation are recognized as mechanisms of β cell dysfunction in diabetes. Published evidence suggests that the CCR4-NOT complex regulates metabolism-related genes via mRNA decay and may be involved in metabolic disorders such as obesity, lipodystrophy and diabetes. Therefore, I hypothesize that the CCR4-NOT complex post-transcriptionally regulates mRNAs governing β cell function and dysregulation of its expression or activity contributes to diabetes pathogenesis.

The main goal of this thesis was to address the function of CCR4-NOT complex in pancreatic β cells and to understand the molecular mechanism of its function. A secondary goal was to elucidate the contribution of the CCR4-NOT complex catalytic subunits in mRNA decay and cell viability in MEFs.

In Chapter two, the objective was to study the role of CNOT3 in pancreatic β cell function in mice. The approach was to delete CNOT3 specifically in β cells and to examine the phenotype of the mice. The function of the islets of Langerhans from mice with β cell-specific *Cnot3* KO was evaluated *in vitro*. Following this, I performed RNA sequencing (RNA-seq) with the purpose of checking the effect of CNOT3 KO on global gene expression in β cells and identifying CNOT3 molecular targets. Being able to unravel previously unknown molecular mechanisms governing β cell function should ultimately contribute to the generation of functionally mature β cells *in vitro* or revert dysfunctional β cells to normal.

In Chapter three, the objective was to compare the two types of CCR4-NOT complex deadenylase subunits: Ccr4-type (CNOT6/6L) and Caf1-type (CNOT7/8) with respect to mRNA deadenylation and cell survival in mammalian cells under normal physiological conditions. The approach was to delete the catalytic subunits in MEFs and to characterize the phenotype of mutant MEFs in terms of CCR4-NOT complex formation, cell survival, global mRNA deadenylation, global gene expression and mRNA stability.

2 Chapter 2: CNOT3 is essential for β cell maturation and maintaining β cell identity

2.1 Introduction

Diabetes mellitus is a metabolic disorder that is ultimately caused by the loss of functional pancreatic β cells (Ashcroft and Rorsman, 2012), the only cells within the body that secrete insulin to regulate blood glucose homeostasis. Whilst T1D involves immune-mediated β cell destruction (Ashcroft and Rorsman, 2012), dedifferentiation and dysfunction, rather than β cell loss *per se*, is implicated in the pathogenesis of T2D (Talchai et al., 2012). A fuller understanding of the molecular mechanisms that govern β cell differentiation *in utero*, maturation after birth, and dedifferentiation in diabetes is likely to be crucial for developing novel prevention and treatment strategies for diabetes.

Pancreatic β cells are defined functionally by the capacity for glucose- (and other nutrient-) stimulated insulin secretion (Rutter, 2004; Rutter et al., 2015). Underlying this is a molecular identity defined by the expression of genes that drive β cell maturation, insulin gene expression, insulin granule formation and exocytosis. Although extensive research has focused on the transcriptional and epigenetic regulation of β cell maturation, the influence of post-transcriptional mechanisms on the β cell gene expression program is relatively less well defined. Nonetheless, glucose is known to stimulate the biosynthesis of insulin and a number of other β cell proteins, particularly those involved in insulin granule biogenesis, from pre-existing mRNAs (Magro and Solimena, 2013; Wicksteed et al., 2003). In addition, several studies (Baroukh et al., 2007; Latreille et al., 2014; Martinez-Sanchez et al., 2015; Nathan et al., 2015; Poy et al., 2004) have implicated non-coding RNAs: long non-coding RNAs (lncRNAs), and miRNAs as important modulators of β cell gene expression and function (Guay et al., 2012; Martinez-Sanchez et al., 2017).

Most eukaryotic mRNAs are polyadenylated, and poly(A) tail lengths are important for post-transcriptional gene regulation (Eckmann et al., 2011; Nousch et al., 2013). Importantly, mRNA deadenylation is the rate-limiting step in mRNA decay (Garneau et al., 2007). Deadenylation involves shortening of poly(A) tail length, reducing the binding of poly(A) tail-binding proteins. This decreases mRNA stability, slowing down translation (Eckmann et al., 2011; Nousch et al., 2013).

In this chapter I investigated whether and how mRNA deadenylation by CCR4-NOT complex regulates β cell function. Earlier studies revealed the involvement of the CCR4–NOT

complex in the development of metabolic disorders such as obesity, diabetes and lipodystrophy (Li et al., 2017; Morita et al., 2011; Takahashi et al., 2019). However, its role in maintaining normal β cell function has not been investigated. I focused on the CNOT3 subunit and presented evidence that CNOT3-dependent deadenylation serves as a post-transcriptional regulatory mechanism governing normal β cell function.

2.2   Materials and Methods

2.2.1   Mice

To suppress *Cnot3* expression in β cells, I crossed mice carrying *Cnot3* floxed alleles (*Cnot3^{flox/flox}*) (Inoue et al., 2015; Li et al., 2017) with *Ins1-Cre* mice (Riken Bioresource Center, # RBRC09525), in which Cre recombinase is knocked in at the *Ins1* locus (Hasegawa et al., 2016). Recombination is expected to be restricted largely to β cells, and to be minimal at other sites, including the brain, where *Ins1* is not expressed (Thorens et al., 2015). *mTmG* reporter mice (Jackson Laboratory, # 007676) were used to trace β cells in which *Ins1-Cre*-mediated recombination was induced (Muzumdar et al., 2007). β cell-specific *Cnot3* knockout mice (*Cnot3*βKO) were used for experiments and their littermates (*Cnot3^{flox/flox}*) were used as controls, unless stated otherwise (*Ins1-Cre* mice were used as controls for *Cnot3*βKO expressing the *mTmG* reporter gene). All experiments were performed on 8-10-week-old male mice, unless stated otherwise. *db/db* mice were used as a model of T2D (Kobayashi et al., 2000) and compared with *+/db* mice (Jackson Laboratory, #000697; purchased from CLEA Japan). Mice were maintained on a 12-hr light/12-hr dark cycle in a temperature-controlled (22° C) barrier facility with free access to water and either a normal chow diet (NCD, CA-1, CLEA Japan) or a HFD (D12492, Research diets). All mouse experiments were approved by the Animal Care and Use Committee in OIST Graduate University.

2.2.2   Genotyping

Tails from 3-week-old mice were lysed in 50 µL of DNA extraction lysis buffer (25mM NaOH, 0.2 mM EDTA) 20 min in 100° C followed by addition of 50 µL of 40 mM Tris-HCl. Samples were then vortexed. 1 µL of lysed tail samples was used as template for PCR amplification as follows. All genotyping primers are listed in Table 3.

PCR mixture:

- 0.4 µL of 10 µM of primers (Forward and Reverse primers)
- 2 µL of 10 ExTaq buffer
- 2 µL of 2.5 mM dNTP
- 0.1 µL of ExTaq
- 1 µL of template DNA
- 14.5 µL of double distilled water

PCR amplification of genomic DNA by cycling for 40 cycles:

- Initial denaturation: 2 min at 95° C,
- 45 s at 95° C,
- 45 s at 60° C,   40 cycles
- 1 min at 72° C.
- Final extension: 5 min at 72° C.

PCR products were run on 2% agarose gel with 10x loading sample buffer.

2.2.3   Islet isolation

Mouse pancreatic islets were isolated as previously described (Graham et al., 2016). Pancreata were perfused with Collagenase P (Sigma) by injection in the common hepatic bile duct at a concentration of 1 mg/mL in Hank's buffered salt solution (HBSS) medium (Invitrogen) supplemented with 1% bovine serum albumin (BSA) (Roche). Pancreata were then removed and dissociated in a 37° C water bath for 16 min. Dissociated pancreata were passed through a metal sieve to remove undigested tissue chunks, followed by washing in HBSS supplemented with 0.1% BSA. Islets were then separated onto a gradient of Histopaque 1077 (Sigma) overlaid with RPMI 1640 medium (Gibco) supplemented with 10% fetal bovine serum (FBS) and 1% penicillin-streptomycin (10,000 U/mL, Gibco). Afterward, islets were collected from the boundary of Histopaque 1077 and RPMI 1640 medium and passed through a 70 μm cell strainer (BD Falcon) into a cell culture dish with RPMI 1640 supplemented with 10% FBS and 1% penicillin/streptomycin from which the islets were hand-picked for experiments to avoid contamination with exocrine tissue.

2.2.4   Cell lines

MIN6 (mouse insulinoma-6) β cell line, a well-established model for the study of the β-cell function, was used for some *in vitro* investigations (Miyazaki et al., 1990). MIN6 cells were cultured in high glucose Dulbecco's modified Eagle's medium (Wako) supplemented with 10% FBS and 1% penicillin-streptomycin (10,000 U/mL, Gibco). For induction of gluco-toxic stress, glucose concentration was increased to 50 mM by dissolving glucose in culture medium followed by sterile filtration.

2.2.5   Fatty acid solution preparation and MIN6 cells treatment

Palmitate stock solution was prepared by dissolving palmitate (Sigma P9767) in 50% ethanol at 70° C to a final concentration of 100 mM. The stock solution was then diluted in culture medium with 0.5% BSA to a final concentration of 0.5 mM. The palmitate was allowed to complex with the BSA for 30 min at 37° C before being added to the cells. Palmitate untreated cells were treated in the same manner, but palmitate stock solution was replaced with vehicle (50% ethanol).

2.2.6   Immunoblot analysis

Pancreatic islets and MIN6 cells were lysed using TNE lysis buffer (1% NP-40, 50 mM Tris–HCl pH 7.5, 150 mM NaCl, 1 mM EDTA, 1 mM phenylmethylsulfonylfluoride, 10 mM NaF). Protein was quantified by Bicinchoninic acid (BCA) assay kit (Thermofisher) following the manufacturer's protocol. All immunoblot analyses were done following SDS-polyacrylamide gel electrophoresis (SDS-PAGE) standard protocols except for MCT1 and LDHA, which were not detected by conventional Western blotting and so the automated Simple Wes system (ProteinSimple) was used for their detection (Harris, 2015).

Immunoblot analysis following SDS-PAGE standard protocols:

In brief, protein samples, adjusted to equal protein amounts and reduced by boiling with sample buffer, were resolved on a 10% polyacrylamide gel. Afterwards, proteins separated on the SDS-PAGE were electro-transferred onto 0.45 μm methanol activated polyvinylidene fluoride (PVDF) membrane at 17V for 70 min using semi-dry transfer system (Biocraft, cat. no. BE-321). PVDF membrane was then blocked in 5% skimmed milk for 1 hr and probed with primary antibodies for overnight at 4° C. Eventually, the blots were visualized using a horseradish

peroxidase (HRP)-conjugated secondary antibody and Western Lightning Plus-ECL enhanced chemiluminescence substrate (PerkinElmer). Blots were imaged using an ImageQuant LAS 4000 mini (GE Healthcare, Tokyo). Protein levels were quantified using ImageJ software and normalized to GAPDH protein levels. Buffers used for SDS-PAGE are listed in Appendix p. 108- 110.

Immunoblot analysis using automated Simple Wes system:

I used an automated Simple Wes system according to the manufacturer's instructions with a 12–230 kDa Separation Module (ProteinSimple SM-W004) and the Anti-Rabbit Detection Module. In brief, 4 µL islet lysates were combined with 1µL Fluorescent Master Mix and heated at 95° C for 5 min. The biotinylated ladder, samples, antibody diluent, primary antibodies (in antibody diluent), HRP-conjugated secondary antibodies and chemiluminescent substrate were pipetted into the plate (part of Separation Module). Instrument default settings were used: stacking and separation at 375 V for 25 min; blocking reagent for 5 min, primary and secondary antibody both for 30 min; luminol/peroxide chemiluminescence detection for ~15 min. Details of primary and secondary antibodies used are listed in Table 4 and Table 5 respectively.

2.2.7   Glucose tolerance tests

Mice were fasted for 16 hrs starting from 19:00, immediately before the onset of the dark phase, followed by fasting blood glucose measurement in tail vein blood samples. Mice were then injected intraperitoneally with 2 g glucose per kg body weight and blood glucose was measured in tail vein blood samples at 15, 30, 60 and 90 min using the Glutest Pro glucometer (Sanwa Kagaku Kenkyusho, Japan).

2.2.8   Glucose-stimulated insulin secretion assay *in vivo*

Mice were fasted for 16 hrs, followed by blood sample collection from the face vein to evaluate serum insulin levels under no glucose stimulation. Mice were then injected intraperitoneally with 2 g glucose per kg body weight and blood samples were collected from the face vein 15 min post- glucose injection. Blood samples were allowed to clot in vacutainer tubes (BD Japan) at room temperature followed by centrifugation for 10 min at 4000 rpm and separation of clear serum. Serum insulin levels were measured using an ultrasensitive mouse insulin ELISA kit (Takara).

2.2.9   Glucose-stimulated insulin secretion assay on islets *ex vivo*

Ten islets were pre-cultured in 450 µL Krebs Ringer buffer (KRB; 140 mM NaCl, 3.6 mM KCl, 0.5 mM NaH_2PO_4, 2 mM $NaHCO_3$, 1.5 mM $CaCl_2$, 0.5 mM $MgSO_4$, 10 mM HEPES) containing 3 mM glucose for 1 hr in opened Eppendorf tubes. Supernatants were discarded and replaced with 450 µL KRB containing 3 mM glucose for 1 hr. Supernatants were collected to measure basal insulin secretion. Islets were then treated with 450 µL KRB containing 17 mM glucose and supernatants were collected after 1 hr. Islets were finally treated with 1 mL 1.5% HCl in ethanol and homogenized by sonication three times (30 seconds on/off). Acid/ethanol lysates were then centrifuged. Supernatants were collected to measure insulin content and residual islet fragments were used for DNA extraction using NucleoSpin Tissue XS (Takara). Insulin in KRB supernatant (released insulin) and islet lysates (islet insulin content) was measured using an ultrasensitive mouse insulin ELISA kit (Takara). Both released insulin and islets insulin content were normalized to islets DNA content.

2.2.10 Tissue preparation and immunohistochemistry

All immunohistochemistry was performed on pancreatic sections from control and *Cnot3*βKO mice, except for CNOT3 immunofluorescence staining, which was performed on islets isolated from control and *Cnot3*βKO mice because the anti-CNOT3 antibody used worked only in isolated islets but showed non-specific signal in pancreatic sections.

Preparation of pancreatic sections and immunohistochemistry:

Mouse pancreata were processed for immunohistochemistry as previously described (Choi et al., 2014). Pancreata were fixed overnight in 4% paraformaldehyde (PFA) in phosphate-buffered solution (Wako) at 4° C. They were then transferred to 70% ethanol and subsequently embedded in paraffin and sectioned at 3 µm. Some sections were stained with hematoxylin and eosin (H & E). Other sections were used for immunofluorescence. All sections for immunofluorescence underwent dewaxing with xylene and rehydration with ethanol (100%, 95%, 70% and 50%) by incubation for 3 min at room temperature. Antigen retrieval was performed using 10 mM sodium citrate buffer, pH6, at 120° C in a pressure cooker for 10 min. After cooling down to room temperature, tissue sections were permeabilized in 0.1% Triton-X 100 in phosphate-buffered saline (PBS) for 30 min, then blocked with blocking buffer (2% BSA solution in PBS and 0.05% Tween) for 30-60 min at room temperature. Samples were then incubated with primary antibodies overnight at 4° C. On the following day, samples were

washed three times in PBS and incubated with secondary antibodies for 1-2 hrs under dark conditions at room temperature. Finally, samples were washed three times in PBS and mounted in Ultracruz hard-set mounting medium (Santa Cruz). Terminal deoxynucleotidyl transferase dUTP nick end labeling (TUNEL) assay was performed using *In Situ* Cell Death Detection Kit, TMR Red (Roche) following the manufacturer's protocol.

Immunofluorescence staining of CNOT3:

Islets were fixed in 4% PFA in phosphate-buffered solution (Wako) for 10 min at room temperature. Then samples were washed twice in PBS for 5 min. Residual PFA was quenched by incubation with 100 mM glycine for 10 min at room temperature, followed by two washes with PBS. Islets were then permeabilized in 0.5% Triton X-100 for 5 min at room temperature and rinsed twice with PBS. Islets were blocked with blocking buffer and incubated with primary and secondary antibodies in the same manner as described for pancreatic sections. Finally, samples were incubated with Ultra Cruz hard-set mounting medium with DAPI (Santa Cruz). Details of primary and secondary antibodies used for Immunofluorescence are listed in Table 6 and Table 7, respectively.

2.2.11 Morphometric image analysis

All immunohistochemistry/immunofluorescent images were acquired using a Leica confocal microscope (TCS SP8 Leica). All images were processed using ImageJ software. To calculate β cell mass, pancreatic sections were stained with anti-insulin antibody. Insulin stained area was taken as β cell area. Then β cell mass was calculated using the following equation:

$$\beta \text{ cell mass (mg)} = \frac{\beta \text{ cell area} \times \text{pancreas weight (mg)}}{\text{Pancreas area}}$$

2.2.12 Transmission electron microscopy

Transmission electron microscopy (TEM) was performed as previously described (Masini et al., 2012). Islets were fixed in 2.5% glutaraldehyde in 0.1 M cacodylate buffer (pH 7.4) for 30 min at room temperature. After three washes with 0.1M cacodylate buffer, islets were fixed in 1% cacodylate-buffered osmium tetroxide for 1 hr at room temperature, then dehydrated in a graded ethanol series and embedded in epoxy resin. Ultrathin sections (50 nm) of islets were cut with a diamond knife (Diatome), placed on copper grids and stained with 4% uranium

acetate for 30 min and then with Sato's lead staining solution. Samples were imaged using a JEOL JEM-1230R TEM.

2.2.13 RNA extraction

Total RNA was extracted from islets and MIN6 cells using Isogen II (Nippon Gene) according to the manufacturer's protocol. RNA purity and concentration were evaluated by spectrophotometry using a NanoDrop ND-2000 (ThermoFisher) instrument. The quality of RNA was assessed using an Agilent 2100 Bioanalyzer microfluidics-based platform (Agilent Technologies, Inc.).

2.2.14 Bulk poly(A) tail assay

Total RNA (2 µg) was labelled with [5′-^{32}P] pCp (cytidine 3′,5′-bis[phosphate]) (0.11 pmol/µL in a total reaction volume of 30 µL) (PerkinElmer; NEG019A) using T4 RNA ligase 1 (NEB, M0204S) at 16º C overnight. Labelled RNAs were incubated at 85º C for 5 min and placed on ice. Then, labelled RNAs were digested with Ribonuclease A (50 ng/µL, Sigma) and Ribonuclease T1 (1.25 U/µl, ThermoFisher Scientific) at 37º C for 2 hrs in digestion buffer (100 mM Tris-HCl [pH7.5], 3M NaCl, 0.5 µg/mL yeast tRNA). The reaction was stopped by adding 5x stop solution (10 mg/mL Proteinase K, 0.125 M EDTA, 2.5% SDS) and subsequently incubating at 37º C for 30 min. After adding 400 µL of RNA precipitation buffer (0.5 M NH$_4$OAc, 10 mM EDTA), the digested RNA samples were purified by phenol-chloroform extraction and isopropanol precipitation. Final products (10 µL) were mixed with RNA Gel loading Dye (NEB, R0641) and incubated at 95º C for 2 min. Then, samples were fractionated on an 8 M urea-10% polyacrylamide denaturing gels (0.8 mm thick). Markers (Prestained Markers for small RNA Plus, BioDynamics Laboratory DM253) were also loaded. The gel was analysed with a Typhoon FLA 9500 Fluorescence Imager (GE Healthcare). Band intensity was quantified using ImageJ software.

2.2.15 RNA sequencing

RNA-seq was performed by the Next Generation Sequencing section at OIST Graduate University for three replicates (each prepared by pooling islets from two mice) per condition. 100 ng of total RNA was used for RNA-seq library preparation with a TruSeq Stranded mRNA Library Prep Kit for NeoPrep (NP-202-1001; Illumina) that allows polyA-oligo(dT)-based

purification of mRNA, according to the manufacturer's protocol with minor modification and optimization as follows. Custom dual index adaptors were ligated at the 5' and 3'-ends of library, and PCR was performed for 11 cycles. 150 base-pair pair-end read RNA-seq was performed with a Hiseq 3000/4000 PE Cluster Kit (PE-410-1001; Illumina) and a Hiseq 3000/4000 SBS Kit (300 Cycles) (FC-410-1003; Illumina) on Hiseq4000 (Illumina), according to the manufacturer's protocol.

2.2.16 Bioinformatic processing of RNA-seq data

Paired-end RNA-seq data were mapped to the *Mus musculus* reference strain mm10 UCSC using, Strand NGS, next generation sequencing analysis software. Counts for each sample were imported into the R statistical environment. Genes without an expression level of at least one read per million mapped reads in at least three samples were removed before differential gene expression testing between control and *Cnot3*βKO islet RNA replicates, was performed with the edgeR function in the Bioconductor package edgeR (Robinson et al., 2010). Genes that were differentially expressed (DE) with a False Discovery Rate (FDR), adjusted *P* value less than 0.05 were considered statistically significant and included in enrichment testing. I identified Gene Ontology (GO) terms enriched among significantly upregulated and down regulated genes using DAVID annotation tool (https://david.ncifcrf.gov/). GO terms were considered significantly enriched if they had an FDR value of less than 0.05.

2.2.17 mRNA stability measurement and qPCR

To measure mRNA stability, islets were treated with actinomycin D (Act. D) (5 μg/mL), a transcription inhibitor, and total RNA was extracted at the indicated time points and subjected to qPCR. Total RNA (1 μg) was used for reverse transcription with oligo(dT)12-18primer (Invitrogen) using the SuperScript III First-Strand Synthesis System (Invitrogen). qPCR reactions were carried out using TB Green Premix Ex Taq (Takara) and ViiA 7 Real-Time PCR System (Applied Biosystems). *Gapdh* mRNA levels were used for normalization. Relative mRNA expression was determined by ΔΔCt method. Primers used for qPCR reactions are listed in Table 8.

2.2.18 Sample preparation for proteomic analysis

Samples were prepared for Liquid Chromatography/Mass Spectrometry (LC/MS) using the Phase-Transfer Surfactant Method (Masuda et al., 2009; Masuda et al., 2008), with minor modifications. First, proteins were extracted from islets and solubilized using buffer containing 12 mM sodium deoxycholate, 12 mM sodium N-dodecanoylsarcosinate, and 100 mM Tris pH 9.0, with EDTA-free Protease Inhibitor Cocktail (Roche, Switzerland). Islets were sonicated for 10 min using a Bioruptor (Cosmo Bio, Japan) on high power with 1-min on/1-min off cycles. Cell debris was removed after centrifugation at 18,000 x g for 20 min at 4°C. Protein concentrations were adjusted to a uniform concentration for a set of samples (0.5-1.0 µg/µL) and between 5-20 µg protein was used for peptide preparation. Cysteine-cysteine disulfide bonds were reduced with 10 mM dithiothreitol at 50° C for 30 min. Free thiol groups were alkylated with 40 mM iodoacetamide in the dark at room temperature for 30 min. Alkylation reactions were quenched with 55 mM cysteine at room temperature for 10 min. Samples were diluted with 2.76 volumes of 50 mM ammonium bicarbonate. Lysyl endopeptidase (Wako, Japan) and trypsin (Promega, USA) were added at a 50:1 ratio of sample protein:enzyme (w/w) and samples were digested for 14 hrs at 37° C. Afterward, 1.77 volumes ethyl acetate were added, and samples were acidified with trifluoroacetic acid (TFA), which was added to 0.46% (v/v). Following centrifugation at 12,000 x g for 5 min at room temperature, samples separated into two phases. The upper organic phase containing sodium deoxycholate was removed, while the lower aqueous phase containing digested tryptic peptides was dried using a centrifugal vacuum concentrator. Digested peptides were dissolved in 300 µL of 0.1% (v/v) TFA in 3% acetonitrile (v/v) and samples were desalted using MonoSpin C_{18} columns (GL Sciences Inc., Japan). Peptides were eluted from C_{18} columns using 0.1% TFA in 50% acetonitrile and dried in a vacuum concentrator. Tryptic peptides were dissolved in 0.1% (v/v) formic acid in 3% (v/v) acetonitrile for MS analysis.

2.2.19 Mass spectrometry measurement

Samples were measured using a Q-Exactive Plus Orbitrap LC-MS/MS System (Thermo Fisher Scientific, USA), equipped with a Nanospray Flex ion source. The same amount of peptide was injected for each sample, which was typically 300-600 ng in a volume of 2 to 5 µL. Peptides were separated on a 3-micrometer particle, 75 micrometer inner diameter, 12 cm filling length C_{18} column (Nikkyo Technos Co., Ltd., Japan). A flow rate of 300 nL/min was used with a two-hr gradient (1% to 34% solvent B in 108 min, 34% to 95% solvent B in 2 min,

with a final wash at 95% solvent B for 10 min, where solvent A was 0.1% (v/v) formic acid in LC/MS grade water and solvent B was 0.1% (v/v) formic acid in 80% (v/v) acetonitrile). The mass spectrometer ion transfer tube temperature was 250° C and 2.0 kV spray voltage was applied during sample measurement.

For data-dependent acquisition (DDA), full MS spectra were acquired from 380 to 1500 m/z at a resolution of 70,000. The AGC target was set to $3e^6$ with a maximum injection time (IT) of 100 ms. MS2 scans were recorded for the top 20 precursors at 17,500 resolution with an AGC of $1e^5$ and a maximum IT of 60 ms. The first mass was fixed at 150 m/z. The default charge state for the MS2 was set to 2. HCD fragmentation was set to normalized collision energy of 27%. The intensity threshold was set to $1.3e^4$, charge states 2–5 were included and the dynamic exclusion was set to 20 s.

For data-independent acquisition (DIA), data were acquired with 1 full MS and 32 overlapping isolation windows constructed covering the precursor mass range of 400-1200 m/z. For full MS, resolution was set to 70,000. The AGC target was set to $5e^6$ and maximum IT was set to 120 ms. DIA segments were acquired at 35,000 resolution with an AGC target of $3e^5$ and an automatic maximum IT. The first mass was fixed at 150 m/z. HCD fragmentation was set to normalized collision energy of 27%.

2.2.20 Protein identification and quantification

Raw files from DDA measurement were searched against the Uniprot mouse database using Proteome Discoverer v2.2 software (Thermo Fisher Scientific, USA). Digestion enzyme specificity was set to Trypsin/P. Precursor and fragment mass tolerance were set to 10 ppm and 0.02 Da, respectively. Modification included carbamidomethylation of cysteine as a fixed modification, with oxidation of methionine and acetyl (protein N-terminus) as variable modifications. Up to 2 missed cleavages were allowed. A decoy database was included to calculate the FDR. Search results were filtered with FDR 0.01 at both peptide and protein levels. The filtered output was used to generate a sample-specific spectral library using Spectronaut software (Biognosys, Switzerland). Raw files from DIA measurements were used for quantification data exaction with the generated spectral library. FDR was estimated with the mProphet approach (Reiter et al., 2011) and set to 0.01 at both peptide precursor level and protein level (Rosenberger et al., 2017). Data were filtered with FDR < 0.01 in at least half of the samples.

2.2.21 RNA immunoprecipitation

RNA immunoprecipitation (RIP) was done on MIN6 cells using anti-CNOT3 antibody (generated by immunizing mice in cooperation with Bio Matrix Research Incorporation). MIN6 cells 80% confluent in 10-cm dishes were lysed with 1mL TNE buffer per dish. MIN6 cell lysates were then incubated with 1μg of either anti-CNOT3 or control IgG antibody in an upside-down tumbling manner for 1 hr at 4° C, and then incubated with 40 μL of protein G Dynabeads (Invitrogen) in an upside-down tumbling manner for 2 hrs at 4° C. Later, beads were separated using a magnetic rack and washed 5 times with TNE buffer. RNAs in immune complexes were isolated using Isogen II, and cDNA was generated with SuperScript Reverse Transcriptase III followed by qPCR. The abundance of each mRNA is quantified as % of input mRNA then mRNA bound to anti-CNOT3 antibody was presented as fold change (FC) relative to mRNA bound to control IgG antibody.

2.2.22 Preparation of Bait RNA and analysis of RBPs

Total RNA was extracted from MIN6 cells as described above followed by reverse transcriptase reaction into cDNA. PCR reactions using Phusion high-fidelity DNA polymerase (New England Biolabs) were carried out to amplify mouse 3'UTRs of *Slc16a1, Ldha, Wnt5b*, and *Abtb2* using cDNA as a template. Primers used for 3'UTR amplification are listed in Table 9. PCR products were then ethanol precipitated and digested with *Xba1* restriction enzyme. Afterward, 3'UTRs were inserted into the pGL3 control vector (Promega). 3'UTR sequences were verified by DNA sequencing. FLAG-tagged 3'UTRs bait RNA were generated by Dr. Shungo Adachi as described previously (Adachi and Natsume, 2015).

For the identification of *Slc16a1*, *Ldha, Wnt5b*, and *Abtb2* 3′-UTRs binding proteins, lysates from MIN6 cells were incubated with 10 pmol FLAG-tagged 3′-UTRs bait RNA for 1 hr at 4° C in an upside-down tumbling manner and then incubated with anti-FLAG M2 antibody (Sigma, F1804) and Dynabeads (Invitrogen) for 2 hrs at 4° C in an upside-down tumbling manner. The bait RNA-protein complexes were eluted by FLAG-peptide elution. Dyna beads were incubated with 20 μL FLAG-peptide (1 mg/mL) for 30 min at room temperature with shaking every 10 min. Finally, bait RBPs were analyzed by immunoblot analysis as described in **section 2.2.6**.

For validating CNOT3 direct interaction with plausible RBPs, FLAG-tagged CNOT3 construct was inserted into pcDNA vector and used for transfecting MIN6 using TransIT-LT1 transfection reagent (Takara). Two days after transfection, cell lysates were prepared. 10% of each lysate was used for immunoblot analysis (Lysates). The rest of each lysate was treated with RNase (1µg/mL) and incubated with anti-FLAG M2 antibody (Sigma, F1804) and Dynabeads (Invitrogen) for 2 hrs at 4° C in an upside-down tumbling manner. Protein complexes were eluted by boiling in 1x sample buffer, and bait RBPs were analyzed by immunoblot analysis as described in **section 2.2.6**.

2.2.23 Statistical Methods

Differences between groups were examined for statistical significance using Student's t-test (two-tailed distribution with two-sample equal variance). Analyses were performed using GraphPad Prism (GraphPad Software v.8.0), RStudio (v.1.1.453) and GSEA (v.4.0.1) developed by Broad Institute (http://software.broadinstitute.org/gsea/index.jsp). *P* value of <0.05 was considered statistically significant.

2.3   Results

2.3.1   Expression of CCR4–NOT complex subunits is deregulated in pancreatic islets in diabetes and obesity

I first asked whether CCR4–NOT complex subunit expression is altered in the diabetic state. Accordingly, I isolated islets from the *db*/*db* mouse model, which lacks the leptin receptor and develops severe obesity associated with diabetes resembling human T2D (Burke et al., 2017; Kobayashi et al., 2000). Immunoblot analysis revealed a decrease in CCR4–NOT subunits CNOT1, CNOT2 and CNOT3 (Figure 2.1a), suggesting impaired deadenylase activity of the CCR4–NOT complex in diabetic islets. I also observed increased expression of CNOT8, one of the deadenylase subunits. To determine whether CCR4–NOT is a possible early effector in the pathogenesis of diabetes, I examined the expression of CCR4–NOT complex subunits in the prediabetic state as well using mice fed on HFD for three months starting at 8 weeks of age and examined at 20 weeks of age. Compared to *db/db* mice, none of the CCR4-NOT complex subunits showed deregulated expression except for CNOT8 that increased by HFD (Figure 2.1b). To find out whether this effect on CCR4–NOT complex subunits was the result of gluco-/lipo-toxicity, I analyzed CCR4–NOT subunit expression in MIN6 cells after chronic exposure

(1 week) to high glucose (50 mM) with or without palmitic acid (0.5 mM). Consistent with the observations in HFD-fed mice, only CNOT8 expression increased with palmitic acid treatment. On the other hand, glucotoxic stress didn't show any obvious effect (Figure 2.1c).
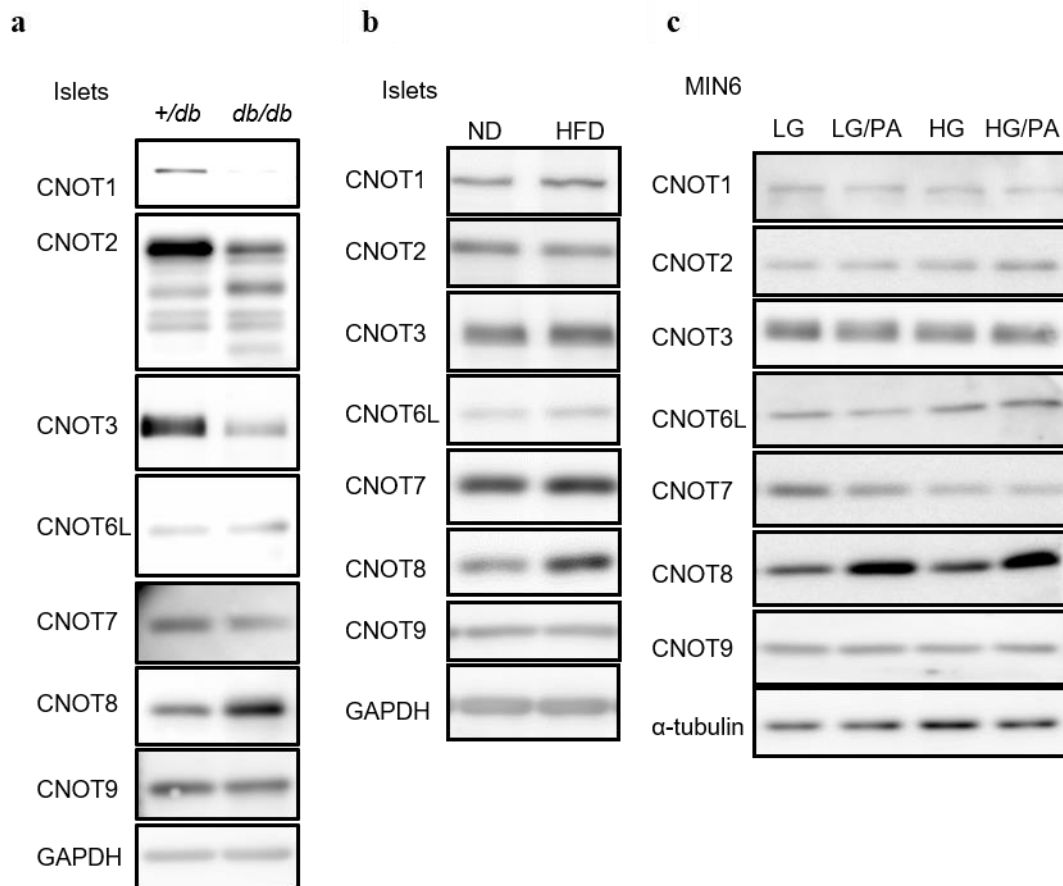
Figure 2.1 Deregulation of CCR4–NOT complex in models of diabetes and obesity
(**a-c**) Immunoblot analysis of CCR4–NOT complex subunits in: (**a**) islet lysates from 16-week-old +/*db* control and *db/db* mice (n=3). (**b**) islet lysates from 20-week-old normal diet (ND) and high-fat diet (HFD) fed mice (n=3). (**c**) MIN6 cells under low/high glucose conditions (LG/HG) with or without palmitic acid (PA) treatment. This HG/PA treatment experiment is a representative of three independent experiments.

2.3.2   Loss of CNOT3 in β cells is associated with impaired CCR4–NOT complex deadenylase activity

In the light of the above findings I sought to investigate the roles of the CCR4–NOT complex in pancreatic β cells, thus I generated *Cnot3*βKO mouse model lacking the *Cnot3* gene in β cells. Successful suppression of CNOT3 in β cells was confirmed by immunoblot analysis and immunofluorescence (Figure 2.2a, b). Consistent with CNOT3 suppression effect on other

CCR4-NOT complex subunits in other tissues (Inoue et al., 2015; Suzuki et al., 2015; Yamaguchi et al., 2018), the abundance of other CCR4-NOT subunits decreased in *Cnot3*βKO islets (Figure 2.2a). Moreover, bulk poly(A) tail analysis showed that the population of poly(A) tail length with longer than 50 nucleotides increased in *Cnot3*βKO islets compared with controls (Figure 2.2c, d), indicating impairment of deadenylase activity.
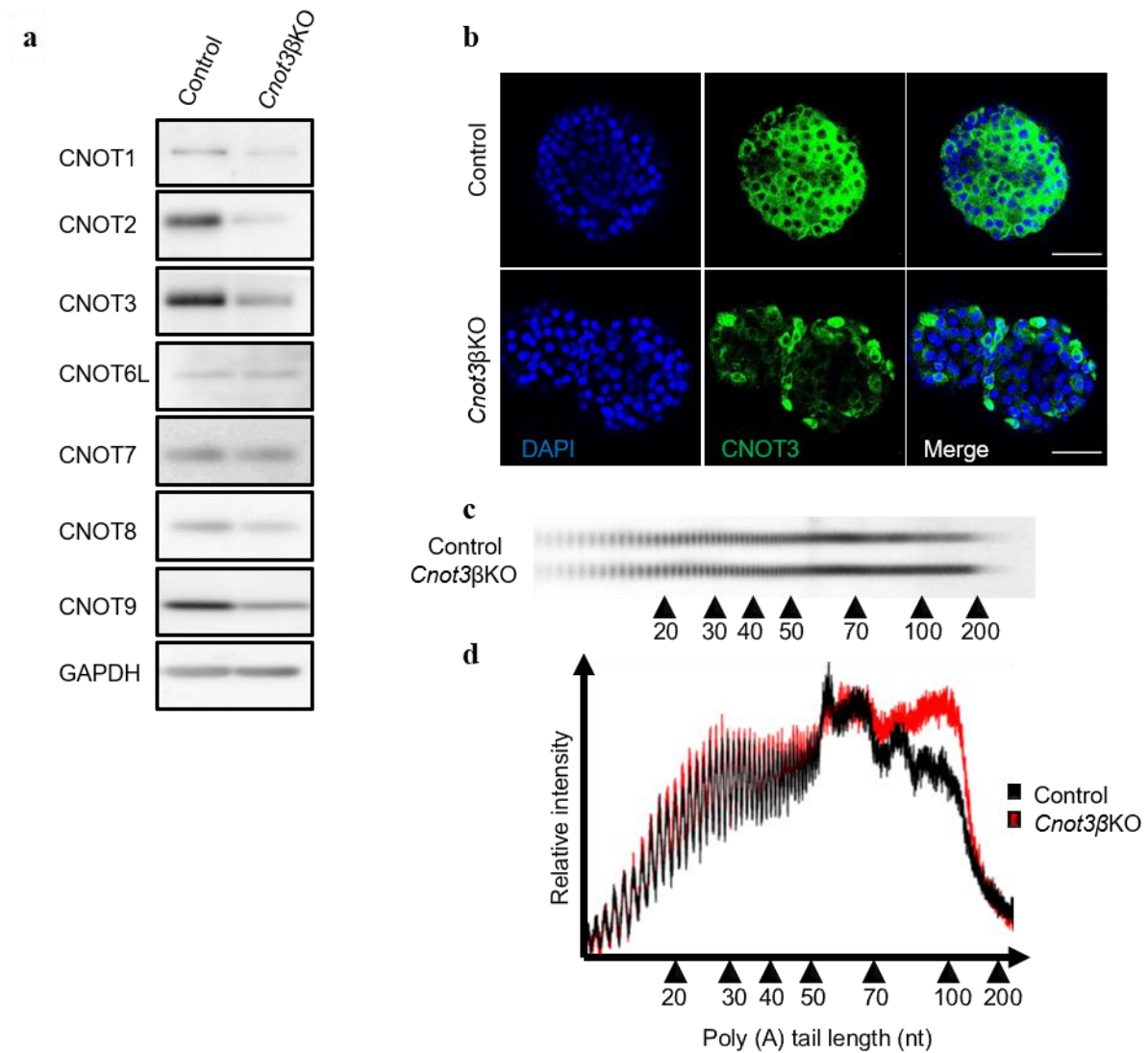
Figure 2.2 Disruption of CCR4–NOT complex deadenylase activity by loss of CNOT3
(**a**) Immunoblot analysis showing decreased CNOT3 in islet lysates from 8-week-old *Cnot3*βKO compared with control mice (n=3). (**b**) Immunofluorescence staining showing CNOT3 (green) suppression as well as its cytosolic localization in islets from 8-week-old *Cnot3*βKO compared with control mice (n=2), DAPI (blue). (**c**) Poly(A) tail lengths of bulk RNA in *Cnot3*βKO compared with control islets (each sample is pooled from 4 mice).

Figure 2.2 (continued). (**d**) Densitograms of poly(A) tail lengths. Bulk poly (A) assay was conducted by Dr. Akiko Yanagiya.

2.3.3   Loss of CNOT3 in β cells causes impaired glucose tolerance and insulin secretion

To determine whether CNOT3 depletion affects β cell function, I first conducted glucose tolerance tests on 4-, 8- and 12-week-old mice to compare glucose metabolism between control and *Cnot3*βKO mice. At 4 weeks of age, *Cnot3*βKO mice showed glucose tolerance and fasting blood glucose levels comparable to those of control mice (Figure 2.3a). While fasting blood glucose levels were still similar between 8-week-old control and *Cnot3*βKO mice, *Cnot3*βKO mice showed impaired glucose tolerance (Figure 2.3b). By 12 weeks of age, *Cnot3*βKO mice developed overt diabetes indicated by significant elevation of fasting blood glucose levels and failure of glucose decrease after the injection (Figure 2.3c). With development of overt diabetes, 12-week-old *Cnot3*βKO mice displayed a general deterioration of their health condition and clinical signs of diabetes, including polyuria, polydipsia (data not shown) and weight loss (Figure 2.3d). These results suggest that the metabolic impairment worsened with age supporting progressive loss of β cell function in *Cnot3*βKO mice. Indeed, blood glucose levels in 8-week-old *Cnot3*βKO mice were significantly elevated above those of control mice under normal feeding conditions (Figure 2.3e).
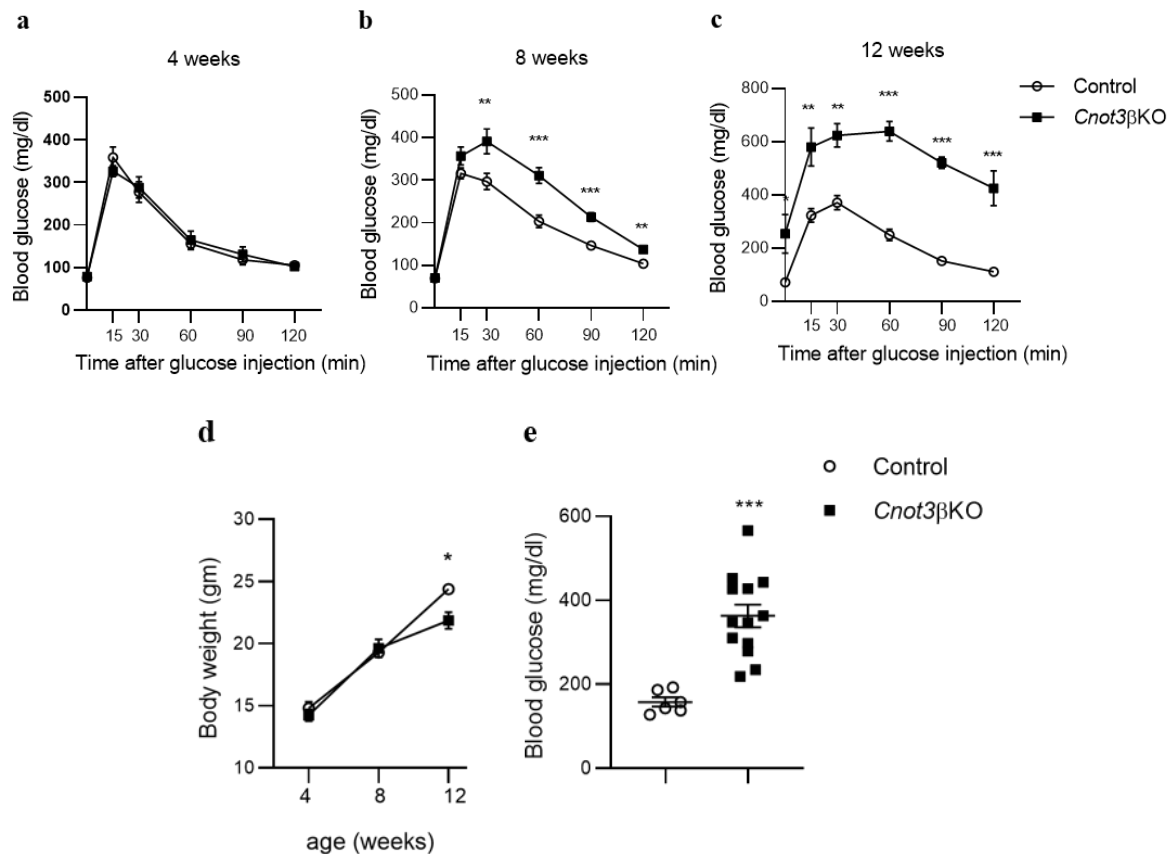
Figure 2.3 Loss of CNOT3 in β cells causes impaired glucose tolerance

(**a-c**) Intraperitoneal glucose tolerance tests in: (**a**) 4-, (**b**) 8- and (**c**) 12- week-old control and *Cnot3*βKO male mice (n=6-9). (**d**) Body weight comparisons between control and *Cnot3*βKO male mice at 4-, 8- and 12- weeks of age (n=6-9). (**e**) Blood glucose measurements of 8-week-old control (n=6) and *Cnot3*βKO (n=13) male mice fed ad-libitum. Data are presented as mean ± standard error of the mean (S.E.M); * $P < 0.05$; ** $P < 0.01$; *** $P < 0.001$

Furthermore, I measured fasting serum insulin levels and serum insulin levels after glucose administration in 8-week-old mice. There was no significant difference in fasting serum insulin levels between *Cnot3*βKO mice and control littermates. Yet, *Cnot3*βKO mice had a significantly lower serum insulin levels measured 15 min after glucose bolus administration compared with control littermates (Figure 2.4a). To evaluate β cell function, I assessed GSIS by islets isolated from 8-week-old *Cnot3*βKO mice and control littermates. *Cnot3*βKO islets displayed normal insulin secretion at low (3 mM) glucose but significantly decreased insulin secretion upon stimulation with high (17 mM) glucose compared with control islets (Figure 2.4b). This provides evidence for a functional impairment of *Cnot3*βKO islets. This *ex vivo* assay result also agrees with the observed normal fasting serum insulin levels in

*Cnot3*βKO mice and decreased serum insulin after *in vivo* glucose stimulation (shown in Figure 2.4a).
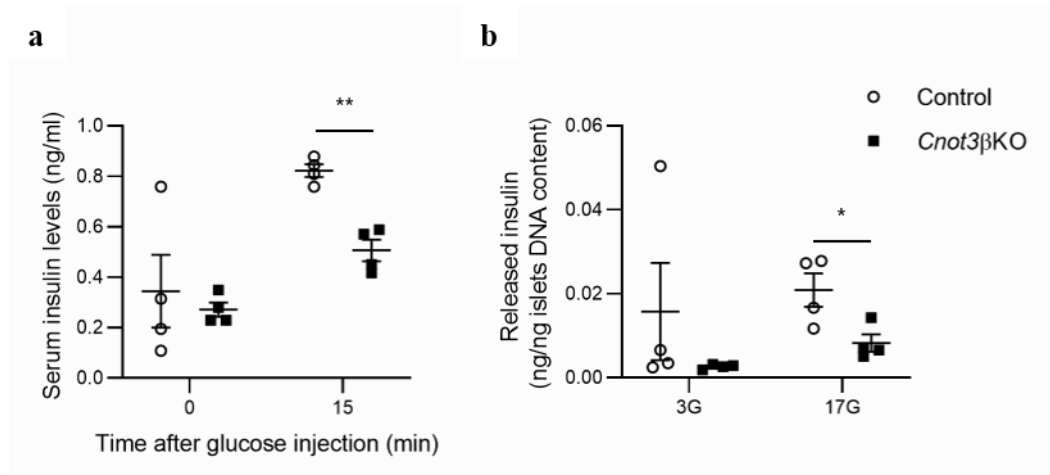
Figure 2.4 Loss of CNOT3 in β cells causes decreased GSIS

(**a**) Serum insulin measured in 8-week-old control and *Cnot3*βKO male mice after 16 hrs fasting (0 min) and 15 min after injection of 2g/kg glucose (n=4). (**b**) Insulin released by islets from 8-week-old control and *Cnot3*βKO male mice in response to low 3mM glucose (3G) and high 17 mM glucose (17G) stimulation of 1 hr. This experiment is a representative of three independent experiments using three different biological replicates (n=3).

Morphological evaluation of islets from 8-week-old *Cnot3*βKO mouse by H&E staining revealed pale nuclear staining with many islets showing abnormal shapes. At 12 weeks of age, almost all *Cnot3*βKO islets displayed abnormal shapes and neovascularization. At 20 weeks of age, *Cnot3*βKO islets were hardly detected and the number of cells in individual islets was markedly reduced in a manner similar to that observed in diabetic Goto-Kakizaki rats (Momose et al., 2006) (Figure 2.5).
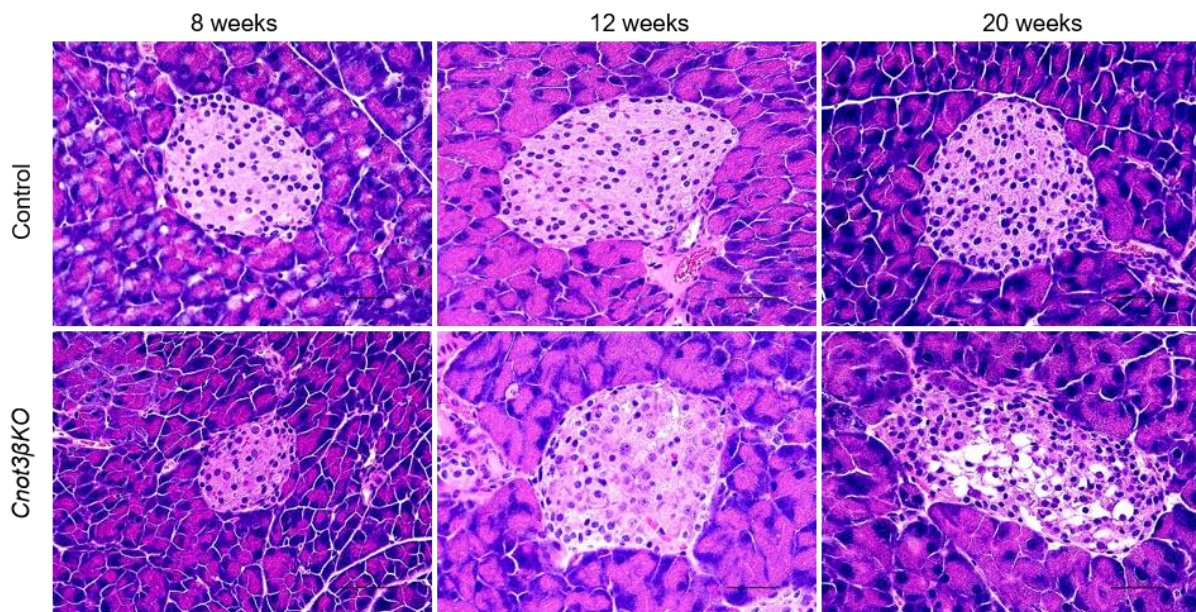
Figure 2.5 *Cnot3*βKO islets display abnormal morphology resembling diabetic islets

H&E-stained pancreatic sections from 8-, 12- and 20-week-old control and *Cnot3*βKO mice.

2.3.4   *Cnot3*βKO mice display reduced numbers of insulin-producing cells

β cell-specific depletion of *Cnot3* led to a significant reduction of the expression of murine insulin gene isoforms (*Ins1* and *Ins2*) as shown in Figure 2.6a. Immunofluorescent staining of pancreatic sections revealed a loss of insulin expression in many β cells in *Cnot3*βKO islets (Figure 2.6b). This was associated with a significant reduction in insulin content in *Cnot3*βKO islets compared with control islets (Figure 2.6c). As expected, on quantifying β cell mass, there was a significant reduction in β cell mass by nearly 50% in *Cnot3*βKO mice (Figure 2.6d). This was not associated with a significant difference in islet number in *Cnot3*βKO mice compared with control mice (Figure 2.6e), but rather with the presence of smaller islets.
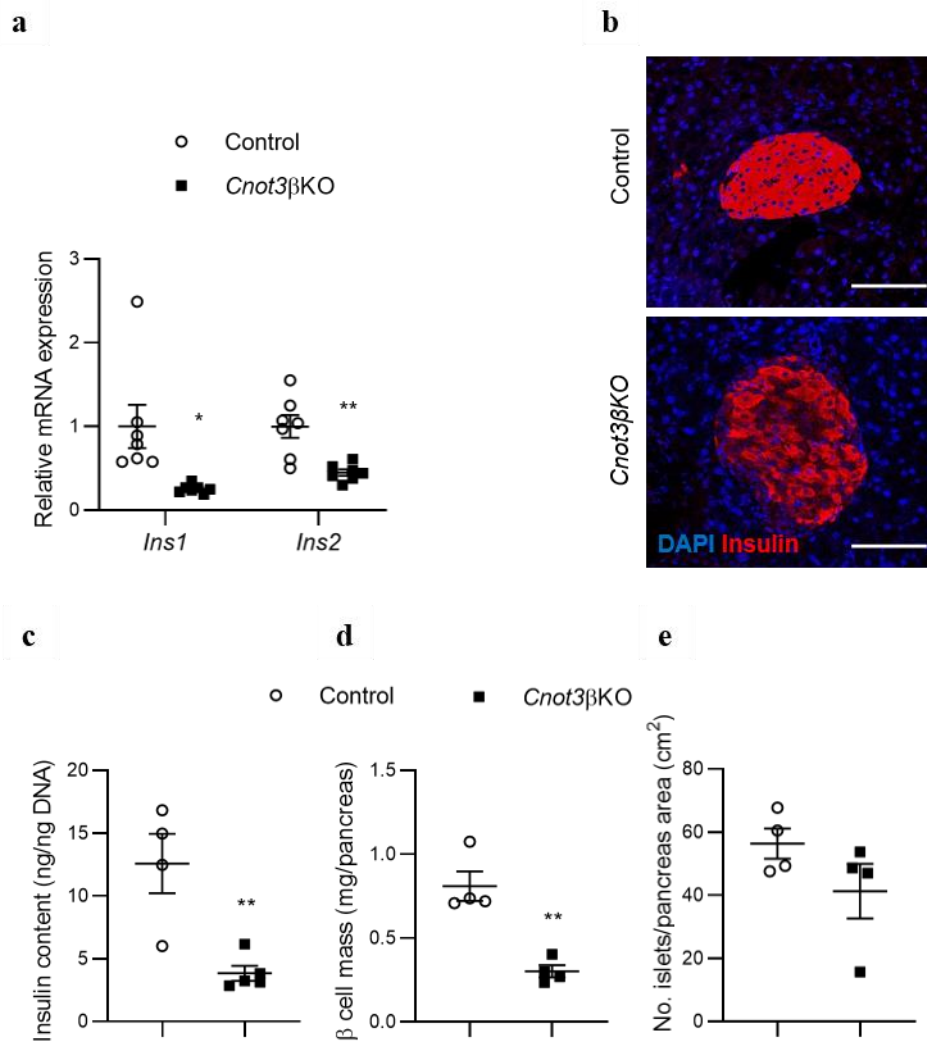
Figure 2.6 Lack of CNOT3 in β cells causes decreased insulin expression

(**a**) qPCR analysis of insulin mRNA isoforms (*Ins1* and *Ins2*), normalized to the *Gapdh* mRNA level, in control and *Cnot3*βKO islets. (**b**) Immunofluorescence staining of insulin (red) and DAPI (blue) in pancreatic sections from 8-week-old control and *Cnot3*βKO male mice (n=4). (**c**) Insulin content of islets from 8-week-old control and *Cnot3*βKO mice (n=3). (**d**) β cell mass measurement in pancreatic sections from 8-week-old control and *Cnot3*βKO male mice (n=4). (**e**) Islet number per pancreas area in pancreatic sections from 8-week-old control and *Cnot3*βKO mice (n=4). Data are presented as mean ± S.E.M; * $P < 0.05$; ** $P < 0.01$; *** $P < 0.001$

These findings prompted me to determine whether decreased pancreatic insulin content and reduced β cell mass were driven by increased β cell death. I examined β cell apoptosis by TUNEL assay. *Cnot3*βKO islets did not show extensive TUNEL staining compared with control islets, even though I observed few TUNEL-positive islet cells in *Cnot3*βKO mice,

suggesting that CNOT3 depletion compromises β cell viability to some extent (Figure 2.7a). Subsequent experiments focused on the majority of β cells that survived *Cnot3* depletion, but lacked insulin expression.

In order to trace *Cnot3* depletion in β cells, I used an *Ins1-Cre mTmG* reporter mouse model in which the successfully recombined cells show green fluorescence from the expression of membrane- localized EGFP (mG) whereas unrecombined cells show red fluorescence of membrane- localized tdTomato (mT). Paraformaldehyde fixation masks mTmG fluorescence, so in order to trace successfully recombined cells I did immunofluorescence staining of EGFP. Immunofluorescence staining of insulin and EGFP in control mice expressing Cre recombinase (Control; *+/Ins1-Cre*) revealed successful labeling of β cells with EGFP. In 8-week-old *Cnot3*βKO islets, many EGFP-positive cells were insulin-negative and did not stain with anti-GLUC, anti-SST and anti-PPT antibodies, indicating that β cells did not transform into other types of islet cells (Figure 2.7b). Furthermore, EGFP-positive cells in *Cnot3*βKO islets stained for the pan-endocrine marker, Synaptophysin (SYP), indicating that these hormone-negative cells are viable and retain their endocrine phenotype (Figure 2.7c).

a

Control; Positive control   Control; Negative control   Control   *Cnot3βKO*

b

c
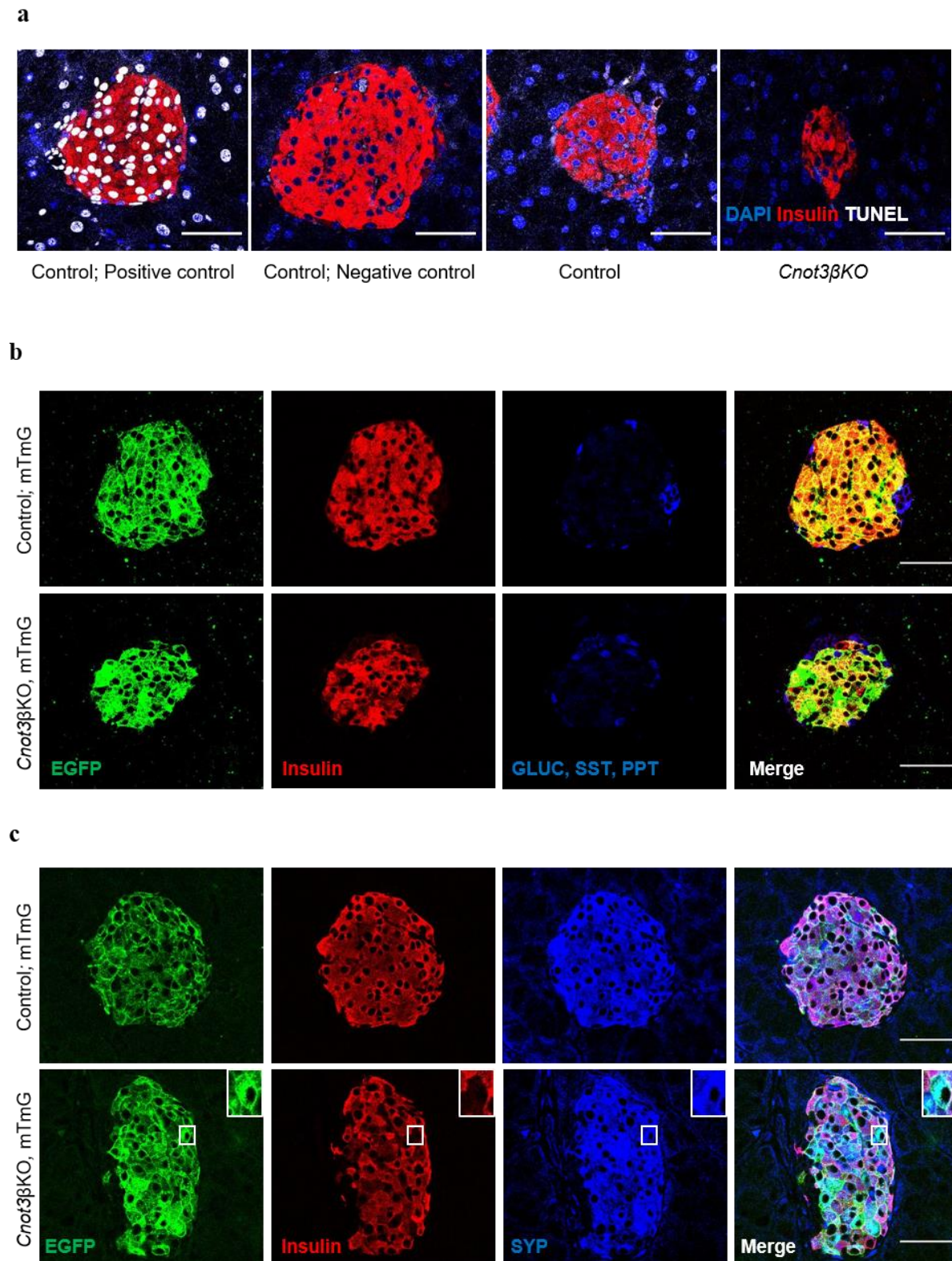
Figure 2.7 Reduced β cell mass was not driven by β cell death

(**a**) TUNEL assay performed on pancreatic sections from 8-week-old control and *Cnot3*βKO male mice, DAPI (blue), Insulin (red) and TUNEL (white).

Figure 2.7 (continued). (**b**) Co-immunofluorescence staining of EGFP (green), insulin (red), GLUC (blue), SST (blue) and PPT (blue) in pancreatic sections from 8-week-old *mTmG* reporter: "control (*Cnot3*^{+,+};*+/Ins1-Cre*) and *Cnot3*βKO" mice. (**c**) Co-immunofluorescence staining of EGFP (green), insulin (red) and SYP (blue) in pancreatic sections from 8-week-old *mTmG* reporter: "control (*Cnot3*^{+,+}; *+/Ins1-Cre*) and *Cnot3*βKO" mice.

2.3.5   CNOT3 KO affects insulin granule formation

I further examined *Cnot3*βKO islets by TEM to detect any ultrastructural alterations in β cells. Control islets possessed β cells with typical insulin granules, bearing characteristic electron-dense crystal cores, and with β cell-β cell contacts displaying tight junctions essential for normal insulin secretion (Benninger and Piston, 2014). In contrast, β cells from *Cnot3*βKO islets were rather heterogeneous in appearance, with few having typical insulin granules. Many were degranulated with few, or abnormally small, insulin granules. Also observed in *Cnot3*βKO islets were β cells in which insulin granules were atypically rod-shaped, or with irregular plasma membranes (Figure 2.8a-d). Of note, despite observed ultrastructural changes, these β cells were viable (as evident from TUNEL assay results, see Figure 2.7a) and maintained their expression of SYP (Figure 2.7c). The above findings suggest that diabetes in *Cnot3*βKO mice is caused by both lack of β cell functional identity and, possibly, failure to attain a fully differentiated state.
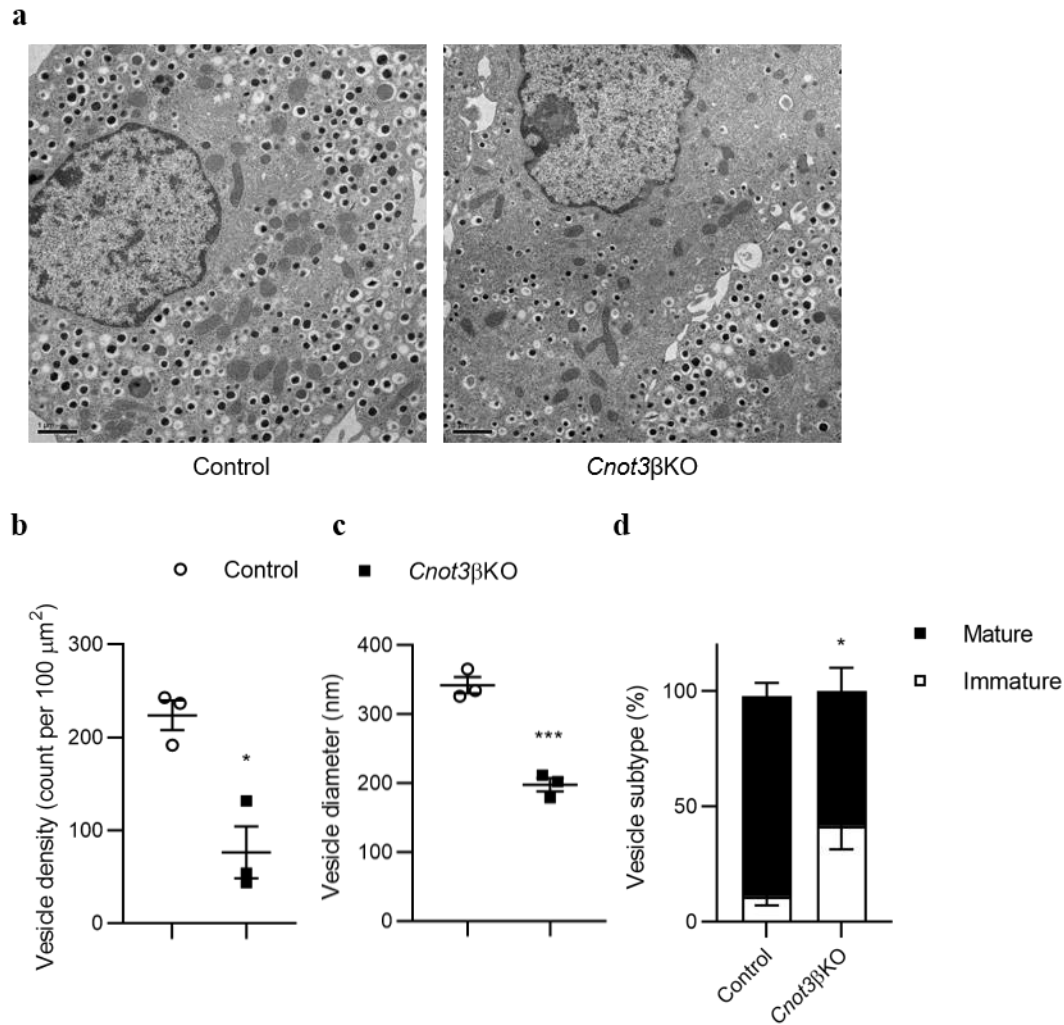
Figure 2.8 Lack of CNOT3 causes ultrastructural changes in β cells relevant to reduced GSIS

(**a-c**) Transmission electron microscopy performed on islets isolated from 8-week-old control and *Cnot3*βKO mice (n=3), including quantification of (**b**) vesicle density, (**c**) vesicle diameter and (**d**) the percentage of mature (black bar) and immature vesicles (white bar). Data are presented as mean ± S.E.M; * $P < 0.05$; ** $P < 0.01$; *** $P < 0.001$.

2.3.6   CNOT3 is essential for β cell maturation and identity

Considering the above observations, my next goal was to investigate dedifferentiation as a possible factor contributing to reduced functional β cell mass. Therefore, I performed qPCR to measure expression of dedifferentiation/progenitor cell markers. I observed significant upregulation of β cell dedifferentiation/progenitor cell markers including *Ngn3, Aldh1a3, Myt1, Dcx* and *Tnfrsf11b* (Figure 2.9a). ALDH1A3 was recently recognized as a

marker of β cell dedifferentiation in diabetes (Cinti et al., 2016; Kim-Muller et al., 2016). Immunoblot analysis of ALDH1A3 revealed its significant upregulation in islets isolated from *Cnot3*βKO mice compared with control islets (Fig. 2.9b, c). This suggests that β cells in *Cnot3*βKO mice exhibits progenitor-like state.
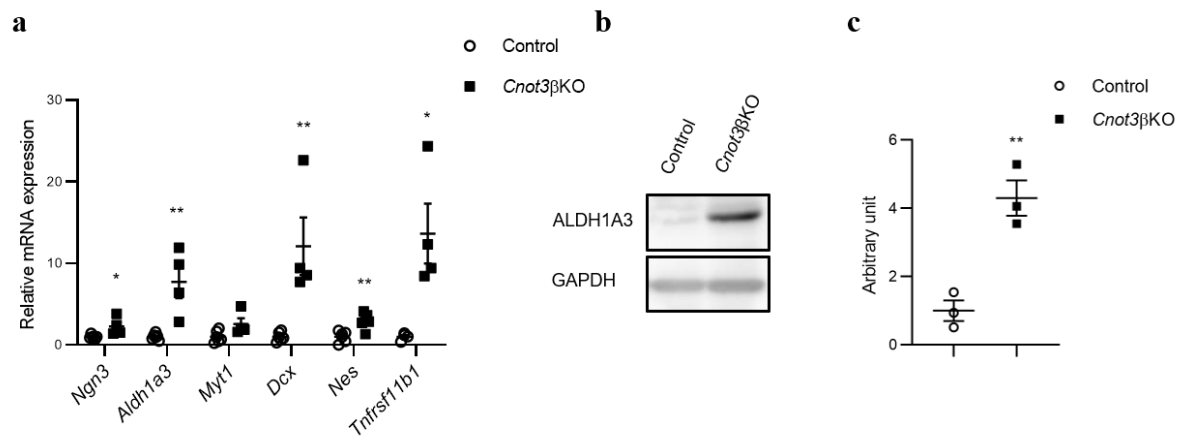
Figure 2.9 *Cnot3*βKO islets display increased expression of progenitor/ dedifferentiation markers

(**a**) qPCR analysis of progenitor cells/dedifferentiation markers, normalized to the *Gapdh* mRNA level, in control and *Cnot3*βKO islets (n=4-6). (**b**) Immunoblot analysis of ALDH1A3 in islet lysates from 8-week-old control and *Cnot3*βKO mice. (**c**) Band quantification of immunoblots of ALDH1A3 (n=3).

In addition, I checked the expression of a number of genes critical for β cell function. Among the transcription factors important for β cell function and insulin transcription tested (*Mafa, Nkx2.2, Nkx6.1, NeuroD1* and *Pdx1*), only *Mafa* mRNA was significantly reduced (Figure 2.10a). *Mafa,* is a key β cell transcription factor and a driver of β cell maturation (Nishimura et al., 2015), that was reduced at the protein level as well (Figure 2.10e). In line with decreased GSIS, MS analysis revealed significant reductions in proteins involved in glucose sensing, insulin secretory granule maturation and insulin secretion (Table 2). Some of the affected proteins did not manifest altered mRNA levels or decreased but not significantly at the mRNA level (Figure 2.10a-d). I observed decreased expression of GLUT2 "encoded by *Slc2a2* gene" in *Cnot3*βKO pancreata (Figure 2.10f). In support of defective maturation of CNOT3-depleted β cells, I found that *Ucn3*, a marker of β cell maturation, that is also reported to be important in GSIS (van der Meulen and Huising, 2014), was unchanged at the mRNA level yet was strongly decreased at the protein level (Figure 2.10d, Table 2). Moreover,

*Cnot3*βKO mice displayed a post-transcriptional defect in insulin biosynthesis where *Cnot3*βKO islets displayed a significant decrease in the expression of genes encoding proteins involved in insulin biosynthesis, such as T2D-associated zinc transporter *Slc30a8*, proinsulin-to-insulin convertase (*Pcsk2*) "encoding PC1" and *Cpe* (Bellomo et al., 2011; Zito et al., 2010) (Figure 2.10c, d, Table 2). These proteins have established roles in insulin processing and/or maturation of insulin secretory granules. These data reveal loss of β cell maturation markers, defects in insulin granule formation and insulin biosynthesis.
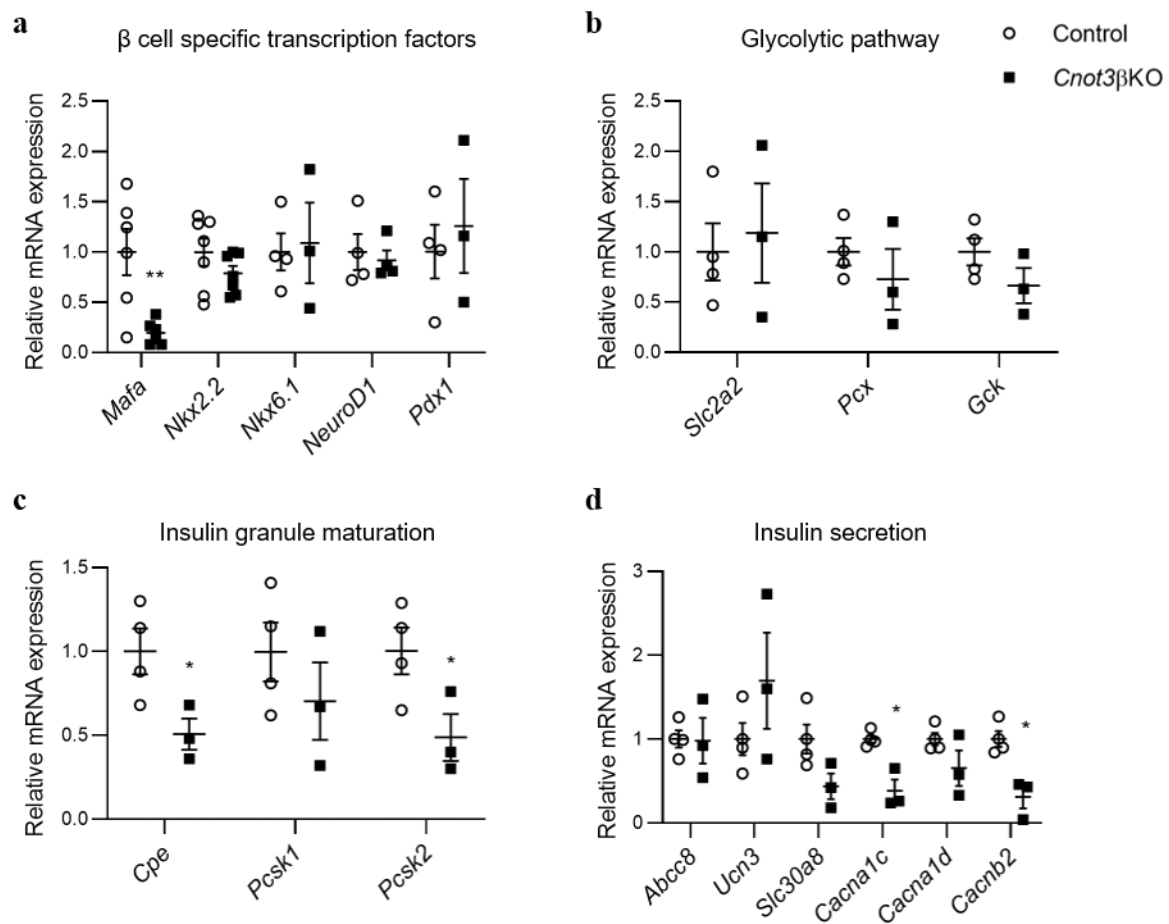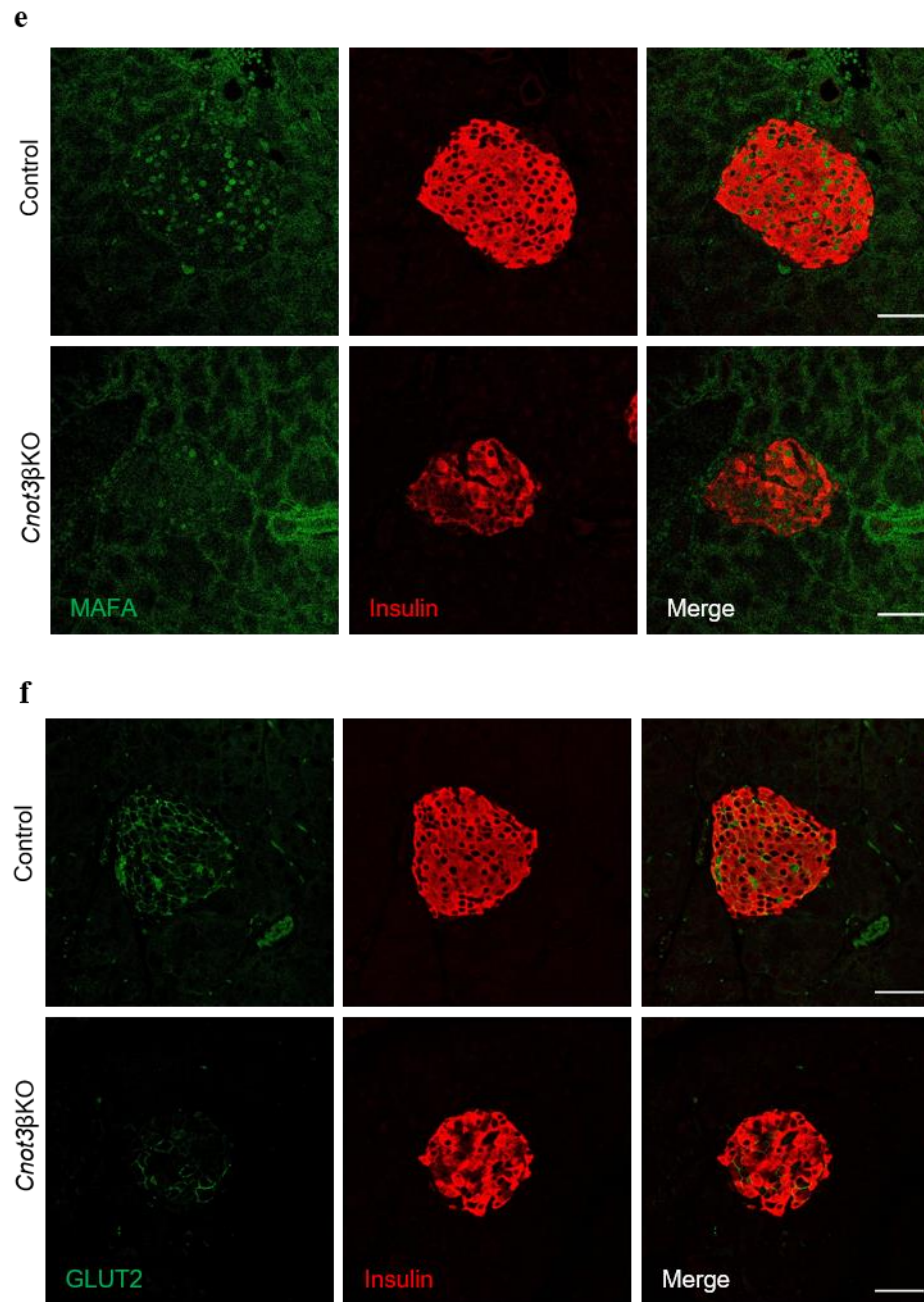
Figure 2.10 *Cnot3* KO causes reduced expression of β cell-specific genes

(**a-d**) qPCR analysis of β cell-specific functional mRNAs expression categorized as: (**a**) β cell-specific transcription factors, (**b**) glycolytic pathway, (**c**) insulin granules maturation and (**d**) insulin secretion mRNAs, normalized to the *Gapdh* mRNA level, in control and *Cnot3*βKO islets (n= 4-7). (**e-f**) Co-immunofluorescence staining of: (**e**) MAFA (green) and insulin (red), (**f**) GLUT2 (green) and insulin (red) in pancreatic sections from 8-week-old control and *Cnot3*βKO male mice (n=4).

In normal mature β cells, insulin secretion is regulated by coupling of glucose metabolism to insulin secretion (Prentki et al., 2013). Glucose first enters the β cell, undergoes glycolysis which is coupled to mitochondrial metabolism that increases the ATP/ADP ratio closing the potassium channels and opening the calcium channels that ultimately allows calcium influx and consequently insulin secretion (Rutter et al., 2015). Multiple genes involved in glycolysis are upregulated in diabetes and interfere with the normal insulin secretion (Haythorne et al., 2019). This prompted me to investigate mRNAs encoding glycolytic enzymes (*Ldha*, *Hk1* and *Hk2*) alongside other mRNAs that are normally selectively repressed in mature β cells (*Slc16a1/Mct1*, *Rest* and *Pdgfra*) and loss of whose repression may result in impaired β cell function (Pullen et al., 2012). I observed significant upregulation of *Slc16a1* and *Ldha*, which belong to the β cell disallowed genes. *Hk1*, *Hk2*, *Rest* and *Pdgfra* were upregulated but the increases were not statistically significant (Figure 2.11a). I confirmed the upregulation of *Slc16a1* protein (MCT1), LDHA and HK1 at the protein level as well (Figure 2.11b, c, Table 2). These data support a metabolic phenotype resembling that of immature/fetal β cells.
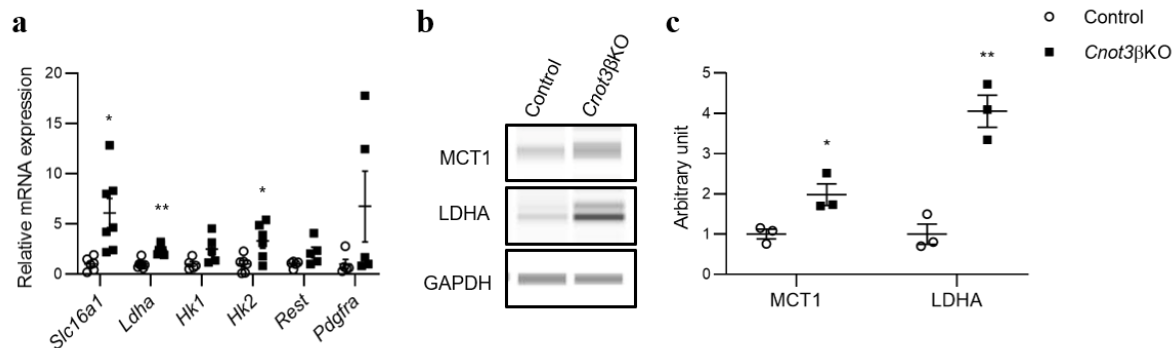
Figure 2.11 *Cnot3*βKO islets display increased expression of immature β cell markers (**a**) qPCR analysis of immature β cell markers, normalized to the *Gapdh* mRNA level, in control and *Cnot3*βKO islets (n=5-7). (**b**) Immunoblot analysis of MCT1 and LDHA in islet lysates from 8-week-old control and *Cnot3*βKO mice. (**c**) Band quantification of immunoblot of MCT1 and LDHA (n=3). Data are presented as mean ± S.E.M; * $P < 0.05$; ** $P < 0.01$; *** $P < 0.001$

Table 2: Categories of proteins affected by Cnot3 KO in β cells obtained from MS analysis of Cnot3βKO islets

Category	Protein symbol
Glycolysis	GCK (FC=1, P=0.4), G6PC2 (FC=1.6, P=0.13)
Glucose sensing and Insulin secretion	**GLUT2** (FC=0.4, P=0.1), **GLP1R** (FC=0.58, P=0.0007), **UCN3** (FC=0.4, P=0.02)
Insulin granule feature	**VAMP2** (FC=0.6, P=0.01), **SLC30A8** (FC=0.4, P=0.049), SYTL4 (FC=0.9, P=0.4), **PC1** (FC=0.48, P=0.09), **PC2** (FC=0.58, P=0.007), **CPE** (FC=0.3, P=0.002)
Immature/ β cell disallowed	**ACOT7** (FC=1.55, P=0.1), **HK1** (FC=2, P=0.003), **ALDOC** (FC=3.1, P=0.02), **LDHA** (FC=1.89, P=0.04) Affected β cell markers are in bold

MS analysis is done by Dr. Yibo Wu

2.3.7   Transcriptome- and proteome-wide changes in *Cnot3*βKO islets

To understand how loss of *Cnot3* affects global gene expression in β cells, I performed RNA-seq of control and *Cnot3*βKO islets (three replicates; each replicate comprised islets pooled from two mice). Comparison of gene expression profiles between control and *Cnot3*βKO islets revealed 3,847 differentially expressed (DE) genes (adjusted *P*< 0.05), of which 2,234 genes were upregulated and 1,613 genes were down regulated (Figure 2.12a). To define the biological processes affected by *Cnot3* depletion, I performed GO analysis of the DE genes using the DAVID gene annotation tool (Huang et al., 2008; Sherman et al., 2008) (Figure 2.12b). Consistent with the diabetic phenotype, GO analysis showed that genes upregulated after *Cnot3* depletion are highly enriched for those involved in: "immune system process", "lipid metabolic processes" and "oxidation/reduction processes", while down regulated genes are highly enriched for those that are involved in regulation of insulin secretion and vesicle-mediated transport.

To gain more insight into the effect of *Cnot3* depletion on the pattern of gene expression in β cells, I applied a stricter threshold by comparing the number of significantly upregulated to down regulated genes that were differentially expressed by more than 2-fold. In line with the molecular function of CNOT3 as a positive modulator of CCR4-NOT complex function in

mRNA decay, most of the differentially expressed genes by more than 2-fold were upregulated (Figure 2.12c).

I next examined whether changes in transcriptome are reflected on proteome of *Cnot3*βKO islets. I compared RNA-seq to MS data from *Cnot3*βKO islets. There was a significant strong correlation between DE genes and proteins in *Cnot3*βKO islets ($R^2 = 0.64$, $P < 2.2e^{-16}$) suggesting that most changes in the transcriptome are mirrored in the proteome (Figure 2.12d).

Steady-state mRNA abundance is mainly determined by rates of RNA transcription and decay. Measuring the mRNA decay rate usually involves performing a time series analysis of mRNA abundance following blockade of transcription by certain chemicals, for example Act. D, or by monitoring the abundance of labeled mRNA using high-throughput pulse-chase methods (Chen et al., 2008). These methods work well for cultured cells but cannot easily be used for measuring mRNA decay rate in tissue samples. Thus, I used transcriptomic data to infer mRNA stability in *Cnot3*βKO islets. While exonic read counts in RNA-seq data correspond to steady-state mRNA abundance, changes in abundance of intronic reads can be used to estimate changes in transcription rate. In this way I was able to infer global mRNA stability from RNA-seq data. I estimated the change in mRNA half-life as the difference of the logarithm of the FC in exonic reads and the logarithm of the FC in intronic reads (Δexon-Δintron) (Gaidatzis et al., 2015). The fact that CNOT3 is involved in mRNA deadenylation and subsequently mRNA decay led me to consider a transcript to be a target of CNOT3 if that transcript was upregulated and stabilized as inferred from RNA-seq data. I found that 80% (254 of 317 mRNAs) of stabilized mRNAs that show differential Δexon-Δintron between *Cnot3*βKO and control islets were among the differentially upregulated mRNAs, suggesting that mRNA stabilization effectively contributed to upregulation of mRNAs in *Cnot3*βKO islets (Figure 2.12e). I compared upregulated stabilized genes in *Cnot3*βKO islets to published RNA-seq data from *db/db* islets (Neelankal John et al., 2018) and found 73 upregulated stabilized genes to be upregulated in *db/db* islets suggesting that CNOT3 is involved in suppressing diabetes-related genes.

Interestingly, transcriptome analysis revealed Aldolase B gene (*Aldob*) to be the most upregulated (almost 1000-fold) of the stabilized genes. *Aldob* is a glycolytic enzyme that is normally silenced in mature β cells (Dhawan et al., 2015; Ni et al., 2017). It was dramatically upregulated at both mRNA and protein levels (Figure 2.12f-h). In addition, the fructose/glucose

transporter, *Slc5a10,* and *Wnt5b* were among the most stabilized genes, and they were upregulated (Figure 2.12f).
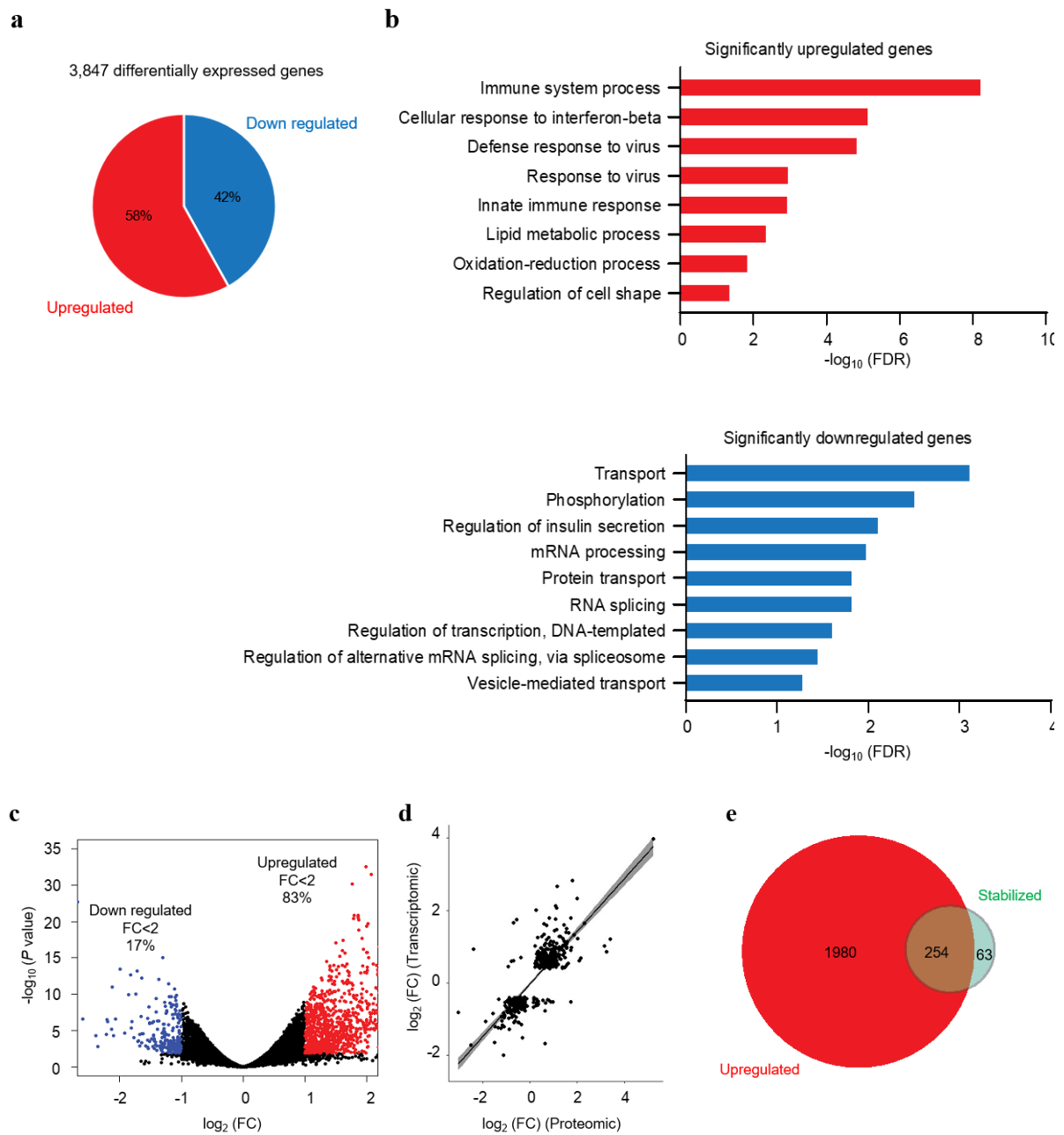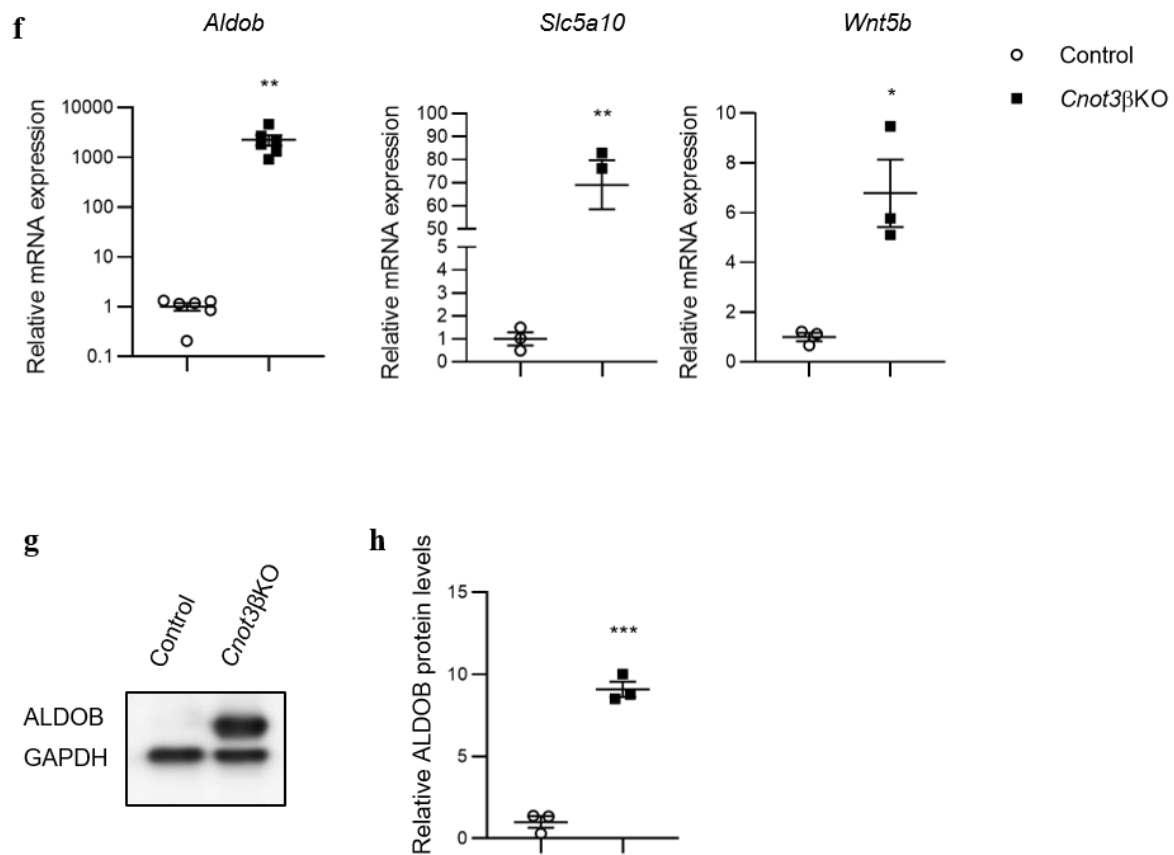
Figure 2.12 Global gene expression changes in *Cnot3*βKO islets

(**a**) 3,847 genes were differentially expressed in islets on CNOT3 depletion in β cells. The graph indicates the percentage distribution of DE genes ($P< 0.05$) in *Cnot3*βKO compared with control islets. (**b**) GO analysis of significantly upregulated (upper) and down regulated (lower) mRNAs in *Cnot3*βKO islets. Bar charts of GO terms (Biological Process) ranked by FDR (< 0.05) are shown. (**c**) Volcano plot of DE genes indicating the percentage distribution of DE genes ($P< 0.05$) with a FC of at least 2, upregulated (red) and down regulated (blue). (**d**) Pearson correlation analysis between DE genes and proteins inferred from RNA-seq analysis and MS analysis of control and *Cnot3*βKO islets. (**e**) Venn diagram showing the overlap of significantly upregulated and stabilized genes in *Cnot3*βKO compared with control islets. (**f**) qPCR analysis of three top upregulated and stabilized mRNAs (*Aldob*, *Slc5a10* and *Wnt5b*), normalized to the *Gapdh* mRNA level, in control and *Cnot3*βKO islets (n=3-6). (**g**), Immunoblot analysis of ALDOB in islet lysates from 8-week-old control and *Cnot3*βKO mice (n=3). (**h**) Band quantification of immunoblots of ALDOB (n=3). Data are presented as mean ± S.E.M; * $P < 0.05$; ** $P <0.01$; *** $P <0.001$.

2.3.8 Derepression and stabilization of β cell disallowed genes in *Cnot3*βKO islets

Based on the findings that CNOT3 affects β cell identity, it was intriguing to find out if CNOT3 is important for the decay of β cell disallowed genes. Two founding studies identified 68 of these genes by microarray analysis (Pullen et al., 2010; Thorrez et al., 2011). More recently, a novel study identified a new list of β cell disallowed genes based on RNA-seq data of islets, β and α cells (Pullen et al., 2017). I performed gene set enrichment analysis (GSEA) of the most recent list of 61 β cell disallowed genes identified in Pullen et al., 2017 study which revealed the enrichment of these β cell disallowed genes in the current study transcriptome data set (Figure 2.13a, b).

I inferred the mRNA stability of some of these disallowed genes together with *Aldob*, *Slc5a10* and *Wnt5b* from transcriptome analysis (Figure 2.12e). Some genes were filtered out in the statistical analysis, due to low expression values, that hindered the assessment of their mRNA stability. I validated this stability analysis by treatment of control and *Cnot3*βKO islets with Act. D and determined their relative abundances after 4 and 8 hrs. *Aldob*, *Wnt5b*, *Cat*, *Abtb2* and *Fgf1* were significantly stabilized (Figure 2.13c). On the other hand, other upregulated *mRNAs*: *Hk1*, *Rest* and *Yap1* were not stabilized (Figure 2.13c). This suggests that the stabilized genes are targets of CNOT3 dependent mRNA decay, whereas the unstabilized genes may be upregulated indirectly by *Cnot3* depletion, rather than via their decay. I couldn't assess the mRNA stability of *Slc5a10, Slc16a1*, *Ldha* and *Pdgfra* experimentally. This could be due to their very low expression levels. Yet, based on statistical evaluation of exon and intron counts, I found that among these genes, *Slc5a10* (logFC= 4.76, FDR=$1.7e^{-17}$) was stabilized in *Cnot3*βKO islets.

To further understand the mechanism by which CNOT3 alters mRNA stability, I asked whether the affected genes interact with CNOT3. To answer this question, I carried out RIP assay using MIN6 cell line lysates with an antibody specific for CNOT3 and negative control immunoglobulin G (IgG). RNA from total extracts (Input), IgG and CNOT3-immunoprecipitated samples were analyzed by qPCR. Among β cell disallowed genes analyzed, *Slc16a1*, *Ldha*, *Cat*, *Abtb2, Fgf1, Igfbp4, Acot7* and *Cxcl12* were significantly enriched in CNOT3-immunoprecipitated samples compared with IgG-immunoprecipitated samples (Figure 2.13d). These data suggest that the above genes interact with CNOT3. Interestingly, among the examined β cell disallowed genes is *Yap1* which I found not interacting with CNOT3 (Figure 2.13d) and whose mRNA decay rate was not affected in *Cnot3*βKO mice

(Figure 2.13c). This observation implies that *Yap1* upregulation after *Cnot3* deletion is an indirect effect (possibly on transcription) rather than a result of reduced decay. Taken together, my data suggest that *Cnot3* depletion resulted in decreased decay rates and increased protein synthesis of target transcripts.

a

Enrichment plot: disallowed genes list

Enrichment score= 0.62
P= 0.0
FDR=0.1

Genes ranked by expression in *Cnot3*βKO vs Control islets

b

c

Time after Act. D treatment (h)
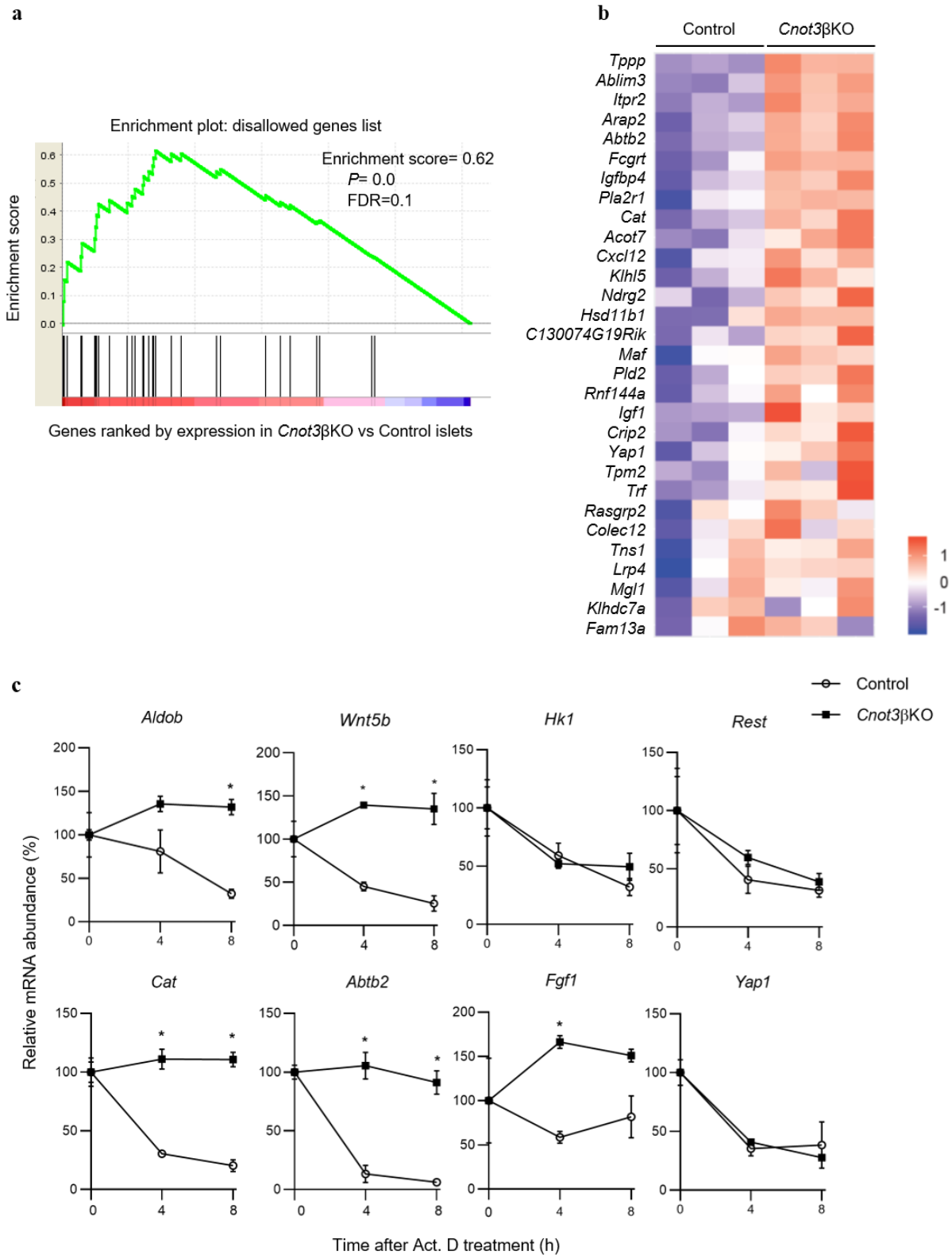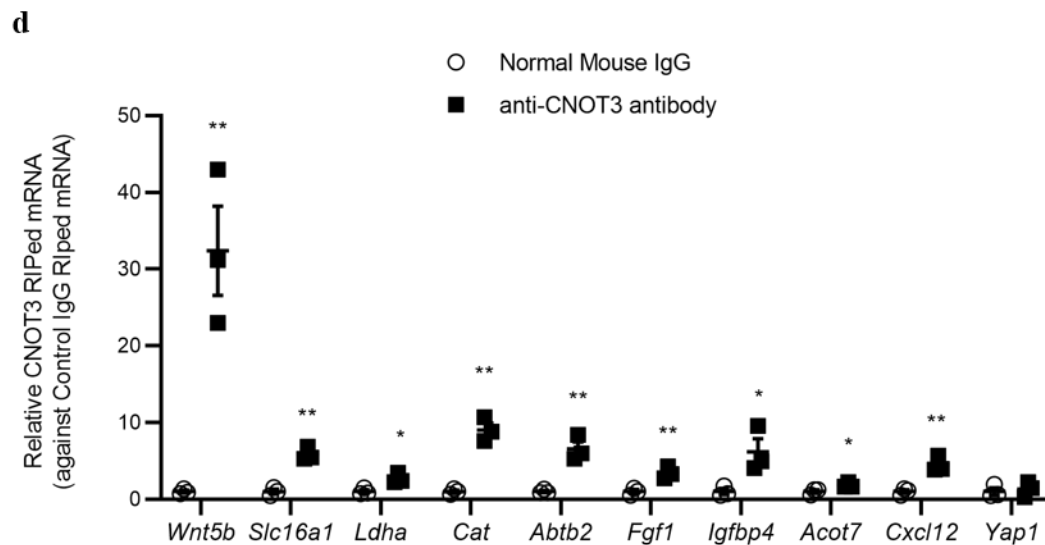
Figure 2.13 Derepression of β cell disallowed genes and their stabilization in *Cnot3*βKO islets

(a) GSEA of β cell disallowed gene list, identified in Pullen et al, 2017 study, in *Cnot3*βKO islets. (**b**) Heatmap of 30 disallowed genes showing mRNA expression obtained from RNA-seq analysis of control and *Cnot3*βKO islets. (**c**) Decay curves of the indicated mRNAs. Total RNA was prepared from control and *Cnot3*βKO islets treated with Act. D (0, 4 or 8h). Relative mRNA levels were determined by qPCR and normalized to the *Gapdh* mRNA level. mRNA level without Act. D treatment (0h) was set to 100% (n=3). (**d**) RIP-qPCR in MIN6 cells using normal anti-mouse and anti-CNOT3 antibodies revealing the interaction of CNOT3 with selected mRNAs that adversely affect β cell function (n=3). Data are presented as mean ± S.E.M; * $P < 0.05$; ** $P < 0.01$; *** $P < 0.001$

To exclude the possibility that the observed immature phenotype is merely caused by hyperglycemia, I performed experiments on euglycemic 4-week-old *Cnot3*βKO mice. I observed significant down regulation of *Mafa*, *Ins1* and *Ins2*, and significant upregulation of *Aldob*, *Slc5a10*, *Wnt5b*, *Hk1* and *Tnfrsf11b,* suggesting that this molecular defect is due to a direct effect of loss of *Cnot3*, rather than to hyperglycemia (Figure 2.14).
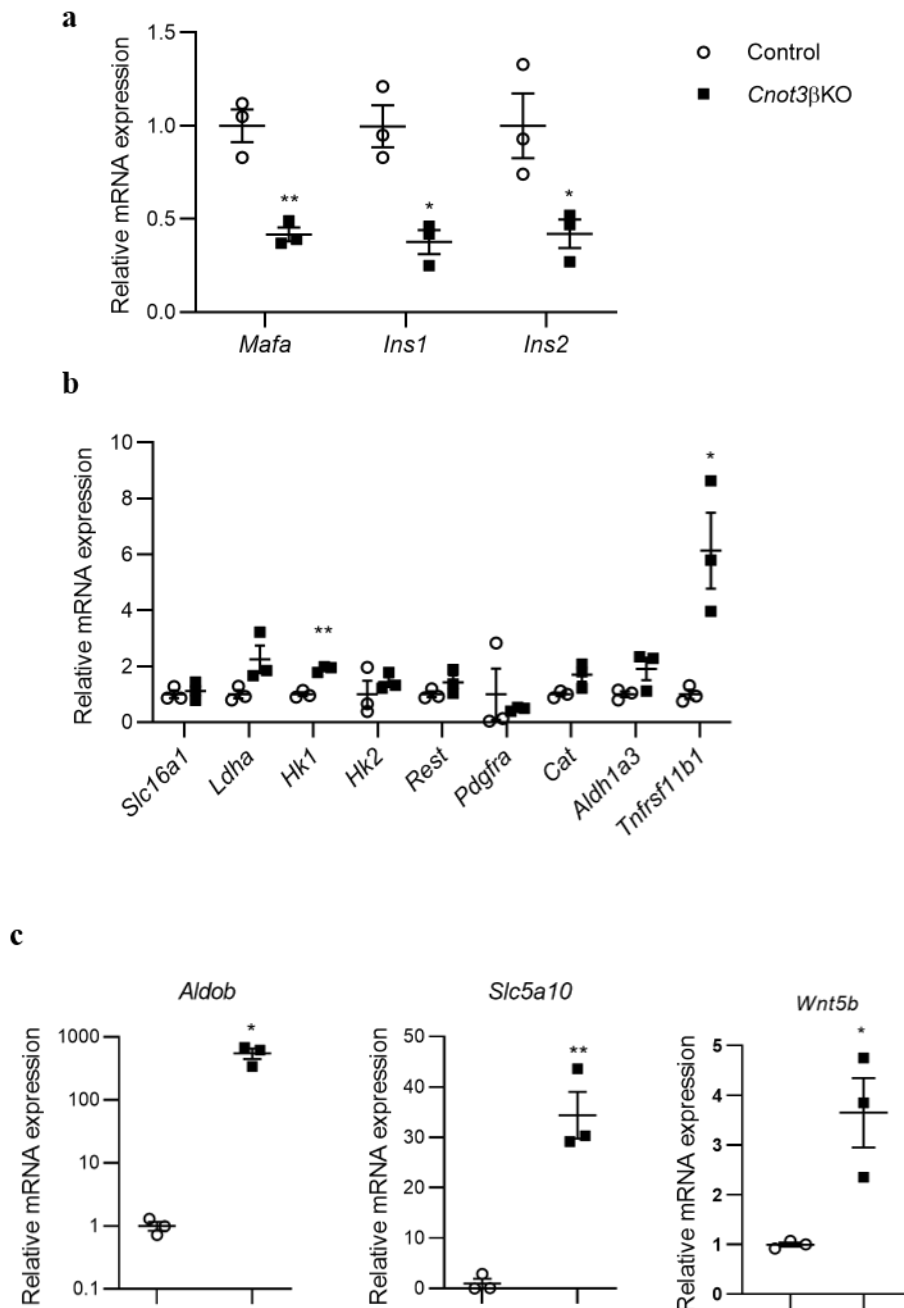
Figure 2.14 Molecular deregulation by CNOT3 loss is observed in 4-week-old mice

qPCR analysis of: (**a**) β cell specific markers, (**b**) Immaturity markers and disallowed genes, and (**c**) top upregulated and stabilized genes as inferred from transcriptome data.

Data are presented as mean ± S.E.M; * P < 0.05; ** P <0.01; *** P <0.001

2.3.9 Roquin recruits CCR4-NOT complex to the 3'UTR of *Slc16a1* mRNA and other plausible target mRNAs for the control of their stability

While direct recruitment of the CCR4–NOT complex to target mRNAs destined for deadenylation and decay is mediated by several RBPs that interact with ARE in 3'UTRs. I tried to identify RBPs that mediate the CCR4-NOT complex interaction with *Slc16a1*, *Ldha, Wnt5b* and *Abtb2* in β cells. To identify proteins that recruit CCR4-NOT complex, cellular extracts of MIN6 cells were incubated with FLAG-tagged fragments of *Slc16a1, Ldha, Wnt5b* and *Abtb2* mRNA 3'UTR for pull down analysis as previously described (Takahashi et al., 2015). The *Slc16a1* 3'UTR was divided into six constructs (*Slc16a1*-1, *Slc16a1*-2, *Slc16a1*-3, *Slc16a1*-4, *Slc16a1*-5 and *Slc16a1*-6), *Wnt5b* 3'UTR into two constructs (*Wnt5b*-1 and *Wnt5b*-2), and *Abtb2* 3'UTR into two constructs (*Abtbt*-1 and *Abtbt*-2) because the technique used for fusing a FLAG tag has a size limitation (Adachi and Natsume, 2015). As shown in Fig. 2.15a, *Slc16a1*-4 interacted with cytoplasmic Roquin whereas the other fragments didn't interact. Also, *Ldha*, *Wnt5b* and *Abtb2* 3'UTR interacted with Roquin (Fig. 2.15b).

To determine whether CNOT3 interacts with Roquin in an RNA-independent manner, cellular extracts of control and FLAG-tagged CNOT3 expressing MIN6 cells were treated with RNase A, and the immunoprecipitates were analyzed and compared by immunoblotting. Roquin showed a direct interaction with CNOT3 whereas HuR, another RBP known to interact with ARE, didn't interact with CNOT3 (Fig. 2.15c).
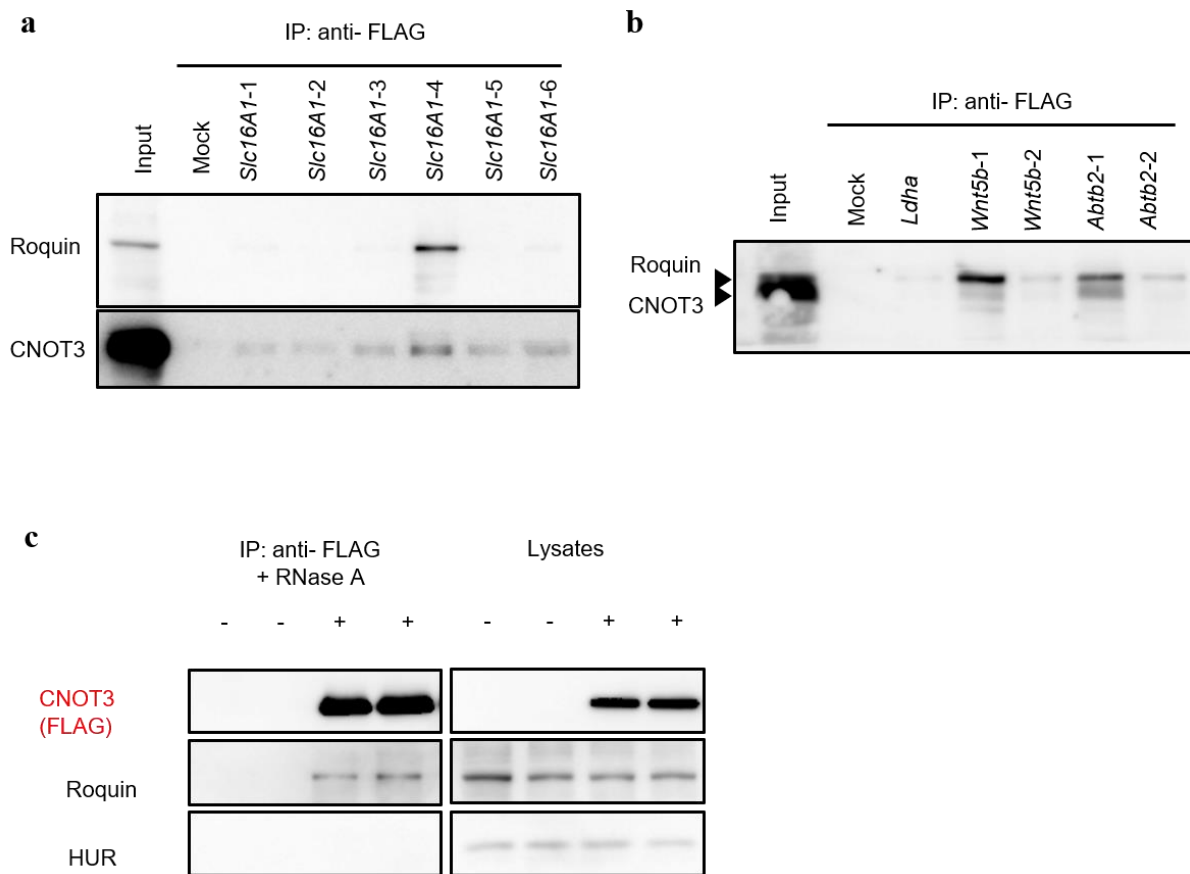
Figure 2.15 Roquin recruits CCR4-NOT complex to the 3'UTR of *Slc16a1*, *Ldha*, *Wnt5b* and *Abtb2* mRNA

(**a-b**) MIN6 cells lysates were incubated with FLAG-tagged (**a**) *Slc16a1*, (**b**) *Ldha*, *Wnt5b* and *Abtb2* 3'UTR fragments and then immunoprecipitated with anti-FLAG antibody. Immune complexes were analyzed by immunoblot analysis with anti-Roquin and anti-CNOT3 antibodies. (**c**) Lysates prepared from MIN6 cells which were transfected with FLAG-tagged CNOT3 and subjected to immunoprecipitation with anti-FLAG antibody. CNOT3 (FLAG) is shown in red to indicate a precipitated molecule. Lysates and IP were analyzed by immunoblot analysis.

2.4   Discussion

Loss of β cell identity and dedifferentiation are increasingly recognized as contributors to impaired β cell function in T2D (Talchai et al., 2012). However, the molecular underpinnings of these events are still unclear. The principal aim of the present study was to elucidate the role of the CCR4-NOT complex, a key regulator of post-transcriptional gene expression, in β cells. I first found that CNOT3, along with CNOT1 and CNOT2, was decreased in diabetic mouse

islets, implying that disruption of the CCR4-NOT complex could be a pathogenic factor in diabetes. To understand the role of the CCR4-NOT complex in β cells I generated *Cnot3βKO* mice in which *Cnot3* is specifically knocked out in β cells by *Ins1-Cre* at the onset of insulin gene expression. In this way, I demonstrated that CNOT3 is crucial for β cell maturation and β cell identity. β cell maturation occurs postnatally in the first few weeks of life when β cells acquire GSIS feature (Blum et al., 2012). This process involves increased expression of β cell-specific genes, such as *Mafa, Gck* and *Ucn3*, and the loss of expression of other genes that would interfere with normal β cell function – β cell disallowed genes (Blum et al., 2012; Pullen et al., 2010; Rutter et al., 2015). Molecular mechanisms governing the process of β cell maturation and acquisition of functional and molecular identities are not fully understood.

The process of GSIS in mature β cells is regulated primarily by the levels of extracellular glucose. Unlike immature β cells, which secrete insulin under low glucose conditions, mature β cells secrete insulin in response to rises in blood glucose, thus maintaining normal glucose homeostasis without causing hypoglycemia (Dhawan et al., 2015). Mature rodent β cells take up glucose via GLUT2 localized to the cell membrane. Upon its uptake, glucose is metabolized by Gck followed by glycolytic breakdown to pyruvate which enters the TCA cycle in the mitochondria to generate ATP. The increased ATP/ADP ratio causes the closure of ATP-sensitive potassium channels, leading to depolarization of the plasma membrane, which opens voltage-dependent calcium channels allowing the influx of calcium. Increased intracellular calcium causes fusion of insulin granules to the plasma membrane for insulin exocytosis (Rorsman and Renström, 2003; Rutter et al., 2015). Here, I show that CNOT3 is essential for both the maintenance of normal β cell mass, as well as the functional, differentiated state of these cells. Notably, GSIS is impaired in *Cnot3βKO* mice, suggesting impaired glucose metabolism. Impaired glucose metabolism could be due to decreased GLUT2 expression and defects in maturity. Expression of glycolytic genes, such as *Hk1*, *Hk2* and *Ldha*, is sharply down regulated during β cell maturation (Liu and Hebrok, 2017). I observed increased expression of these glycolytic genes alongside with other markers of immature β cell: *Slc16a1*, *Rest* and *Pdgfra* (Figure 2.11). Ectopic expression of *Hk1*, *Slc16a1* and *Ldha* has been reported to impair glucose metabolism and GSIS (Alcazar et al., 2000; Becker et al., 1994; Pullen et al., 2012; Zhao and Rutter, 1998). Moreover, decreased expression of *Pdgfra* during maturation is responsible for decreased proliferation in the mature β cell necessary for normal GSIS (Chen et al., 2011b).

Nearly all fully processed eukaryotic mRNAs possess poly (A) tails at their 3' ends. Poly(A) tail length is suggested to influence mRNA stability (Eckmann et al., 2011; Norbury, 2013). Deadenylation of these 3' tails is the rate-limiting step in mRNA decay and translational silencing. Suppression of any of the CCR4-NOT complex subunits in cell lines and tissues results in stabilization of its target genes due to elongation of the poly(A) tail (Ito et al., 2011b; Suzuki et al., 2019). In my study, the β cell dysfunction and lack of β cell maturation in *Cnot3*βKO mice, which cannot deadenylate mRNAs in β cells (Figure 2.2 c, d), is coincident with the upregulation and stabilization of various genes. Among these genes are *Aldob*, *Slc5a10* and *Wnt5b* (Figure 2.12 f), whose upregulation is shown to be correlated with diabetes (Gerst et al., 2018; Haythorne et al., 2019; Lee et al., 2008; Solimena et al., 2018). ALDOB is a glycolytic enzyme that is positively correlated with glycated hemoglobin in T2D patients and negatively correlated with insulin secretion (Gerst et al., 2018). Increases of the glucose/fructose transporter, SLC5A10, are associated with inhibition of mitochondrial metabolism and decreased insulin secretion (Haythorne et al., 2019). *Wnt5b*, a member of the *Wnt* gene family, has been identified as a candidate gene for susceptibility to T2D (Kanazawa et al., 2004), but it has not been determined whether this occurs through a direct effect on the islets or in peripheral tissues. Moreover, it is still not known whether Wnt signaling in islets plays a role in pathogenesis of diabetes or whether it is activated as a compensatory mechanism during the progression of the disease. Interestingly, prolonged activation of Wnt signaling is shown to affect the differentiated state of β cells (Heiser et al., 2006; Lee et al., 2008). In addition, there is an inverse correlation between Wnt signaling activation and insulin gene expression, which suggests a deleterious effect of Wnt signaling activation on β cell function (Lee et al., 2008). These results are in agreement with previous findings that the CCR4-NOT complex is involved in regulation of energy metabolism genes (Li et al., 2017; Morita et al., 2011; Takahashi et al., 2015). Moreover, I demonstrated that disallowed genes are preferentially upregulated by *Cnot3* KO (Figure 2.13 a, b). Therefore, it is conceivable that CNOT3 is involved in silencing of these genes.

β cell disallowed genes are selectively silenced in β cells. Their repression is part of β cell identity acquired during postnatal maturation and ensures normal GSIS (Pullen and Rutter, 2013), but their roles in affecting normal β cell function are not fully elucidated. However, repression of *Slc16a1* and *Ldha*, two founder members of β cell disallowed genes, were proposed to prevent lactate and pyruvate, produced from muscle during exercise, from inappropriately stimulating insulin release (Thorrez et al., 2011). The molecular mechanisms

involved in repressing these genes are largely unknown. Thus, it is currently unclear whether there is a general silencing mechanism for all disallowed genes, or several molecular mechanisms are involved. Transcriptional epigenetic mechanisms such as DNA methylation are shown to be involved in repressing several disallowed genes (*Pdgfra*, *Acot7*, *Igfbp4* and *Fgf1*) (Ni et al., 2017). Of note, DNA methylation is generally essential for β cell maturation and contributes to repression of immature β cell genes including *Aldob*, *Hk1*, *Hk2* and *Ldha* (Dhawan et al., 2015). Histone methylation may also be involved. The trimethylation of histone H3 on lysine 27 (H3K27me3), was found in the *Slc16a1* promoter (van Arensbergen et al., 2010) and several other disallowed genes (*Cxcl12*, *Acot7*, *Nfib*, *Mgst1*, *Maf*) (Pullen and Rutter, 2013). Several studies have revealed that miRNAs down regulate *Slc16a1*, *Acot7*, *Fcgrt*, *Igfbp4*, *Maf*, *Oat* and *Pdgfra* (Martinez-Sanchez et al., 2015; Martinez-Sanchez et al., 2016; Pullen et al., 2011). One possible mechanism of the CCR4–NOT complex target recognition is through miRNAs (Chekulaeva et al., 2011; Fabian et al., 2011). It is conceivable that the CCR4–NOT complex is involved in post-transcriptional regulation of relevant miRNA targets in β cells.

The current study provides evidence that deadenylation by the CCR4–NOT complex is involved in repressing *Aldob*, *Slc5a10*, *Wnt5b* and several disallowed genes through both direct and indirect mechanisms. I considered that upregulated stabilized genes were more likely to be directly regulated by CNOT3-dependent deadenylation by the CCR4-NOT complex. Investigations of mRNA stability have shown that *Cnot3* KO results in increased stability of *Aldob, Slc5a10, Wnt5b, Cat, Abtb2* and *Fgf1* (Figure 2.13 c). Moreover, the finding that CNOT3 directly interacts with *Wnt5b*, *Cat*, *Abtb2* and *Fgf1* (Figure 2.13 d) supports direct repression of these genes by CNOT3. However, I could not determine the mRNA stability of some of the investigated disallowed genes in Act. D chase experiments. Other methods for assessing mRNA stability, such as monitoring the abundance of labeled mRNA using high-throughput pulse-chase methods could not be applied to islets owing to the low quantity of RNA that could be extracted from them. Also, we were only able to assess bulk poly(A) tail length elongation in *Cnot3*βKO islets (Figure 2.2c, d). However, owing to the very low expression levels of most target genes, I couldn't assess their poly(A) tail lengths using currently available techniques. For the same reason, I was unable to detect direct binding of CNOT3 to its plausible targets, *Aldob* and *Slc5a10*, using a conventional RIP assay.

On the other hand, indirect effects of CNOT3 suppression on gene expression likely involve changes in expression of key transcription factors. Of note, it was recently reported

that MafA (Nishimura et al., 2015), Pax6 (Swisa et al., 2017), Rfx6 (Piccand et al., 2014) and Nkx2.2 (Gutierrez et al., 2017) act as repressors of several disallowed genes and changes in any of these factors may be involved in upregulation of disallowed genes. Among these repressors only MafA was significantly decreased in *Cnot3*βKO islets (Figure 2.10 a, e). Therefore, I cannot exclude the possibility that repression of MafA in *Cnot3*βKO islets also contributes to increased expression of disallowed genes. Moreover, down regulation of MafA could explain upregulation of endocrine progenitor cell markers observed in *Cnot3*βKO islets (Figure 2.9 a-c). Upregulation of these progenitor markers, as a result of MafA down regulation, hallmarks dedifferentiation state in β cells and upregulates β cell disallowed genes (Nishimura et al., 2015). Indeed, *Slc16a1* was upregulated but not stabilized. Thus, I propose that *Slc16a1* is upregulated indirectly by CNOT3 through MafA repression. This comes in agreement with its upregulation observed in dedifferentiated β cells of *Mafa* KO mice (Nishimura et al., 2015). The *Mafa* suppression mechanism was not determined in this study. Taken together, my data and that of others' data suggest that repression of disallowed genes is achieved by multiple mechanisms.

I showed here that CNOT3 is required for normal β cell maturation, sustaining expression of β cell-specific genes and repressing that of disallowed genes. These findings, together with the observed decreased expression of CNOT3 in *db*/*db* diabetic mouse model (Burke et al., 2017), raise the possibility that disruption of the CCR4–NOT complex could be behind the loss of β cell identity in diabetes, possibly through loss of repression of immature β cell and disallowed genes. I found that glucotoxicity and lipotoxicity did not change CNOT3 levels; thus, I propose that other factors in diabetes may be involved in perturbing its protein levels. Interestingly, proteomic analysis of human islets revealed significant reduction of CNOT3 during high glucose treatment (Schrimpe-Rutledge et al., 2012). Further studies are required to identify the molecular mechanisms that control CNOT3 levels during diabetes.

In the mammalian CCR4-NOT complex, CNOT3 does not have well-defined RNA binding motifs but rather forms a platform for interaction with RBPs via direct protein-protein interactions. The recognition of target mRNAs by the CCR4-NOT complex is, hence, likely mediated through RBPs. One of the well characterized cis-acting elements for regulation of mRNA stability is AU-rich elements (ARE) found in the 3′UTRs (Bhandari et al., 2014; Braun et al., 2011; Leppek et al., 2013; Sgromo et al., 2017; Van Etten et al., 2012). Previous research by our group and others elucidated the recruitment of the CCR4-NOT complex to target 3'UTRs by TTP protein family (Fabian et al., 2013; Takahashi et al., 2015). I was unable

to detect this family of proteins in β cells (data not shown). On the other hand, I identified Roquin, an mRNA binding protein, that interacts specifically with a stem loop constitutive decay element in 3'UTR (Leppek et al., 2013) and recruits CNOT3 to some of investigated mRNAs: *Slc16a1*, *Ldha*, *Wnt5b* and *Abtb2* 3'UTRs. Interestingly, Roquin was found to interact directly with *Slc16a1* in HEK293 cells and MEFs by Photoactivatable-Ribonucleoside-Enhanced Crosslinking and Immunoprecipitation (PAR-CLIP) technique (Essig et al., 2018; Murakawa et al., 2015). Future investigations are needed to identify sequences in the investigated target mRNAs to which Roquin interacts and examine the mRNA stability of these target mRNAs in the absence of Roquin.

In conclusion, this study identifies CNOT3 as a key post-transcriptional regulator of β cell identity and function, and raises the possibility that changes in CNOT3 expression or activity contribute to β cell failure in diabetes.

3 Chapter 3: Essential functions of the CNOT7/8 catalytic subunits of the CCR4-NOT complex in mRNA regulation and cell viability

3.1 Introduction

Regulation of mRNA decay in the cytoplasm is important for proper gene expression, and its dysregulation causes various disorders. Shortening of mRNA poly(A) tails by deadenylation is the initial, rate-limiting step in the exonucleolytic mRNA decay pathway, which is also relevant to translational suppression (Garneau et al., 2007; Parker, 2012). mRNA deadenylation occurs via two distinct steps. First, PAN2-PAN3 trims long poly(A) tails to ~110 nucleotides (nt) and subsequently, the CCR4-NOT complex completes deadenylation (Wahle and Winkler, 2013; Yamashita et al., 2005).

The CCR4-NOT complex is critical to a variety of physiological functions in mammals, including energy metabolism, B-cell development, heart function, and liver maturation, via mRNA deadenylation and subsequent degradation (Inoue et al., 2015; Morita et al., 2011; Suzuki et al., 2019; Yamaguchi et al., 2018). Mouse embryonic development also requires CCR4-NOT complex activity, as mice lacking the *Cnot1* or *Cnot3* genes (*Cnot1*-KO or *Cnot3*-KO mice, respectively) show embryonic lethality (Morita et al., 2011; Yamaguchi et al., 2018). Furthermore, suppression of CCR4-NOT activity leads to cell death via apoptosis or necroptosis, indicating the importance of the CCR4-NOT complex in cell viability (Inoue et al., 2015; Ito et al., 2011b; Mittal et al., 2011; Suzuki et al., 2019; Suzuki et al., 2015; Yamaguchi et al., 2018).

Several studies have described different roles of the catalytic subunits in deadenylase activity and biological processes, but their individual biological roles are not fully understood. In yeast, current evidence suggests that Ccr4, the ortholog of CNOT6/6L, is the dominant deadenylase subunit of CCR4-NOT (Tucker et al., 2001). On the other hand, DEDD family proteins: Ccf1 (Caf1 ortholog) and CNOT7/8 possess the main activity in *C. elegans* and mammals respectively (Nousch et al., 2013; Piao et al., 2010). Suppression of *Cnot6l* or both *Cnot6/6l* in human cancer cell lines leads to proliferation arrest and cell death in a deadenylase activity-dependent manner, indicating the importance of CNOT6/6L in mammals (Mittal et al., 2011; Morita et al., 2007). In the same study, it was shown that CNOT6/6L and CNOT7/8 regulate distinct groups of genes (Mittal et al., 2011). Therefore, CNOT6/6L and CNOT7/8 serve different functions, depending on cell types, biological processes, and target genes.

Importantly, recent studies show that CNOT6/6L and CNOT7/8 display distinct biochemical activities in deadenylation. These differences possibly explain why two different types of ribonuclease in a single complex (Webster et al., 2018; Yi et al., 2018). The two paralogs, CNOT6/6L and CNOT7/8, in mammals have been considered basically redundant. *Cnot6l*-KO or *Cnot7*-KO mice are viable and normally grow to adulthood, supporting their functional redundancy, at least in mouse embryonic development and in embryo-to-adult viability (Berthet et al., 2004; Morita et al., 2019; Nakamura et al., 2004). On the other hand, while CNOT7 and CNOT8 have overlapping roles in some cases, as in growth of human breast cancer cell line, MCF7 cells (Aslam et al., 2009), they also have unique roles in other contexts. For instance, male *Cnot7*-KO mice are sterile due to defects in spermatogenesis, suggesting that CNOT8 cannot compensate for loss of CNOT7 in this process (Berthet et al., 2004; Nakamura et al., 2004). To better understand the different biological roles of the four catalytic subunits, further analyses are necessary to clarify their distinctive functions in various biological contexts.

In this chapter, I addressed the contribution of CNOT7/8 and CNOT6/6L to CCR4-NOT complex deadenylase activity and viability of primary MEFs. I used primary MEFs prepared from mice lacking CCR4-NOT complex subunits. Since *Cnot1*-KO, *Cnot3*-KO, and *Cnot8*-KO mice are embryonically lethal (Morita et al., 2011; Neely et al., 2010; Yamaguchi et al., 2018), I prepared MEFs from mice possessing conditional alleles in which loxP sequences were inserted, and I deleted the corresponding targets using Cre-mediated somatic recombination. Given that primary MEFs lacking CCR4-NOT complex-dependent deadenylation undergo cell death (Suzuki et al., 2015), roles of the catalytic subunits in cell viability were investigated.

3.2   Materials and Methods

3.2.1   Cell culture

MEFs were prepared as described previously (Suzuki et al., 2015). A timed mating was set between male and female mice. On the following day, plug was checked. The day when the plug is detected is considered E0.5. MEFs were prepared from E14.5 embryos extracted from pregnant mice. The pregnant mice were anaesthetized using isoflurane and euthanized by cervical dislocation, then the embryos were retrieved. The head and internal organs were carefully removed and discarded. Part of the head was used for genotyping. Then, embryos

were minced by scissors and dissociated in 0.25% trypsin (Gibco) at 37° C for 5 min. Trypsin was diluted by adding low glucose Dulbecco's modified Eagle's medium (Wako) supplemented with 10% FBS and 1% penicillin-streptomycin. Then, the cells were washed once in medium. Afterwards, the cells were plated on tissue culture flask in low glucose Dulbecco's modified Eagle's medium containing 10% FBS and 1% Penicillin-Streptomycin, cultured at 37° C until confluency.

I used *Cnot1*-flox MEFs infected with mock retrovirus and *Cnot7*$^{+/+}$; *Cnot8*-flox MEFs (littermates of *Cnot7*-KO; *Cnot8*-flox MEFs) infected with mock retrovirus, as controls for *Cnot1*-KO and *Cnot7/8*-dKO MEFs, respectively. I used wild-type (WT) MEFs with the same passage number as controls for *Cnot6/6l*-dKO MEFs.

3.2.2   Virus infection

MEFs infection with retrovirus (mock or Cre) was performed as described previously (Suzuki et al., 2002). Retroviruses (mock and Cre) were produced by transfecting Plat-E packaging cells with 2 μg empty pMX-puro plasmid or 2 μg pMX-puro-Cre plasmid (Suzuki et al., 2015) using TransIT-LT1 transfection reagent (Takara). Two days after transfection, cell culture supernatants containing the retroviruses were filtered and polybrene (0.5 μg/mL) was added. The resultant viral solutions were used for infection of MEFs that were 40% confluent. Two days after viral infection, cells were diluted following trypsinization and cultured in the presence of puromycin (1 µg/mL) for an additional 2 days to select infected cell populations.

In the series of rescue experiments: FLAG-tagged CNOT7-WT and CNOT7-mutants: catalytically negative (CNOT7-CN) and dominant negative (CNOT7-DN) constructs were inserted into pMX vectors and used for retrovirus production for infecting MEFs as shown above for mock and Cre retrovirus infection. Adenovirus infection [control (GFP) and Cre] was performed 2 days after retrovirus infection at MOI 7.5. Two days later, adenovirus-infected MEFs were used for immunoprecipitation. For cell death analysis, MEFs were cultured in the presence of puromycin (1 µg/mL) for additional 2 days.

3.2.3   Immunoprecipitation and immunoblotting

MEFs were lysed with TNE lysis buffer (1% NP-40, 50 mM Tris–HCl [pH 7.5], 150 mM NaCl, 1 mM EDTA, 1 mM phenylmethylsulfonylfluoride, and 10 mM NaF). I used 5% of each lysate for immunoblot analysis (Lysates). The remainder of each lysate was used for

immunoprecipitation and were incubated with anti-CNOT3 antibody for 1 hr at 4° C in an upside-down tumbling manner followed by incubation with Protein G Sepharose (GE Healthcare) for 2 hrs at 4° C in an upside-down tumbling manner. Immune complexes were subjected to immunoblot analysis following SDS-PAGE standard protocols described in **section 2.2.6**. Primary and secondary antibodies used are listed in Table 4 and Table 5 respectively.

3.2.4   Measurement of cell survival rate

Cell viability was measured by the ability of cells to exclude propidium iodide (PI). Cell culture supernatants containing floating dead cells were collected and attached cells were treated with 0.1% Trypsin, collected by centrifugation, washed once with phosphate-buffered saline (PBS), and resuspended in PBS containing 5 µg/mL of PI (Sigma). Levels of PI incorporation were quantified using FACS Calibur (Becton Dickinson).

3.2.5   RNA extraction

Total RNA was extracted from MEFs as described in **section 2.2.13.**

3.2.6   mRNA stability measurement and qPCR

To measure mRNA stability, 4 days after viral infection including the two days of puromycin selection, cells were treated with Act. D (2.5 µg/mL); and total RNA was extracted at 0, 4 and 8 hrs and used for RNA-seq and qPCR. Total RNA (1 µg) was used for reverse transcription with oligo(dT)12-18primer (Invitrogen) using the SuperScript III First-Strand Synthesis System (Invitrogen). qPCR reactions were carried out using TB Green Premix Ex Taq (Takara) and the ViiA 7 Real-Time PCR System (Applied Biosystems). *Gapdh* mRNA levels were used for normalization. Relative mRNA expression was determined by the ΔΔCT method. Primers for qPCR reactions are listed in Table 8.

3.2.7   Bulk poly(A) tail assay

Total RNA (10 µg) was used for bulk poly(A) tail analysis following the same protocol described in **section 2.2.14**.

3.2.8   RNA sequencing

RNA-seq was performed by the Next Generation Sequencing section at OIST Graduate University for two biological replicates per condition; following the same protocol described in **section 2.2.15.**

3.2.9   RNA sequencing data analysis

Paired-end RNA-seq data were mapped to the *Mus musculus* reference strain mm10 UCSC using Strand NGS software (Strand Genomics). Transcript abundance for each replicate was measured in Fragments Per Kilobase Mapped (FPKM). *Genes* with FPKM < 0.1 were filtered out, and only "protein-coding genes" were considered. For comparison, I used gene expression values defined as *Gene* FPKMs normalized with *Gapdh* FPKM. Fold changes in gene expression values (KO against control MEFs) were determined. Half-lives were calculated based on the decay rate of each transcript after suppression of transcription. Total RNA was prepared at 0, 4, and 8 h after Act. D treatment, and subjected to RNA-seq. To calculate the mRNA degradation rate constant ($k_{degradation}$), gene expression values were plotted on a semilogarithmic scale as a function of time (t). The line that best fit the data was identified using linear regression, then $k_{degradation}$ was obtained from the slope. The $t_{1/2}$ was calculated by substitution in the equation:

$$t_{1/2} = \ln(2) / k_{degradation}$$

mRNAs having half-lives less than 0 h or more than 50 h were excluded as unreliable. *Cnot1*-flox or *Cnot8*-flox MEFs infected with mock virus were used as controls for *Cnot1*-KO and *Cnot7/8*-dKO MEFs, respectively. WT MEFs were used as controls for *Cnot6/6l*-dKO MEFs. mRNAs having more than 2-fold longer half-lives compared to controls were considered stabilized genes. GO enrichment analysis was performed with DAVID Bioinformatics Resources 6.8 (https://david.ncifcrf.gov).

3.2.10   Statistical analysis

Differences between groups were examined for statistical significance using Student's t-test (two-tailed distribution with two-sample equal variance). *P* value of <0.05 was considered statistically significant.

3.3   Results

3.3.1   Simultaneous suppression of *Cnot7* and *Cnot8* causes marked cell death in MEFs

Based on embryonic phenotypes of mice lacking each catalytic subunit in the CCR4-NOT complex, I prepared MEFs from mice with *Cnot8*-flox alleles (*Cnot8*-flox MEFs) and subsequently deleted the *Cnot8* gene with Cre-mediated recombination to generate *Cnot8*-KO MEFs. I employed recombinant retrovirus to introduce Cre in MEFs. *Cnot6*-KO, *Cnot6l*-KO, *Cnot7*-KO (32), and *Cnot6/6l*-dKO MEFs were prepared from the corresponding KO mouse embryos. I also prepared *Cnot7*-KO/*Cnot8*-flox MEFs by crossing *Cnot7*-Het/*Cnot8*-flox pairs. Using Cre-mediated recombination, I generated *Cnot7/8*-dKO MEFs. For controls, mock-infected MEFs were used. MEFs were also prepared from mice with *Cnot1*-flox alleles followed by Cre-mediated deletion of the *Cnot1* gene (*Cnot1*-KO MEFs). Immunoblot analysis confirmed that expression of CNOT1 protein was substantially decreased (Figure 3.1a, b). CNOT1 protein was still detected after *Cnot1* gene deletion. Our group previously observed a similar result in *Cnot3*-KO MEFs (Suzuki et al., 2015). I speculate that cells which had comparably high levels of CNOT1 protein before Cre-mediated gene deletion survived until the time of our analysis, while cells with reduced CNOT1 levels died. It is also possible that some cells escaped gene deletion due to insufficient Cre expression, because random integration of the *Cre* gene into the host genome leads to heterogeneous cell populations that vary in Cre expression. Expression of other CCR4-NOT complex subunits also decreased in *Cnot1*-KO MEFs, resulting in decreased expression of the whole complex, as shown by immunoprecipitation using anti-CNOT3 antibody (Figure 3.1a, b). Furthermore, the appearance of floating cells and a significant increase in the number of PI-incorporated cells indicated that *Cnot1*-KO MEFs underwent cell death (Figure 3c, d). Thereafter, I used *Cnot1*-KO MEFs as a model of loss of viability due to loss of CCR4-NOT complex function, because they largely lack the CCR4-NOT complex.

a

b

☐ Control   ■ *Cnot1*-KO

c

Control   *Cnot1*-KO

d

☐ Control
■ *Cnot1*-KO
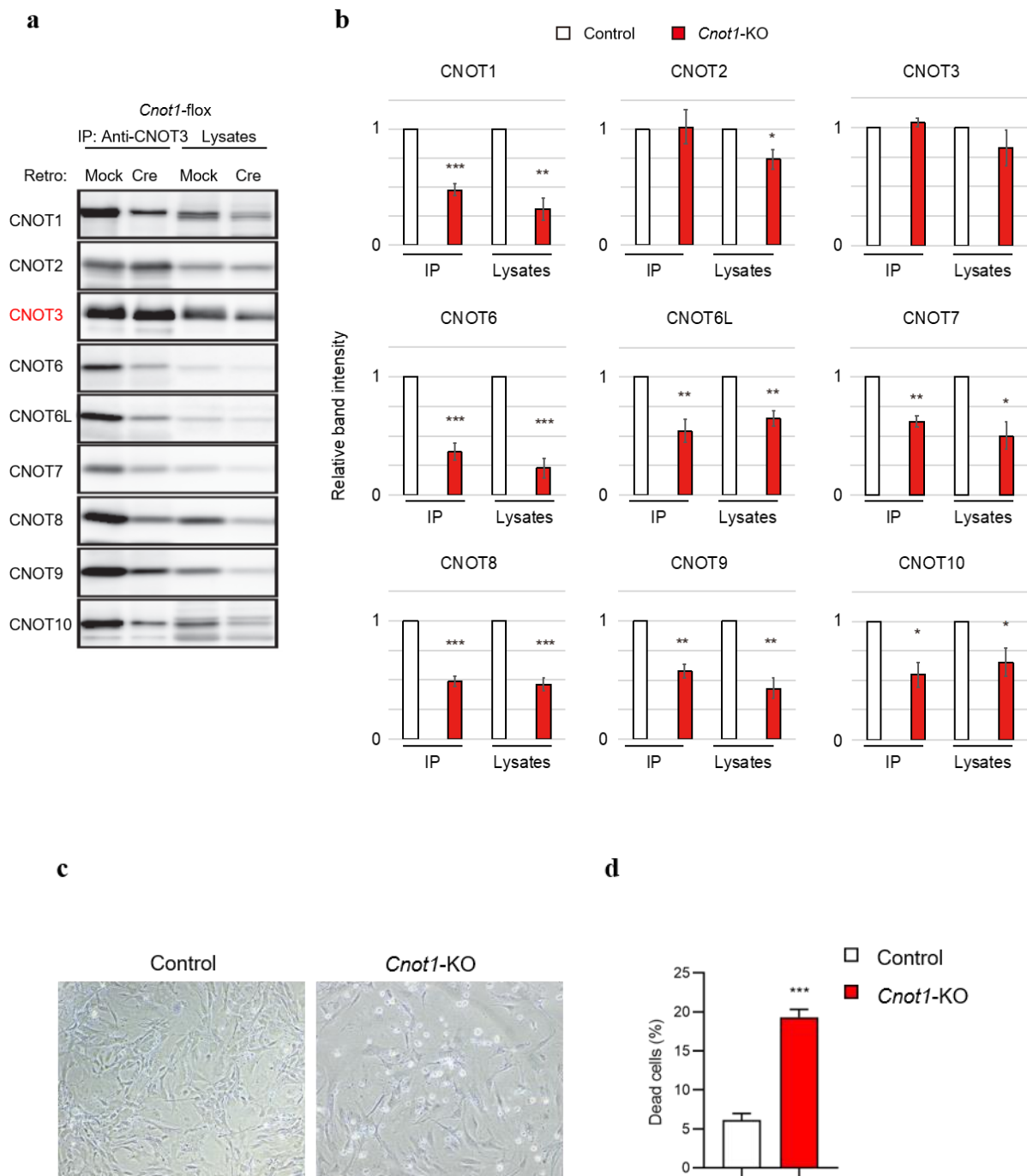
Figure 3.1 *Cnot1*-KO MEFs undergo cell death

(**a**) Lysates were prepared from *Cnot1*-flox MEFs that were infected with mock or Cre-expressing retrovirus and subjected to immunoprecipitation with anti-CNOT3 antibody. CNOT3 are shown in red to indicate a precipitated molecule. Lysates and immunoprecipitates (IP) were analyzed by immunoblot with the indicated antibodies. (**b**) Quantification of the immunoblot data in Figure 3.1a. Relative band intensities normalized to those of IP or lysates in control MEFs are shown (n=3). Data are presented as mean ± S.E.M. (**c**) Morphology of *Cnot1*-flox MEFs infected with mock (Control) or Cre-expressing retrovirus (*Cnot1*-KO).

Figure 3.1 (continued). Photographs are at the same magnification and represent one of three independent experiments. Dead cells that were about to lose adhesion were observed in *Cnot1-*KO MEFs. (**d**) Cell death was assessed by propidium iodide uptake using flow cytometry (n=3). Data are presented as mean ± S.E.M. *P<0.05, **P<0.01, ***P< 0.001.

Then, I examined viability of *Cnot7/8*-dKO and *Cnot6/6l*-dKO MEFs. *Cnot7/8*-dKO MEFs underwent cell death, while such outcomes were not observed in *Cnot7*-KO, *Cnot8*-KO, and mock-infected MEFs (Figure 3.2a, b). There was no significant difference in PI-incorporated cells among *Cnot6*-KO, *Cnot6l*-KO, *Cnot6/6l*-dKO, and WT MEFs (Figure 3.2a, b). Therefore, CNOT6/6L are dispensable for MEF viability. In contrast, CNOT7 and CNOT8 have redundant functions in maintaining MEF viability.
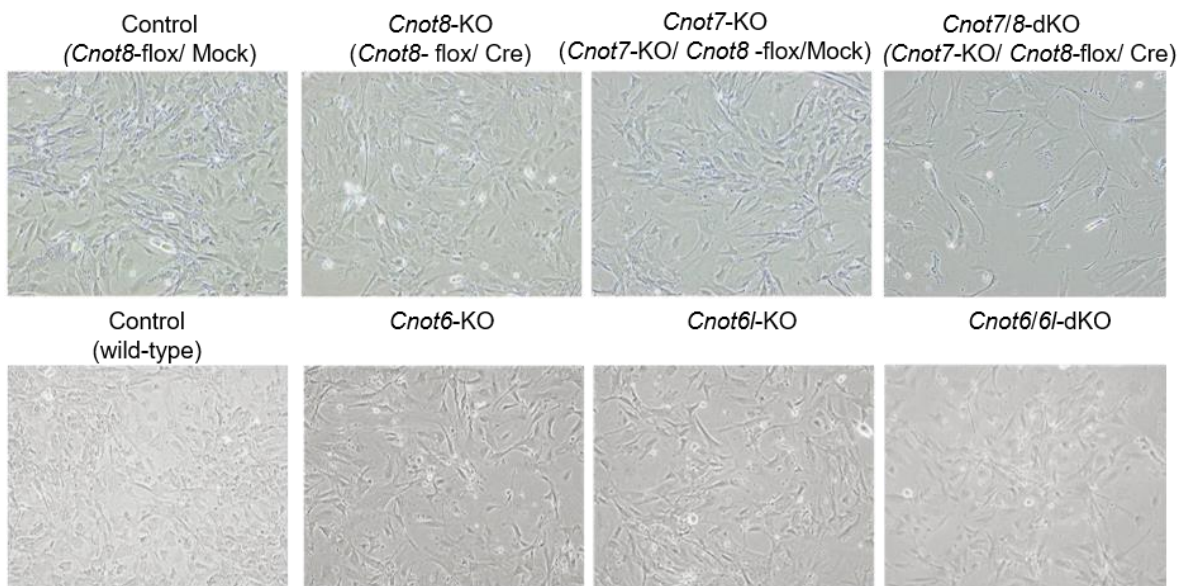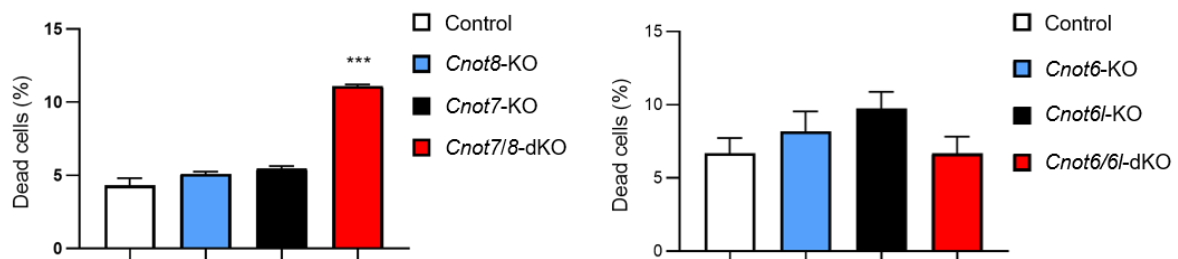
Figure 3.2 Suppression of CNOT7/8, but not CNOT6/6L, affects viability of MEFs

Figure 3.2 (continued). (**a**) Morphology of MEFs with the indicated genotypes. Mock and Cre represent cells infected with retrovirus. (**b**) Cell death was assessed as in Figure 3.1d (n=3). Data are presented as mean ± S.E.M. ***$P < 0.001$.

3.3.2   *Cnot7/8* suppression results in loss of catalytic subunits from the CCR4-NOT complex

Decreased levels of intact CCR4-NOT complex result in decreased MEF viability ((Suzuki et al., 2015), and Figure 3.1). I performed co-immunoprecipitation experiments to examine the effects of CNOT6/6L or CNOT7/8 suppression on complex formation. CNOT8 protein was still detected after *Cnot8* gene deletion (Figure 3.3a), probably for the same reasons described in the case of *Cnot1*-KO MEFs (Figure 3.1a, see above). Importantly, immunoprecipitation of lysates from *Cnot7/8*-dKO MEFs with anti-CNOT3 antibody showed that levels of co-immunoprecipitated CNOT6 and CNOT6L decreased substantially compared to control MEFs (Figure 3.3a), indicating that few catalytic subunits were associated with core subunits (CNOT1-3) of the CCR4-NOT complex in *Cnot7/8*-dKO MEFs. This is consistent with a study demonstrating CNOT7/8 bridge interaction between CNOT6/6L and CNOT1 (Clark et al., 2004). I found that CNOT1, CNOT2, CNOT3, CNOT7, CNOT8, CNOT9, and CNOT10 existed at similar levels in anti-CNOT3 immunoprecipitates among WT, *Cnot6*-KO, *Cnot6l*-KO and *Cnot6/6l*-dKO MEFs (Figure 3.3b). These data suggest that loss of CNOT6/6L does not affect association of other CCR4-NOT complex subunits.
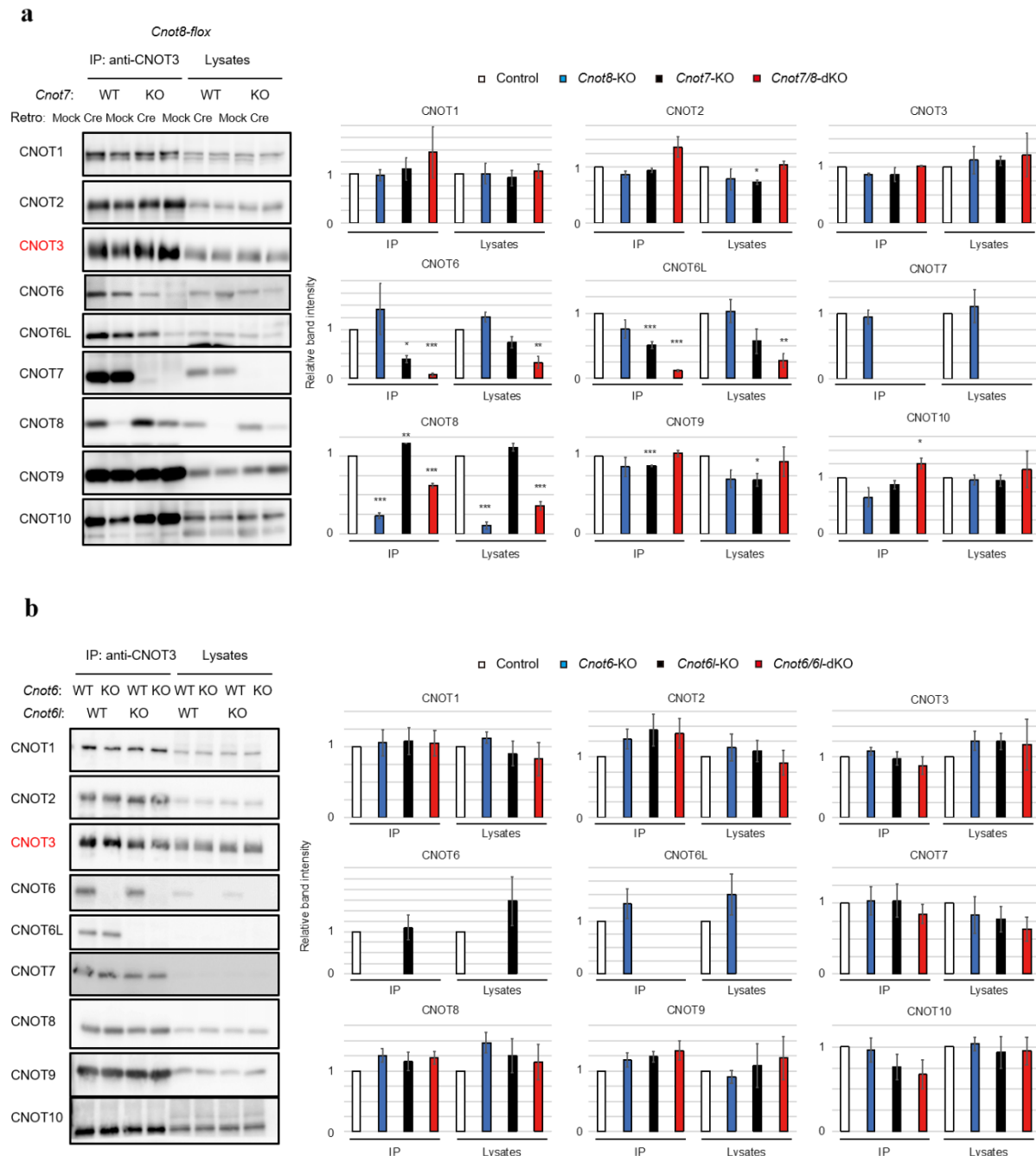
Figure 3.3 CNOT6/6L are not part of CCR4-NOT complex in *Cnot7/8*-dKO MEFs

(**a**) Lysates were prepared from *Cnot8*-flox MEFs with the indicated genotypes, which were infected with mock or Cre-expressing retrovirus and subjected to immunoprecipitation with anti-CNOT3 antibody. CNOT3 is shown in red to indicate a precipitated molecule. Lysates and IP were analyzed by immunoblot with the indicated antibodies. WT: wild-type, KO: knockout. (**b**) Lysates were prepared from MEFs with the indicated genotypes and subjected to immunoprecipitation with anti-CNOT3 antibody. Lysates and IP were analyzed by immunoblot. Data are presented as mean ± S.E.M. *$P<0.05$, **$P<0.01$, ***$P< 0.001$.

3.3.3 CNOT7 catalytic activity is essential to maintain MEF viability

Rates of cell death were not increased in MEFs lacking CNOT6/6L relative to control cells, indicating that CNOT7/8 are sufficient for MEF viability (Figure 3.2a, b). To examine whether CNOT7/8 catalytic activity is critically involved in MEF viability, I introduced either FLAG epitope-tagged CNOT7-WT or CNOT7 mutants into *Cnot7/8*-dKO MEFs, using a recombinant retrovirus. CNOT7 mutants used included a catalytically negative mutant (CN; D40A/E42A), and a dominant negative mutant (DN; D40A/E42A/C67E/L71E), which lacked both catalytic activity and the capacity to bind CNOT6/6L (Mishima and Tomari, 2016). I first characterized CNOT7 mutants by overexpressing them in WT-MEFs. Results of immunoprecipitation with anti-FLAG antibody confirmed that CNOT7-WT and CNOT7-CN, but not CNOT7-DN, interacted with CNOT6/6L, whereas CNOT1 and CNOT3 were co-precipitated with all CNOT7 constructs (Figure 3.4a). I found that both CNOT7-CN and CNOT7-DN induced death in WT-MEFs (Figure 3.4b), suggesting that these mutants have a dominant negative effect on MEF viability.
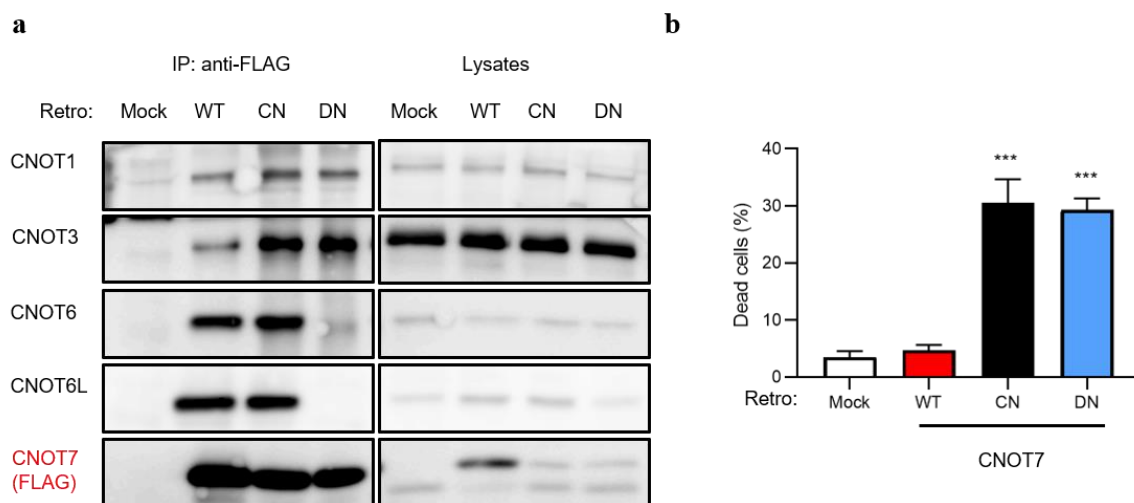
Figure 3.4 Characterization of CNOT7 mutants

(**a**) Lysates prepared from WT MEFs which were infected with the indicated retrovirus and subjected to immunoprecipitation with anti-FLAG antibody. CNOT7 (FLAG) is shown in red to indicate a precipitated molecule. Lysates and IP were analyzed by immunoblot. WT: CNOT7 wild-type, CN: CNOT7 lacking catalytic activity, DN: CNOT7 dominant negative mutant which lacks catalytic activity and an ability to bind to CNOT6/6L. (**b**) Cell death was assessed as in Figure 3.1d (n=3). Cell death assay for this experiment was done by Dr. Toru Suzuki. Data are presented as mean ± S.E.M. ***$P < 0.001$.

In the series of the coming rescue experiments, I used a recombinant adenovirus expressing Cre to delete the *Cnot8* gene. When CNOT7-WT was reintroduced into *Cnot7/8*-dKO MEFs, cell viability was comparable to that of control (GFP) virus-infected MEFs (Figure 3.5a, b). Expression of either CNOT7-CN or CNOT7-DN failed to recover viability, but further induced cell death (Figure 3.5a, b). This effect was likely caused by a dominant negative effect of CNOT7-CN and CNOT7-DN. Immunoblot analyses revealed the successful expression of FLAG-CNOT7-WT and mutants in *Cnot7/8*-dKO MEFs (Figure 3.5c, d). I found that the amount of CNOT6/6L in anti-CNOT3 immunoprecipitates from *Cnot7/8*-dKO MEFs expressing CNOT7-WT or CNOT7-CN was comparable to that from control MEFs, while much less CNOT6/6L was detected in *Cnot7/8*-dKO MEFs and those expressing CNOT7-DN (Figure 3.5c, d). These data demonstrate that recruitment of CNOT6/6L to the complex by CN mutant is not sufficient to rescue the phenotype in *Cnot7/8*-dKO MEFs suggesting that the catalytic activity of DEDD family proteins (CNOT7/8) in the CCR4-NOT complex is essential for cell viability.
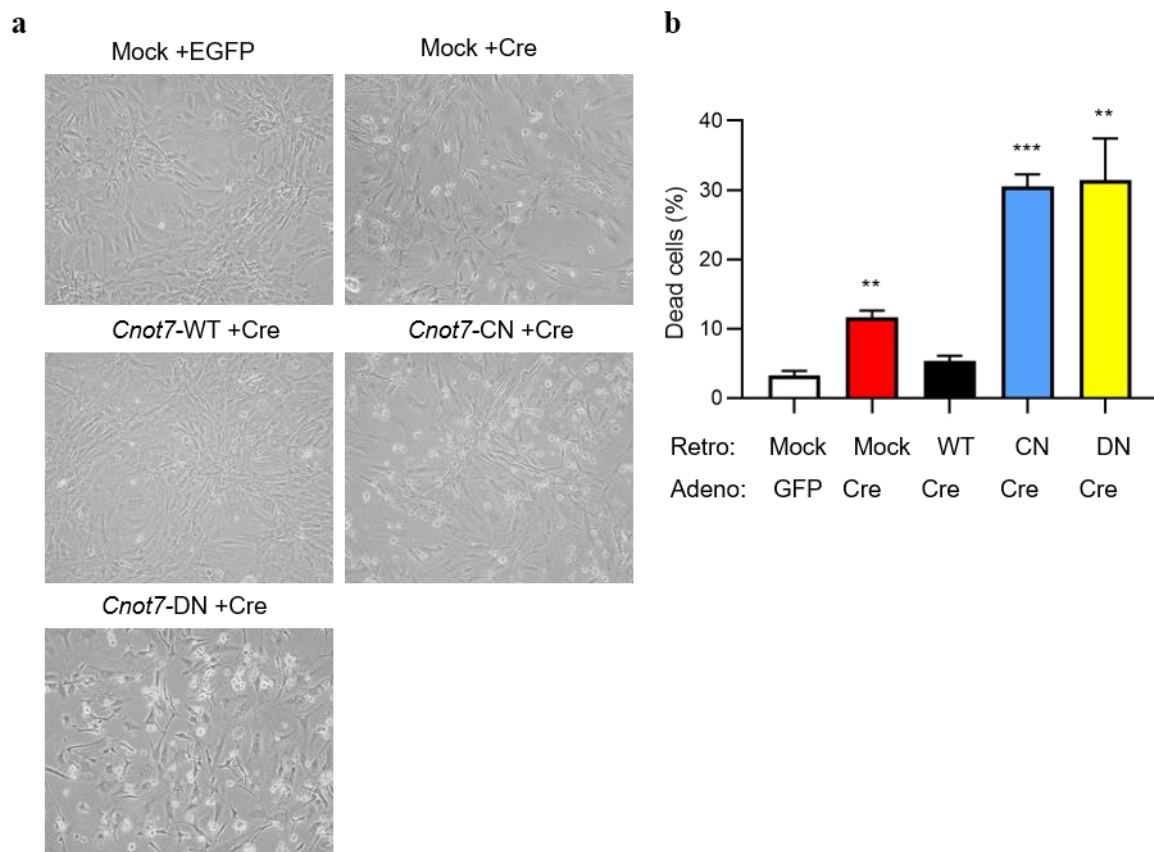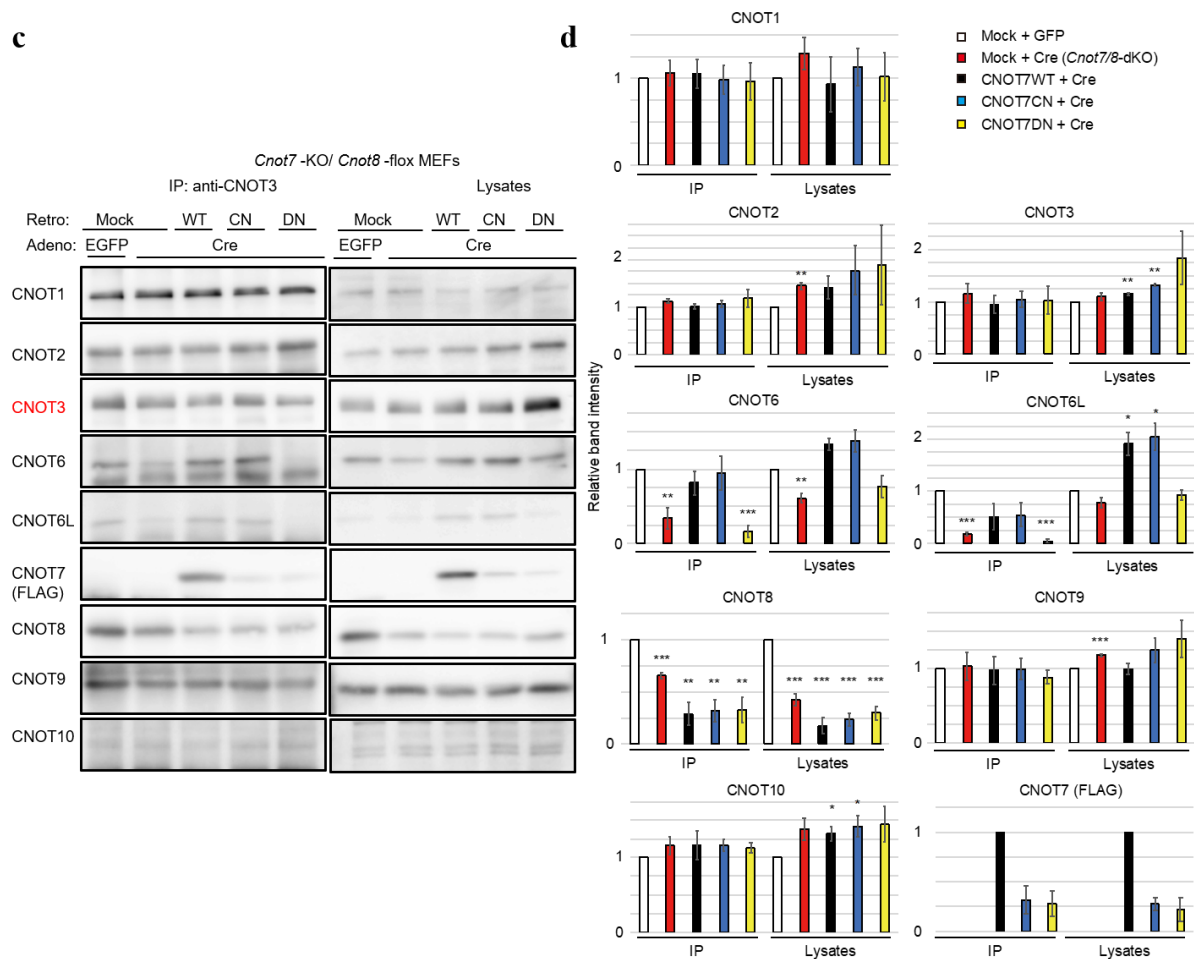
Figure 3.5 CNOT7 catalytic activity is sufficient to maintain MEF viability

(a) Morphology of *Cnot7*-KO/*Cnot8*-flox MEFs infected with the indicated (retro + adeno) viruses. (**b**) Cell death was assessed as in Figure 3.1d (n=3). (**c**) Lysates were prepared from *Cnot7*-KO/*Cnot8*-flox MEFs infected with the indicated viruses and subjected to immunoprecipitation with anti-CNOT3 antibody. CNOT3 is shown in red to indicate a precipitated molecule. Lysates and IP were analyzed by immunoblot. WT: CNOT7 wild-type, CN: CNOT7 lacking catalytic activity, DN: CNOT7 dominant negative mutant which lacks catalytic activity and an ability to bind to CNOT6/6L. (**d**) Quantification of the immunoblot data in Figure 3.5c. Relative band intensities normalized to those of IP or lysates in control MEFs are shown (n=3). Data are presented as mean ± S.E.M. *$P<0.05$, **$P<0.01$, ***$P< 0.001$.

3.3.4   Poly(A) tail length of bulk RNAs is elongated in *Cnot1*-KO and *Cnot7/8*-dKO MEFs

I next compared deadenylase activity in *Cnot1*-KO, *Cnot7/8*-dKO, and *Cnot6/6l*-dKO MEFs with their respective controls, and then examined poly(A) tail lengths of bulk RNAs. In *Cnot1*-KO and *Cnot7/8*-dKO MEFs, the population of mRNAs with poly(A) tail lengths longer than 50 nt increased, while the population of mRNAs with poly(A) tail lengths shorter than 40 nt decreased (Figure 3.6a, b). On the other hand, the distribution of poly(A) tail lengths was similar in control and *Cnot6/6l*-dKO MEFs (Figure 3.6c). I observed a slight increase in the population of mRNAs with poly(A) tail lengths of 50 to 100 nt, which is reminiscent of what occurs in poly(A)-binding protein (PABP)-mediated prevention of deadenylation, though the effect was smaller than in human cancer cell lines (30). These data suggest that deadenylase activity is largely impaired in *Cnot1*-KO and *Cnot7/8*-dKO, but not in *Cnot6/6l*-dKO MEFs.

a

b

c
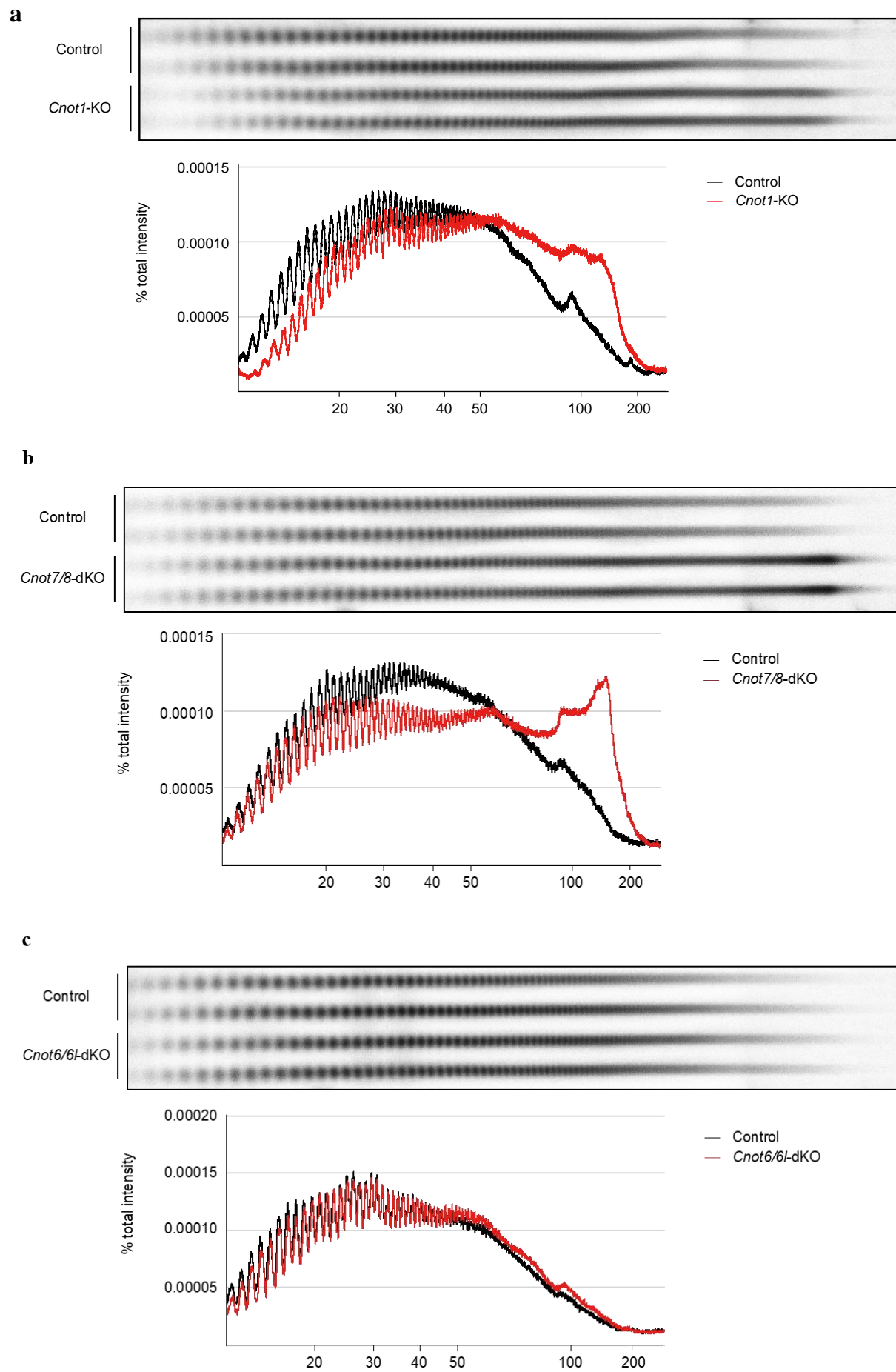
Figure 3.6 (previous page) RNAs in *Cnot1*-KO and *Cnot7/8*-dKO MEFs have longer poly(A) tails compared to those in *Cnot6/6l*-dKO MEFs

(**a-c**) Poly(A) tail lengths of bulk RNA in *Cnot1*-KO (**a**), *Cnot7/8*-dKO (**b**) and *Cnot6/6l*-dKO MEFs (**c**) (n=2 for each genotype). *Cnot1*-flox MEFs infected with mock retrovirus, *Cnot7*$^{+/+}$; *Cnot8*-flox MEFs infected with mock retrovirus, and WT MEFs were used as controls, respectively. Densitograms of poly(A) tail lengths are shown below each image. The mean of two independent experiments was used. This experiment was done by Dr. Akiko Yanagiya.

3.3.5 Upregulation and stabilization of mRNAs in *Cnot1*-KO and *Cnot7/8*-dKO MEFs compared to *Cnot6/6l*-dKO MEFs

To examine the effects of impaired deadenylation on global gene expression, I performed total RNA-seq analysis on *Cnot1*-KO, *Cnot7/8*-dKO, *Cnot6/6l*-dKO MEFs and their respective controls. I found that 8257, 1344, and 710 mRNAs were upregulated more than 2-fold in *Cnot1*-KO, *Cnot7/8*-dKO, and *Cnot6/6l*-dKO MEFs, respectively, compared with controls (Figure 3.7a). The number of upregulated mRNAs in *Cnot7/8*-dKO MEFs was much smaller than that in *Cnot1*-KO MEFs (Figure 3.3a). In addition, only a few mRNAs decreased in *Cnot1*-KO MEFs, whereas 662 mRNAs decreased in *Cnot7/8*-dKO MEFs when compared with their respective controls (Figure 3.7a). Similar results were observed in MCF7 (Aslam et al., 2009). These data suggest that CNOT7/8 have deadenylation-independent, CNOT1-independent roles. The difference in gene expression between control and *Cnot6/6l*-dKO MEFs was less prominent (Figure 3.7a).

I next assessed stability of mRNAs based on calculation of mRNA half-lives following Act. D chase. The number of stabilized mRNAs was much greater than that of destabilized mRNAs in both *Cnot1*-KO and *Cnot7/8*-dKO MEFs (Figure 3.7b). While around 2000 mRNAs were stabilized in *Cnot6/6l*-dKO MEFs, a similar number of mRNAs was destabilized (Figure 3.7b). More than 70% of upregulated mRNAs in *Cnot7/8*-dKO or *Cnot6/6l*-dKO MEFs overlapped with those in *Cnot1*-KO MEFs (Figure 3.7c). Similar results were observed in stabilized mRNAs (Figure 3.7d). In contrast, less than 50% of upregulated or stabilized mRNAs in *Cnot6/6l*-dKO were observed in *Cnot7/8*-dKO MEFs (Figure 3.7c, d). These data, together with MEF viability data, suggest that the upregulated and stabilized mRNAs common to both *Cnot1*-KO and *Cnot7/8*-dKO, but not *Cnot6/6l*-dKO MEFs, are relevant to death of MEFs. Gene ontology (GO) analysis indicated that stabilized mRNAs overlapping between *Cnot1*-KO and *Cnot7/8*-dKO, but not *Cnot6/6l*-dKO MEFs showed significant enrichment for

molecules pertaining to "response to DNA damage stimulus" and "DNA damage repair" (Figure 3.7e).

e

Stabilized in *Cnot1*-KO and *Cnot7/8*-dKO but not *Cnot6/6l*-dKO

Stabilized in *Cnot1*-KO and *Cnot6/6l*-dKO but not *Cnot7/8*-dKO
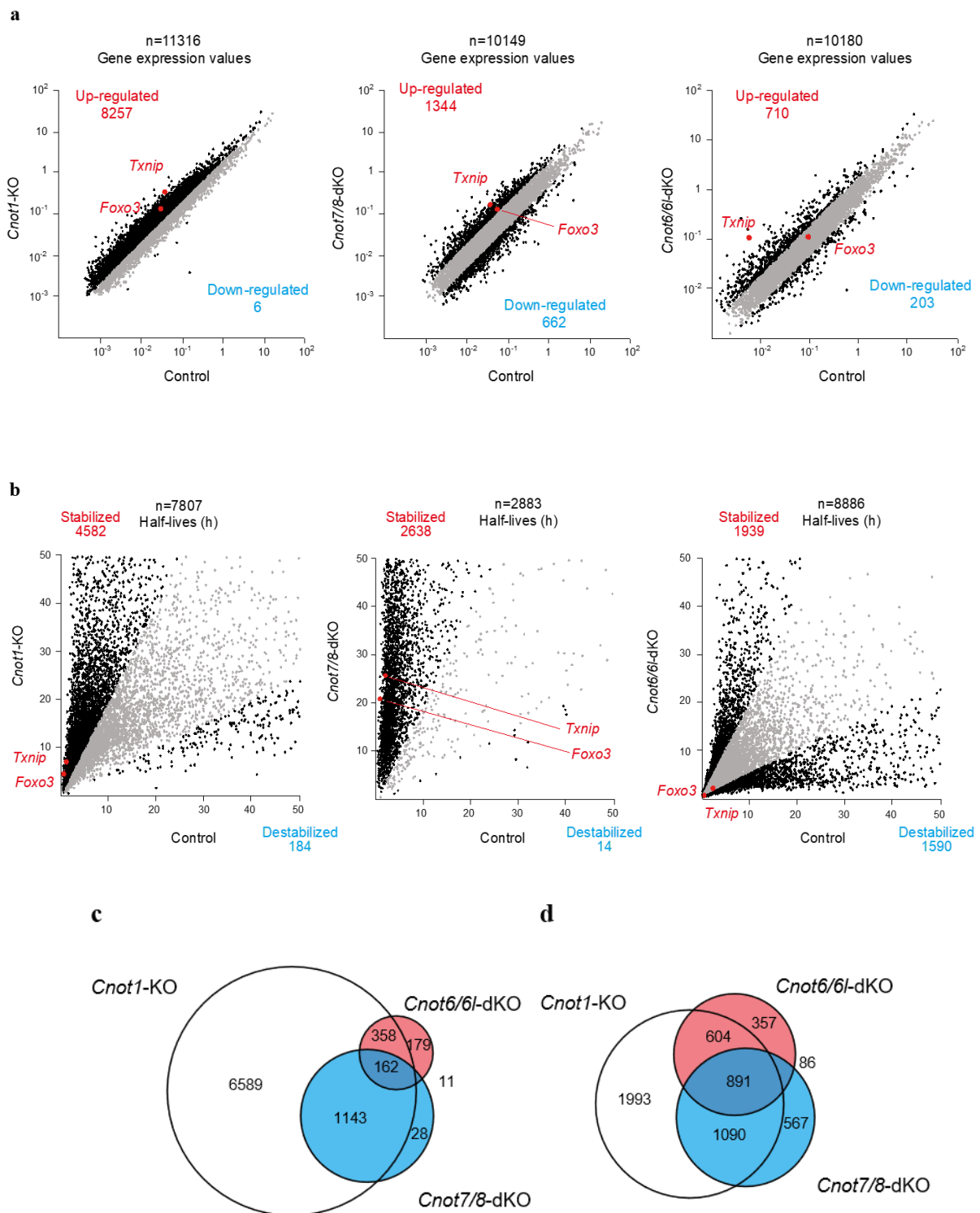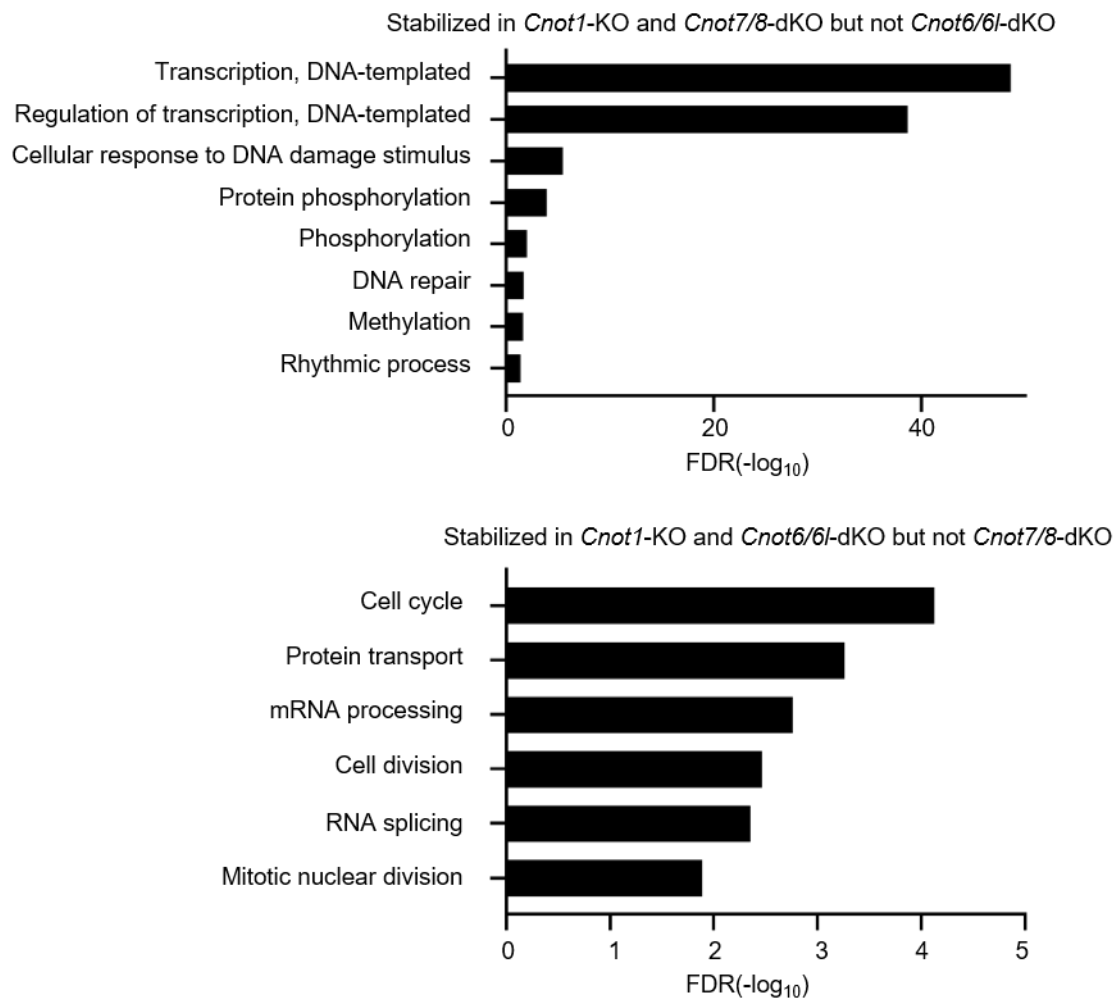
Figure 3.7 Gene expression and mRNA stability differ among *Cnot1*-KO, *Cnot7/8*-dKO and *Cnot6/6l*-dKO MEFs

RNA-seq analysis of *Cnot1*-KO, *Cnot7/8*-dKO and *Cnot6/6l*-dKO MEFs compared to controls: *Cnot1*-flox MEFs infected with mock retrovirus, *Cnot7*$^{+/+}$; *Cnot8*-flox MEFs infected with mock retrovirus and WT MEFs, respectively (n=2). (**a**, **b**) Scatter plots comparing gene expression values (**a**) or mRNA half-lives (**b**). mRNAs showing expression (**a**) or half-lives (**b**) that differed more than 2-fold are displayed in black. All values represent means of two independent experiments. (**c**, **d**) Venn diagrams showing overlap of upregulated (**c**) or stabilized genes (**d**) (more than 2-fold) in *Cnot*1-KO, *Cnot7/8*-dKO and *Cnot6/6l*-dKO MEFs compared to controls. (**e**) GO analysis of mRNAs stabilized in *Cnot1*-KO and *Cnot7/8*-dKO but not *Cnot6/6l*-dKO (upper), or *Cnot1*-KO and *Cnot6/6l*-dKO but not *Cnot7/8*-dKO MEFs (lower). Bar charts of the GO terms (Biological Process) ranked by FDR (< 0.05) are shown.

Finally, I validated the results of RNA-seq by performing qPCR analysis. I first examined levels of *Foxo3* and *Txnip* mRNAs, which are stabilized in both *Cnot1*-KO and *Cnot7/8*-dKO, but not *Cnot6/6l*-dKO MEFs in our RNA-seq results (Figure 3.7b). *Foxo3* and *Txnip* mRNAs were significantly upregulated in *Cnot1*-KO and *Cnot7/8*-dKO MEFs, but not in *Cnot6/6l*-dKO MEFs, compared to controls (Figure 3.8a). I next assessed their stability using total RNAs from Act. D-treated cells. Consistent with the results of RNA-seq, both *Foxo3* and *Txnip* mRNAs had significantly elongated half-lives in *Cnot1*-KO and *Cnot7/8*-dKO MEFs, compared to controls (Figure 3.8b). Elongation of their half-lives was less obvious in *Cnot6/6l*-dKO MEFs (Figure 3.8b).
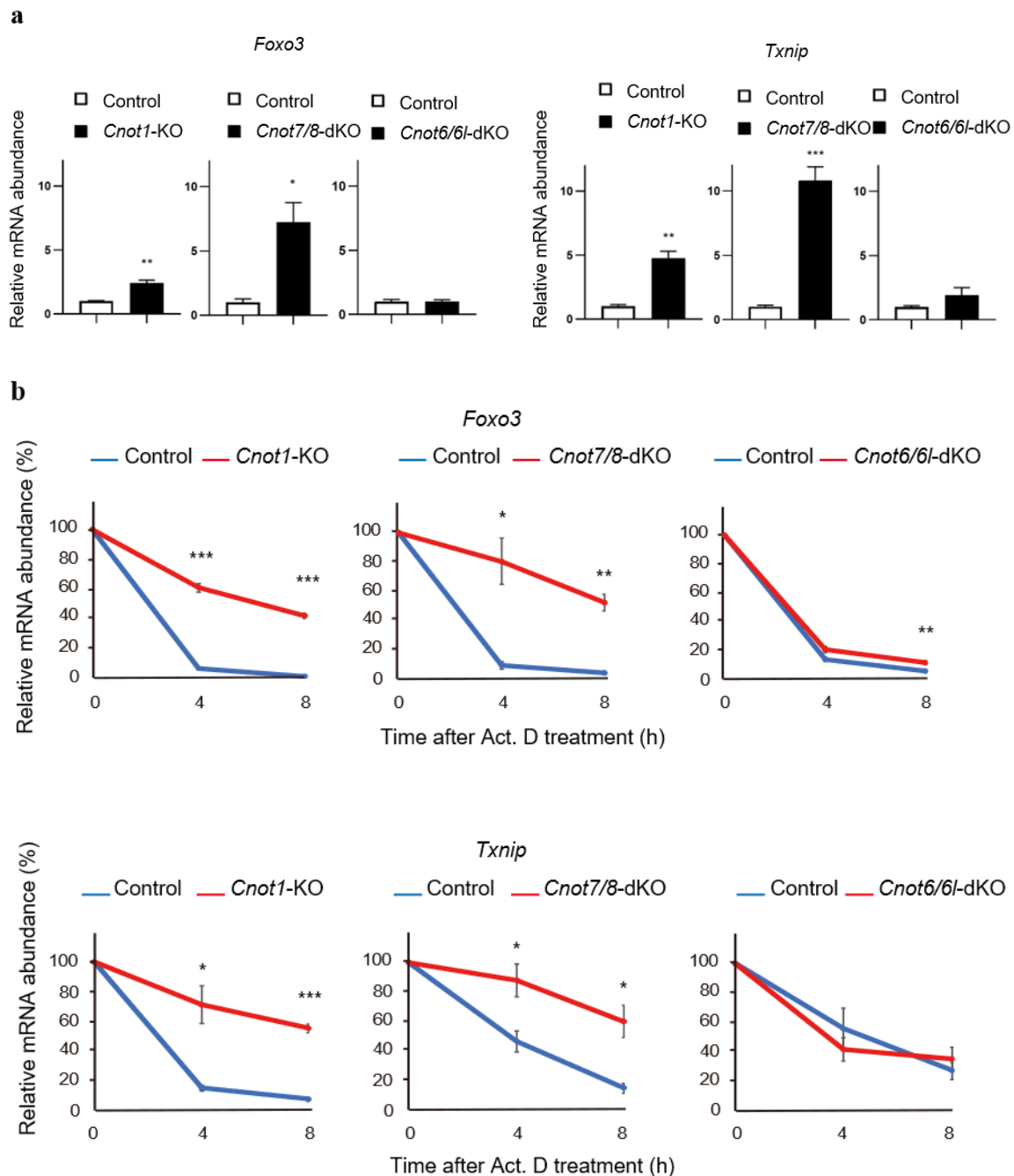
Figure 3.8 *Foxo3* and *Txnip* mRNAs are upregulated and stabilized in *Cnot1*-KO and *Cnot7/8*-dKO MEFs

(**a**) qPCR analysis of the indicated mRNAs in *Cnot1*-KO, *Cnot7/8*-dKO and *Cnot6/6l*-dKO MEFs together with their controls, as in Figure 3.7. Relative mRNA levels were determined by qPCR and normalized to the *Gapdh* mRNA level (n=3). (**b**) Decay curves of mRNAs. Total RNAs were prepared from the indicated MEFs treated with Act. D (0, 4 or 8h). Relative mRNA levels were determined as in (**a**). mRNA levels without Act. D treatment (0h) were set to 100% (n=3). Data are presented as mean ± S.E.M. *$P<0.05$, **$P<0.01$, ***$P<0.001$.

3.4   Discussion

Suppression of the CCR4-NOT complex causes severe defects in cytoplasmic deadenylation and subsequent degradation of mRNA (Bartlam and Yamamoto, 2010; Collart and Panasenko, 2012; Tucker et al., 2001). Although many studies have addressed its function in various organisms, it was not clear whether its different catalytic subunits serve distinct biological functions. In this study, I showed that CNOT7/8, but not CNOT6/6L, are essential for viability in MEFs. It is important to emphasize that I evaluated the roles of the CCR4-NOT complex in normal cells, by using primary fibroblasts with a less likelihood of mutation, in contrast to cancer cell lines. The latter usually contain genetic mutations that promote tumorigenesis, with the consequence that malignant cells are governed by different molecular mechanisms and signaling pathways than normal cells.

The decreased viability of *Cnot7/8*-dKO MEFs was concomitant with a lack of all the catalytic subunits in the CCR4-NOT complex (Figure 3.2 and 3.3a). Reintroduction of CNOT7-WT in *Cnot7/8*-dKO MEFs recovered cell viability; however, expression of CNOT7-CN and CNOT-DN mutants did not (Figure 3.5). This suggests that CNOT7 catalytic activity is critical in maintenance of viability because the existence of CNOT6/6L in the complex with the introduction of CNOT7-CN mutant didn't recover MEF viability. Thus, a complex composed of CNOT6/6L, catalytically inactive CNOT7, CNOT1 and other subunits fails to function as an intact deadenylation complex for maintenance of cell viability.

Gene expression profiling using RNA-seq revealed a larger contribution of CNOT7/8 than CNOT6/6L in regulation of global gene expression in MEFs. Similar results have been observed in human cell lines, trypanosomes and *Drosophila* (Schwede et al., 2008; Temme et al., 2004). Remarkably, the catalytic effect of CNOT7/8 was more prominent than that of CNOT6/6L, as is evident from the results of bulk poly(A) tail analysis, which are clearly reflected in mRNA expression (Mittal et al., 2011; Temme et al., 2004) and this study. Absence of all known catalytic subunits may partly explain the greater differences in gene expression and mRNA stability observed in *Cnot7/8*-dKO MEFs compared to *Cnot6/6l*-dKO MEFs, as in cell viability. Although CNOT6/6L are not anymore part of the CCR4-NOT complex in *Cnot7/8*-dKO MEFs, genes affected by *Cnot6/6l*-dKO were not mostly contained within the set of mRNAs affected by *Cnot7/8*-dKO. A similar observation was reported in a previous study (Mittal et al., 2011). It is possible that CNOT6/6L deadenylate distinct set of genes apart from its association with CNOT7/8 in the CCR4-NOT complex. Interestingly, purified

CNOT7/8 and CNOT6/6L exhibit deadenylase activity *in vitro* (Horiuchi et al., 2009; Raisch et al., 2019; Wang et al., 2010). It would be intriguing to examine whether there are complex-independent CNOT7/8 and CNOT6/6L functions *in vivo*.

While target mRNAs and biological processes vary by species (human or mouse) or cellular status (transformed or non-transformed), there seems to be a common mechanism by which CNOT7/8 and CNOT6/6L regulate distinct groups of mRNAs and biological processes. In MCF7, CNOT7/8 are required for cell proliferation, whereas CNOT6/6L are required for cell viability (Mittal et al., 2011). Furthermore, upon CNOT7/8 suppression, upregulated or stabilized mRNAs showed limited overlap with those upregulated or stabilized by CNOT6/6L suppression. A recently proposed model of deadenylation considers the critical involvement of PABP on mRNAs, suggesting distinct roles of CNOT7/8 and CNOT6/6L. Specifically, CNOT7/8 deadenylate PABP-free poly(A) tails until they encounter PABP, and then CNOT6/6L take over, removing PABP and subsequently deadenylating mRNAs (Webster et al., 2018; Yi et al., 2018). Importantly, different cell types and cells under different conditions vary in their PABP local availability (Yi et al., 2018). This may partly explain the context-dependent deadenylation activity of CNOT7/8 and CNOT6/6L. In *S. cerevisiae*, mRNAs have higher Pab1 (PABP in yeast) occupancy and consequently, Ccr4, rather than Caf1, contributes significantly to deadenylation (Webster et al., 2018). Similarly, mRNAs are saturated with PABP in HeLa cells and are deadenylated mainly by CNOT6/6L (Yi et al., 2018). Posttranscriptional regulators as miRNA could affect PABP availability. Active translation state is relevant to the abundance of PABP on mRNA. Binding of PABP to mRNA is important for translation initiation and elongation, because the translation initiation factor complex and PABP interact on mRNAs to form closed-loop messenger ribonucleoprotein complexes (Wells et al., 1998). On the other hand, miRNA-mediated translational repression causes dissociation of PABP from mRNA, leading to mRNA degradation (Zekri et al., 2013). It is possible that CNOT6/6L or CNOT7/8 preferentially target mRNAs which are translationally active (abundant PABP) or silent (less PABP), respectively, resulting in different biological roles. Global analysis of translation status using ribosome profiling should be useful to determine whether CNOT6/6L and CNOT7/8 activities are dependent on the mRNA translation status.

Several lines of evidence show that in addition to its function as a deadenylase, the CCR4-NOT complex has nuclear roles in transcription and mRNA export (Collart, 2016). In *S. cerevisiae*, the CCR4-NOT complex interacts with TATA binding protein (TBP) and TBP-associated factor (TAF) to suppress transcription initiation (Badarinarayana et al., 2000; Collart

and Struhl, 1994). It also stimulates transcription elongation through its association with RNA polymerase II complexes (Kruk et al., 2011). Moreover, the CCR4-NOT complex is involved in transcriptional regulation in mammals (Cejas et al., 2017; Garapaty et al., 2008; Hu et al., 2009; Neely et al., 2010; Winkler et al., 2006). In our RNA-seq results, not all upregulated mRNAs in *Cnot1*-KO MEFs corresponded to stabilized mRNAs (Figure 3.7). Our group previously observed dysregulation in transcriptional mechanisms upon suppression of CNOT1 or CNOT3 in adipose tissue and in liver, respectively (Suzuki et al., 2019; Takahashi et al., 2019). These data suggest that suppression of the CCR4-NOT complex transcriptional and other nuclear roles could be responsible for upregulation of a subset of genes. Moreover, down regulation of a significant number of genes in *Cnot7/8*-dKO is possibly due to loss of the catalytic activity-independent function of CNOT7/8, which positively affects transcription. Indeed, CNOT7/8 play a positive role in regulating transcription mediated by the nuclear receptors, ERα and RARβ (Morel et al., 2003; Nakamura et al., 2004; Prevot et al., 2001).

There was not any obvious abnormalities in mouse embryonic development (Mostafa et al, 2020), growth to adulthood, or MEF viability in the absence of CNOT6/6L, suggesting that CNOT6/6L do not target mRNAs encoding molecules involved in those processes. It is also possible that CNOT7/8-mediated deadenylation is sufficient to regulate those mRNAs. Yet, CNOT6/6L-mediated mRNA decay is still central to certain biological events. For example, CNOT6/6L are critical to survival of MCF7 (Mittal et al., 2011). In NIH3T3 mouse fibroblasts, knockdown of CNOT6L causes a severe reduction in proliferation, concomitant with significant stabilization of *p27kip1* mRNA (Morita et al., 2007). I found that mRNAs encoding molecules involved in cell proliferation were enriched among stabilized mRNAs in *Cnot6/6l*-dKO MEFs. Therefore, CNOT6/6L likely regulate proliferation of fibroblasts without affecting viability. Furthermore, *Cnot6l*-KO mice exhibit resistance to diet-induced obesity, enhanced energy expenditure, and improved insulin sensitivity (Morita et al., 2019).

While both *Cnot7*-KO and *Cnot8*-KO MEFs are viable, *Cnot7/8*-dKO MEFs undergo death. This is consistent with functional redundancy of CNOT7 and CNOT8, owing to their high amino acid sequence similarity (Aslam et al., 2009). Despite this functional redundancy in some contexts, as in MEFs (in this study) and MCF7 cells (Aslam et al., 2009), they play distinct roles (Berthet et al., 2004; Koch et al., 2014; Nakamura et al., 2004). *Cnot8*-KO mice die in embryo (Mostafa et al, 2020). A specific developmental role of CNOT8 is also observed in zebrafish (Koch et al., 2014). Attenuation of *Cnot8* in zebrafish caused upregulation of developmental control genes and early lethality (Koch et al., 2014). Reciprocally, *Cnot7*-KO

male mice have defects in spermatogenesis, even in the presence of CNOT8 (Berthet et al., 2004; Nakamura et al., 2004). Differential expression of CNOT7 and CNOT8 could be relevant to their specific roles, as previously reported in mouse neural tissues (Chen et al., 2011a). Furthermore, their interaction with different proteins may affect their substrate specificities and consequently their biological roles. For instance, SMG5/7 endonucleases, which function in nonsense-mediated mRNA decay (NMD), preferentially interact with CNOT8 rather than with CNOT7 (Loh et al., 2013). Importantly, NMD is essential for embryonic development and viability (Hwang and Maquat, 2011). In such a way, I cannot exclude the possibility that CNOT8 functions in zebrafish or mouse embryonic development independently of its catalytic activity in the CCR4-NOT complex. Further analyses are necessary to address the molecular basis for the distinctive functions of CNOT7 and CNOT8.

To conclude, the data presented in this chapter suggest that maintenance of cell viability is one of the fundamental roles of the CCR4-NOT complex, which is mediated mainly by the catalytic activity of the CNOT7/8. Their vital importance in regulating global mRNA expression is clearly reflected in global gene expression. On the other hand, CNOT6/6L are dispensable in MEF viability. However, relatively few biological processes have been examined to date. Mouse strains generated with null or conditional alleles for catalytic subunits of the CCR4-NOT complex are valuable tools to analyze functions of each catalytic subunit in various tissues and biological contexts.

4   Conclusion and Future prospects

In this thesis, I uncovered a novel physiological role of CNOT3 in pancreatic β cells. In line with my observation that the CCR4-NOT complex expression is deregulated in islets from diabetic mice, suppression of the CCR4-NOT complex activity in β cells by knocking out *Cnot3* led to glucose intolerance and diabetes. These findings raise the possibility that changes in CNOT3 expression may contribute to β cell failure in T2D in humans. Thus, it would be informative to investigate the expression of CNOT3 in diabetic patients versus healthy donor β cells.

In my model, CNOT3 deletion occurs embryonically at the onset of insulin gene expression. Thus, the data I presented here support the role of CNOT3 in the maturation of β cells especially the classical markers of β cell maturation such as: MAFA and UCN3 were suppressed in *Cnot3*βKO islets. These data may contribute to the development of diabetes therapy through enabling the understanding of the molecular mechanisms that are critical for β cell maturation. Achieving β cell maturation presents a major challenge in the generation of functional β cells *in vitro* from embryonic stem cells (D'Amour et al., 2006) or replication from existing β cells (Russ et al., 2008) and this can only be tackled with a clear understanding of the complex genetic programs that produce and maintain functional β cells. It is currently tempting to check if CNOT3 expression varies between different developmental stages: progenitor cells, fetal, immature and mature β cells. Studying the effects of knocking out CNOT3 at each of these stages would determine whether CNOT3 plays a role in differentiation and progression from one stage to another. Moreover, in this study I focused on elucidating the role of CNOT3 in β cells only. It will be interesting to investigate its role in other islet cells.

A detailed molecular mechanism of CNOT3 role in pancreatic β cell function is yet to be investigated. Future efforts could shed novel light on RBPs that mediate the interaction of CNOT3 with its target genes in β cells. Other mechanisms of CNOT3 function rather than mRNA decay are still possible. Global elongation of bulk poly(A) tails in *Cnot3*βKO islets motivated me to find out mRNA targets that CNOT3 is involved in their decay. I suggested that CNOT3 is involved in mRNA decay of *Aldob* and *Slc5a10* that are known to be upregulated in T2D islets and cause β cell dysfunction (Haythorne et al., 2019). Additionally, I suggested the involvement of CNOT3 in the regulation of β cell disallowed genes through direct and indirect mechanisms. β cell disallowed genes are presently attractive to study as little is known about their functions and the mechanisms involved in their suppression. They hold a

good promise as targets for treatment of diabetes because their de-repression contributes to T2D.

A secondary goal of my thesis was to compare the effect of the deletion of the deadenylase subunits on CCR4-NOT complex structure and function in MEFs. I concluded that either Ccr4-type or Caf1-type deadenylase can have the main deadenylase activity depending on the context. The specific KO MEFs I generated in this study form important set of tools that will be highly useful to untangle paralog-specific molecular functions of CNOT7 and/or CNOT8 and CNOT6 and/or CNOT6L.

Finally, the work in this thesis complements functional studies of the CCR4-NOT complex in mammals. Particularly studies investigating its physiological roles, contribution to development and pathological implications. Obviously, loss of subunits of the CCR4-NOT complex results in serious abnormalities in embryonic development and tissue function, suggesting that it is worth to continue studying the biological activities of this complex. This may pave the way for eventual development of therapeutics.

5 References

1. Adachi, S., and Natsume, T. (2015). Purification of noncoding RNA and bound proteins using FLAG peptide-conjugated antisense-oligonucleotides. In Nuclear Bodies and Noncoding RNAs: Methods and Protocols, S. Nakagawa, and T. Hirose, eds. (New York, NY: Springer New York), pp. 265-274.

2. Alcazar, O., Tiedge, M., and Lenzen, S. (2000). Importance of lactate dehydrogenase for the regulation of glycolytic flux and insulin secretion in insulin-producing cells. Biochemical Journal *352*, 373-380.

3. Andrali, Sreenath S., Sampley, Megan L., Vanderford, Nathan L., and Özcan, S. (2008). Glucose regulation of insulin gene expression in pancreatic β-cells. Biochemical Journal *415*, 1-10.

4. Ashcroft, F., and Rorsman, P. (2004). Type 2 diabetes mellitus: not quite exciting enough? Human Molecular Genetics *13,* 21-31.

5. Ashcroft, Frances M., and Rorsman, P. (2012). Diabetes mellitus and the β Cell: the last ten years. Cell *148*, 1160-1171.

6. Ashworth, W., Stoney, P.N., and Yamamoto, T. (2019). States of decay: The systems biology of mRNA stability. Current Opinion in Systems Biology *15*, 48-57.

7. Aslam, A., Mittal, S., Koch, F., Andrau, J.-C., and Winkler, G.S. (2009). The Ccr4-NOT deadenylase subunits CNOT7 and CNOT8 have overlapping roles and modulate cell proliferation. Molecular Biology of the Cell *20*, 3840-3850.

8. Azzouz, N., Panasenko, O.O., Deluen, C., Hsieh, J., Theiler, G., and Collart, M.A. (2009). Specific roles for the Ccr4-Not complex subunits in expression of the genome. RNA *15*, 377-383.

9. Badarinarayana, V., Chiang, Y.C., and Denis, C.L. (2000). Functional interaction of CCR4-NOT proteins with TATAA-binding protein (TBP) and its associated factors in yeast. Genetics *155*, 1045-1054.

10. Baroukh, N., Ravier, M.A., Loder, M.K., Hill, E.V., Bounacer, A., Scharfmann, R., Rutter, G.A., and Van Obberghen, E. (2007). MicroRNA-124a regulates Foxa2 expression and intracellular signaling in pancreatic β-cells lines. Journal of Biological Chemistry *282*, 19575-19588.

11. Bartel, D.P. (2009). MicroRNA target recognition and regulatory functions. Cell *136*, 215-233.

12. Bartlam, M., and Yamamoto, T. (2010). The structural basis for deadenylation by the CCR4-NOT complex. Protein & Cell *1*, 443-452.

13. Basquin, J., Roudko, V.V., Rode, M., Basquin, C., Séraphin, B., and Conti, E. (2012). Architecture of the nuclease module of the yeast Ccr4-Not complex: the Not1-Caf1-Ccr4 interaction. Molecular Cell *48*, 207-218.

14. Bawankar, P., Loh, B., Wohlbold, L., Schmidt, S., and Izaurralde, E. (2013). NOT10 and C2orf29/NOT11 form a conserved module of the CCR4-NOT complex that docks onto the NOT1 N-terminal domain. RNA biology *10*, 228-244.

15. Becker, T.C., BeltrandelRio, H., Noel, R.J., Johnson, J.H., and Newgard, C.B. (1994). Overexpression of hexokinase I in isolated islets of Langerhans via recombinant adenovirus. Enhancement of glucose metabolism and insulin secretion at basal but not stimulatory glucose levels. Journal of Biological Chemistry *269*, 21234-21238.

16. Behm-Ansmant, I., Rehwinkel, J., Doerks, T., Stark, A., Bork, P., and Izaurralde, E. (2006). mRNA degradation by miRNAs and GW182 requires both CCR4:NOT deadenylase and DCP1:DCP2 decapping complexes. Genes & Development *20*, 1885-1898.

17. Bellomo, E.A., Meur, G., and Rutter, G.A. (2011). Glucose regulates free cytosolic Zn2+ concentration, Slc39 (ZiP), and metallothionein gene expression in primary pancreatic islet β-Cells. Journal of Biological Chemistry *286*, 25778-25789.

18. Benninger, R.K., and Piston, D.W. (2014). Cellular communication and heterogeneity in pancreatic islet insulin secretion dynamics. Trends in Endocrinology and Metabolism *25*, 399-406.

19. Berthet, C., Morera, A.M., Asensio, M.J., Chauvin, M.A., Morel, A.P., Dijoud, F., Magaud, J.P., Durand, P., and Rouault, J.P. (2004). CCR4-associated factor CAF1 is an essential factor for spermatogenesis. Molecular Cellular Biology *24*, 5808-5820.

20. Bhandari, D., Raisch, T., Weichenrieder, O., Jonas, S., and Izaurralde, E. (2014). Structural basis for the Nanos-mediated recruitment of the CCR4–NOT complex and translational repression. Genes & Development *28*, 888-901.

21. Blandino-Rosano, M., Scheys, J.O., Jimenez-Palomares, M., Barbaresso, R., Bender, A.S., Yanagiya, A., Liu, M., Rui, L., Sonenberg, N., and Bernal-Mizrachi, E. (2016). 4E-BP2/SH2B1/IRS2 are part of a novel feedback loop that controls β-cell mass. Diabetes *65*, 2235-2248.

22. Blum, B., Hrvatin, S., Schuetz, C., Bonal, C., Rezania, A., and Melton, D.A. (2012). Functional beta-cell maturation is marked by an increased glucose threshold and by expression of urocortin 3. Nature Biotechnology *30*, 261-264.

23. Boland, A., Chen, Y., Raisch, T., Jonas, S., Kuzuoğlu-Öztürk, D., Wohlbold, L., Weichenrieder, O., and Izaurralde, E. (2013). Structure and assembly of the NOT module of the human CCR4–NOT complex. Nature Structural & Molecular Biology *20*, 1289-1297.

24. Braun, Joerg E., Huntzinger, E., Fauser, M., and Izaurralde, E. (2011). GW182 proteins directly recruit cytoplasmic deadenylase complexes to miRNA targets. Molecular Cell *44*, 120-133.

25. Braun, J.E., Huntzinger, E., and Izaurralde, E. (2013). The role of GW182 proteins in miRNA-mediated gene silencing. In Ten Years of Progress in GW/P Body Research, L.E.K. Chan, and J.M. Fritzler, eds. (New York, NY: Springer New York), pp. 147-163.

26. Brennan, C.M., and Steitz, J.A. (2001). HuR and mRNA stability. Cellular and Molecular Life Sciences CMLS *58*, 266-277.

27. Burke, S.J., Batdorf, H.M., Burk, D.H., Noland, R.C., Eder, A.E., Boulos, M.S., Karlstad, M.D., and Collier, J.J. (2017). db/db mice exhibit features of human type 2 diabetes that are not present in weight-matched C57BL/6J mice fed a western diet. Journal of Diabetes Research *2017*, 8503754-8503754.

28. Butler, A.E., Janson, J., Bonner-Weir, S., Ritzel, R., Rizza, R.A., and Butler, P.C. (2003). β-cell deficit and increased β-cell apoptosis in humans with type 2 diabetes. Diabetes *52*, 102-110.

29. Cejas, P., Cavazza, A., Yandava, C.N., Moreno, V., Horst, D., Moreno-Rubio, J., Burgos, E., Mendiola, M., Taing, L., Goel, A.*, et al.* (2017). Transcriptional regulator CNOT3 defines an aggressive colorectal cancer subtype. Cancer Research *77*, 766-779.

30. Cerf, M.E. (2006). Transcription factors regulating beta-cell function. European Journal of Endocrinology *155*, 671-679.

31. Chekulaeva, M., Mathys, H., Zipprich, J.T., Attig, J., Colic, M., Parker, R., and Filipowicz, W. (2011). miRNA repression involves GW182-mediated recruitment of CCR4–NOT through conserved W-containing motifs. Nature Structural & Molecular Biology *18*, 10.1038/nsmb.2166.

32. Chen, C.-Y.A., Ezzeddine, N., and Shyu, A.-B. (2008). Messenger RNA half-life measurements in mammalian cells. Methods in Enzymology *448*, 335-357.

33. Chen, C.-Y.A., and Shyu, A.-B. (2011). Mechanisms of deadenylation-dependent decay. WIREs RNA *2*, 167-183.

34. Chen, C.-Y.A., Zheng, D., Xia, Z., and Shyu, A.-B. (2009). Ago-TNRC6 complex triggers microRNA-mediated mRNA decay by promoting biphasic deadenylation followed by decapping. Nature Structural & Molecular Biology *16*, 1160-1166.

35. Chen, C., Ito, K., Takahashi, A., Wang, G., Suzuki, T., Nakazawa, T., Yamamoto, T., and Yokoyama, K. (2011a). Distinct expression patterns of the subunits of the CCR4–NOT deadenylase complex during neural development. Biochemical and Biophysical Research Communications *411*, 360-364.

36. Chen, H., Gu, X., Liu, Y., Wang, J., Wirt, S.E., Bottino, R., Schorle, H., Sage, J., and Kim, S.K. (2011b). PDGF signalling controls age-dependent proliferation in pancreatic β-cells. Nature *478*, 349-355.

37. Chen, Y., Boland, A., Kuzuoğlu-Öztürk, D., Bawankar, P., Loh, B., Chang, C.-T., Weichenrieder, O., and Izaurralde, E. (2014). A DDX6-CNOT1 Complex and W-Binding Pockets in CNOT9 Reveal Direct Links between miRNA Target Recognition and Silencing. Molecular cell *54*, 737-750.

38. Chera, S., Baronnier, D., Ghila, L., Cigliola, V., Jensen, J.N., Gu, G., Furuyama, K., Thorel, F., Gribble, F.M., Reimann, F., *et al.* (2014). Diabetes recovery by age-dependent conversion of pancreatic [dgr]-cells into insulin producers. Nature *514*, 503-507.

39. Chicoine, J., Benoit, P., Gamberi, C., Paliouras, M., Simonelig, M., and Lasko, P. (2007). Bicaudal-C recruits CCR4-NOT deadenylase to target mRNAs and regulates oogenesis, cytoskeletal organization, and its own expression. Developmental Cell *13*, 691-704.

40. Choi, W., Kaufman, R.J., and Back, S.H. (2014). TRIPLE (Insulin, Glucagon and EGFP) immunofluorescence staining protocol in pancreas. Bio-protocol *4*, e1056.

41. Cinti, F., Bouchi, R., Kim-Muller, J.Y., Ohmura, Y., Sandoval, P.R., Masini, M., Marselli, L., Suleiman, M., Ratner, L.E., Marchetti, P., *et al.* (2016). Evidence of beta-Cell dedifferentiation in human type 2 diabetes. The Journal of Clinical Endocrinology and Metabolism *101*, 1044-1054.

42. Clark, L.B., Viswanathan, P., Quigley, G., Chiang, Y.-C., McMahon, J.S., Yao, G., Chen, J., Nelsbach, A., and Denis, C.L. (2004). Systematic mutagenesis of the Leucine-rich repeat (LRR) domain of CCR4 reveals specific sites for binding to CAF1 and a separate critical role for the LRR in CCR4 deadenylase activity. Journal of Biological Chemistry *279*, 13616-13623.

43. Collart, M.A. (2016). The Ccr4-Not complex is a key regulator of eukaryotic gene expression. Wiley Interdisciplinary Reviews: RNA *7*, 438-454.

44. Collart, M.A., and Panasenko, O.O. (2012). The Ccr4–Not complex. Gene *492*, 42-53.

45. Collart, M.A., and Struhl, K. (1994). NOT1(CDC39), NOT2(CDC36), NOT3, and NOT4 encode a global-negative regulator of transcription that differentially affects TATA-element utilization. Genes & Development *8*, 525-537.

46. D'Amour, K.A., Bang, A.G., Eliazer, S., Kelly, O.G., Agulnick, A.D., Smart, N.G., Moorman, M.A., Kroon, E., Carpenter, M.K., and Baetge, E.E. (2006). Production of pancreatic hormone–expressing endocrine cells from human embryonic stem cells. Nature Biotechnology *24*, 1392-1401.

47. Dhawan, S., Tschen, S.-I., Zeng, C., Guo, T., Hebrok, M., Matveyenko, A., and Bhushan, A. (2015). DNA methylation directs functional maturation of pancreatic β cells. The Journal of Clinical Investigation *125*, 2851-2860.

48. Doidge, R., Mittal, S., Aslam, A., and Winkler, G.S. (2012). Deadenylation of cytoplasmic mRNA by the mammalian Ccr4–Not complex. Biochemical Society Transactions *40*, 896-901.

49. Eckmann, C.R., Rammelt, C., and Wahle, E. (2011). Control of poly(A) tail length. Wiley Interdisciplinary Reviews RNA *2*, 348-361.

50. Edlund, H. (2002). Pancreatic organogenesis -developmental mechanisms and implications for therapy. Nature Reviews Genetics *3*, 524-532.

51. Eliasson, L., Abdulkader, F., Braun, M., Galvanovskis, J., Hoppa, M.B., and Rorsman, P. (2008). Novel aspects of the molecular mechanisms controlling insulin secretion. The Journal of Physiology *586*, 3313-3324.

52. Essig, K., Kronbeck, N., Guimaraes, J.C., Lohs, C., Schlundt, A., Hoffmann, A., Behrens, G., Brenner, S., Kowalska, J., Lopez-Rodriguez, C.*, et al.* (2018). Roquin targets mRNAs in a 3′ -UTR-specific manner by different modes of regulation. Nature Communications *9*, 3810.

53. Eulalio, A., Huntzinger, E., Nishihara, T., Rehwinkel, J., Fauser, M., and Izaurralde, E. (2009). Deadenylation is a widespread effect of miRNA regulation. RNA *15*, 21-32.

54. Fabian, M.R., Cieplak, M.K., Frank, F., Morita, M., Green, J., Srikumar, T., Nagar, B., Yamamoto, T., Raught, B., Duchaine, T.F.*, et al.* (2011). miRNA-mediated deadenylation is orchestrated by GW182 through two conserved motifs that interact with CCR4–NOT. Nature Structural and Molecular Biology *18*, 1211-1217.

55. Fabian, M.R., Frank, F., Rouya, C., Siddiqui, N., Lai, W.S., Karetnikov, A., Blackshear, P.J., Nagar, B., and Sonenberg, N. (2013). Structural basis for the recruitment of the human CCR4–NOT deadenylase complex by tristetraprolin. Nature Structural and Molecular Biology *20*, 735-739.

56. Fabian, M.R., Mathonnet, G., Sundermeier, T., Mathys, H., Zipprich, J.T., Svitkin, Y.V., Rivas, F., Jinek, M., Wohlschlegel, J., Doudna, J.A.*, et al.* (2009). Mammalian miRNA

RISC recruits CAF1 and PABP to affect PABP-dependent deadenylation. Molecular Cell *35*, 868-880.

57. Gaidatzis, D., Burger, L., Florescu, M., and Stadler, M.B. (2015). Analysis of intronic and exonic reads in RNA-seq data characterizes transcriptional and post-transcriptional regulation. Nature Biotechnology *33*, 722-729.

58. Garapaty, S., Mahajan, M.A., and Samuels, H.H. (2008). Components of the CCR4-NOT complex function as nuclear hormone receptor coactivators via association with the NRC-interacting Factor NIF-1. Journal of Biological Chemistry *283*, 6806-6816.

59. Garneau, N.L., Wilusz, J., and Wilusz, C.J. (2007). The highways and byways of mRNA decay. Nature Reviews Molecular Cellular Biology *8*, 113-126.

60. Georgia, S., and Bhushan, A. (2004). β cell replication is the primary mechanism for maintaining postnatal β cell mass. Journal of Clinical Investigation *114*, 963-968.

61. Gerst, F., Jaghutriz, B.A., Staiger, H., Schulte, A.M., Lorza-Gil, E., Kaiser, G., Panse, M., Haug, S., Heni, M., Schütz, M.*, et al.* (2018). The expression of Aldolase B in islets is negatively associated with insulin secretion in humans. The Journal of Clinical Endocrinology & Metabolism *103*, 4373-4383.

62. Goodge, K.A., and Hutton, J.C. (2000). Translational regulation of proinsulin biosynthesis and proinsulin conversion in the pancreaticβ-cell. Seminars in Cell & Developmental Biology *11*, 235-242.

63. Graham, K.L., Fynch, S., Papas, E.G., Tan, C., Kay, T.W.H., and Thomas, H.E. (2016). isolation and culture of the islets of Langerhans from mouse pancreas. Bio-protocol *6*, e1840.

64. Guay, C., Jacovetti, C., Nesca, V., Motterle, A., Tugay, K., and Regazzi, R. (2012). Emerging roles of non-coding RNAs in pancreatic β-cell function and dysfunction. Diabetes, Obesity and Metabolism *14*, 12-21.

65. Guay, C., and Regazzi, R. (2015). Role of islet microRNAs in diabetes: which model for which question? Diabetologia *58*, 456-463.

66. Gutierrez, G.D., Bender, A.S., Cirulli, V., Mastracci, T.L., Kelly, S.M., Tsirigos, A., Kaestner, K.H., and Sussel, L. (2017). Pancreatic beta cell identity requires continual repression of non-beta cell programs. Journal of Clinical Investigation *127*, 244-259.

67. Halban, P.A., Wollheim, C.B., Blondel, B., Meda, P., Niesor, E.N., and Mintz, D.H. (1982). The possible importance of contact between pancreatic islet cells for the control of insulin release. Endocrinology *111*, 86-94.

68. Harris, V.M. (2015). Protein detection by Simple Western™ Analysis. In Western Blotting: Methods and Protocols, B.T. Kurien, and R.H. Scofield, eds. (New York, NY: Springer New York), pp. 465-468.

69. Hasegawa, Y., Hoshino, Y., Ibrahim, A.E., Kato, K., Daitoku, Y., Tanimoto, Y., Ikeda, Y., Oishi, H., Takahashi, S., Yoshiki, A.*, et al.* (2016). Generation of CRISPR/Cas9-mediated bicistronic knock-in *Ins1-Cre* driver mice. Experimental Animals *65*, 319-327.

70. Haythorne, E., Rohm, M., van de Bunt, M., Brereton, M.F., Tarasov, A.I., Blacker, T.S., Sachse, G., Silva dos Santos, M., Terron Exposito, R., Davis, S.*, et al.* (2019). Diabetes causes marked inhibition of mitochondrial metabolism in pancreatic β-cells. Nature Communications *10*, 2474.

71. Heiser, P.W., Lau, J., Taketo, M.M., Herrera, P.L., and Hebrok, M. (2006). Stabilization of β-catenin impacts pancreas growth. Development *133*, 2023-2032.

72. Horiuchi, M., Takeuchi, K., Noda, N., Muroya, N., Suzuki, T., Nakamura, T., Kawamura-Tsuzuku, J., Takahasi, K., Yamamoto, T., and Inagaki, F. (2009). Structural basis for the antiproliferative activity of the Tob-hCaf1 complex. The Journal of Biological Chemistry *284*, 13244-13255.

73. Hu, G., Kim, J., Xu, Q., Leng, Y., Orkin, S.H., and Elledge, S.J. (2009). A genome-wide RNAi screen identifies a new transcriptional module required for self-renewal. Genes & Development *23*, 837-848.

74. Huang, D.W., Sherman, B.T., and Lempicki, R.A. (2008). Systematic and integrative analysis of large gene lists using DAVID bioinformatics resources. Nature Protocols *4*, 44-57.

75. Hwang, J., and Maquat, L.E. (2011). Nonsense-mediated mRNA decay (NMD) in animal embryogenesis: to die or not to die, that is the question. Curr Opin Genet Dev *21*, 422-430.

76. IDF Diabetes Atlas ninth edition (2019).

77. Inada, T., and Makino, S. (2014). Novel roles of the multi-functional CCR4-NOT complex in post-transcriptional regulation. Frontiers in genetics *5*.

78. Inoue, T., Morita, M., Hijikata, A., Fukuda-Yuzawa, Y., Adachi, S., Isono, K., Ikawa, T., Kawamoto, H., Koseki, H., Natsume, T.*, et al.* (2015). CNOT3 contributes to early B cell development by controlling Igh rearrangement and p53 mRNA stability. The Journal of Experimental Medicine *212*, 1465-1479.

79. Ito, K., Inoue, T., Yokoyama, K., Morita, M., Suzuki, T., and Yamamoto, T. (2011a). CNOT2 depletion disrupts and inhibits the CCR4–NOT deadenylase complex and induces apoptotic cell death. Genes to Cells *16*, 368-379.

80. Ito, K., Takahashi, A., Morita, M., Suzuki, T., and Yamamoto, T. (2011b). The role of the CNOT1 subunit of the CCR4-NOT complex in mRNA deadenylation and cell viability. Protein & Cell *2*, 755-763.

81. Kanazawa, A., Tsukada, S., Sekine, A., Tsunoda, T., Takahashi, A., Kashiwagi, A., Tanaka, Y., Babazono, T., Matsuda, M., Kaku, K.*, et al.* (2004). Association of the Gene Encoding Wingless-Type Mammary Tumor Virus Integration-Site Family Member 5B (WNT5B) with Type 2 Diabetes. The American Journal of Human Genetics *75*, 832-843.

82. Kim-Muller, J.Y., Fan, J., Kim, Y.J.R., Lee, S.-A., Ishida, E., Blaner, W.S., and Accili, D. (2016). Aldehyde dehydrogenase 1a3 defines a subset of failing pancreatic β cells in diabetic mice. Nature Communications *7*, 12631.

83. Kim, V.N., Han, J., and Siomi, M.C. (2009). Biogenesis of small RNAs in animals. Nature Reviews Molecular Cell Biology *10*, 126-139.

84. Knox, J., Rees, K., Zbornik, T., Morin, M., and Bowden, S. (2016). Exploration of the Role of the CCR4-NOT Deadenylase Complex Subunit Regena/NOT2 in MicroRNA-mediated Gene Silencing. The FASEB Journal *30*, 1060

85. Kobayashi, K., Forte, T.M., Taniguchi, S., Ishida, B.Y., Oka, K., and Chan, L. (2000). The db/db mouse, a model for diabetic dyslipidemia: Molecular characterization and effects of western diet feeding. Metabolism *49*, 22-31.

86. Koch, P., Löhr, H.B., and Driever, W. (2014). A mutation in cnot8, component of the Ccr4-not complex regulating transcript stability, affects expression levels of developmental regulators and reveals a role of Fgf3 in development of caudal hypothalamic dopaminergic neurons. PLOS ONE *9*, e113829.

87. Kruk, J.A., Dutta, A., Fu, J., Gilmour, D.S., and Reese, J.C. (2011). The multifunctional Ccr4–Not complex directly promotes transcription elongation. Genes & Development *25*, 581-593.

88. Latreille, M., Hausser, J., Stützer, I., Zhang, Q., Hastoy, B., Gargani, S., Kerr-Conte, J., Pattou, F., Zavolan, M., Esguerra, J.L.S.*, et al.* (2014). MicroRNA-7a regulates pancreatic β cell function. The Journal of Clinical Investigation *124*, 2722-2735.

89. Lau, N.-C., Kolkman, A., van Schaik, Frederik M.A., Mulder, Klaas W., Pijnappel, W.W.M.P., Heck, Albert J.R., and Timmers, H.T.M. (2009). Human Ccr4–Not complexes contain variable deadenylase subunits. Biochemical Journal *422*, 443-453.

90. Lee, S.-H., Demeterco, C., Geron, I., Abrahamsson, A., Levine, F., and Itkin-Ansari, P. (2008). Islet specific Wnt activation in human type II diabetes. Experimental Diabetes Research *2008*, 13.

91. Lemaire, K., Granvik, M., Schraenen, A., Goyvaerts, L., Van Lommel, L., Gómez-Ruiz, A., in 't Veld, P., Gilon, P., and Schuit, F. (2017). How stable is repression of disallowed genes in pancreatic islets in response to metabolic stress? PLOS ONE *12*, e0181651.

92. Lemaire, K., Thorrez, L., and Schuit, F. (2016). Disallowed and allowed gene expression: two faces of mature islet beta cells. Annual Review of Nutrition *36*, 45-71.

93. Leppek, K., Schott, J., Reitter, S., Poetz, F., Hammond, M.C., and Stoecklin, G. (2013). Roquin promotes constitutive mRNA decay via a conserved class of stem-loop recognition motifs. Cell *153*, 869-881.

94. Li, X., Morita, M., Kikuguchi, C., Takahashi, A., Suzuki, T., and Yamamoto, T. (2017). Adipocyte-specific disruption of mouse Cnot3 causes lipodystrophy. FEBS Letters *591*, 358-368.

95. Liu, J.S.E., and Hebrok, M. (2017). All mixed up: defining roles for β-cell subtypes in mature islets. Genes & Development *31*, 228-240.

96. Loh, B., Jonas, S., and Izaurralde, E. (2013). The SMG5–SMG7 heterodimer directly recruits the CCR4–NOT deadenylase complex to mRNAs containing nonsense codons via interaction with POP2. Genes & Development *27*, 2125-2138.

97. Lovis, P., Gattesco, S., and Regazzi, R. (2008a). Regulation of the expression of components of the exocytotic machinery of insulin-secreting cells by microRNAs. Biological Chemistry *389*, 305-312.

98. Lovis, P., Roggli, E., Laybutt, D.R., Gattesco, S., Yang, J.-Y., Widmann, C., Abderrahmani, A., and Regazzi, R. (2008b). Alterations in microRNA expression contribute to fatty acid–induced pancreatic β-cell dysfunction. Diabetes *57*, 2728-2736.

99. Lykke-Andersen, J., and Wagner, E. (2005). Recruitment and activation of mRNA decay enzymes by two ARE-mediated decay activation domains in the proteins TTP and BRF-1. Genes & Development *19*, 351-361.

100. Lynn, F.C., Skewes-Cox, P., Kosaka, Y., McManus, M.T., Harfe, B.D., and German, M.S. (2007). MicroRNA expression is required for pancreatic islet cell genesis in the mouse. Diabetes *56*, 2938-2945.

101. MacDonald, P.E., and Rorsman, P. (2006). Oscillations, intercellular coupling, and insulin secretion in pancreatic β cells. PLOS Biology *4*, e49.

102. Magro, M.G., and Solimena, M. (2013). Regulation of beta-cell function by RNA-binding proteins. Molecular Metabolism *2*, 348-355.

103. Martinez-Sanchez, A., Nguyen-Tu, M.-S., and Rutter, G.A. (2015). Dicer inactivation identifies pancreatic β-cell "disallowed" genes targeted by microRNAs. Molecular Endocrinology *29*, 1067-1079.

104. Martinez-Sanchez, A., Pullen, T.J., Chabosseau, P., Zhang, Q., Haythorne, E., Cane, M.C., Nguyen-Tu, M.-S., Sayers, S.R., and Rutter, G.A. (2016). Disallowance of *Acot7* in β-Cells Is Required for Normal Glucose Tolerance and Insulin Secretion. Diabetes *65*, 1268-1282.

105. Martinez-Sanchez, A., Rutter, G.A., and Latreille, M. (2017). MiRNAs in β-Cell development, identity, and disease. Frontiers in Genetics *7*.

106. Masini, M., Marselli, L., Bugliani, M., Martino, L., Masiello, P., Marchetti, P., and De Tata, V. (2012). Ultrastructural morphometric analysis of insulin secretory granules in human type 2 diabetes. Acta Diabetologica *49,* 247-252.

107. Masuda, T., Saito, N., Tomita, M., and Ishihama, Y. (2009). Unbiased quantitation of Escherichia coli membrane proteome using phase transfer surfactants. Molecular Cell Proteomics *8*, 2770-2777.

108. Masuda, T., Tomita, M., and Ishihama, Y. (2008). Phase transfer surfactant-aided trypsin digestion for membrane proteome analysis. Journal of Proteome Research *7*, 731-740.

109. Meier, J.J., Butler, A.E., Saisho, Y., Monchamp, T., Galasso, R., Bhushan, A., Rizza, R.A., and Butler, P.C. (2008). β-cell replication is the primary mechanism subserving the postnatal expansion of β-cell mass in humans. Diabetes *57*, 1584-1594.

110. Melkman-Zehavi, T., Oren, R., Kredo-Russo, S., Shapira, T., Mandelbaum, A.D., Rivkin, N., Nir, T., Lennox, K.A., Behlke, M.A., Dor, Y.*, et al.* (2011). miRNAs control insulin content in pancreatic beta-cells via downregulation of transcriptional repressors. The EMBO Journal *30*, 835-845.

111. Miller, J.E., and Reese, J.C. (2012). Ccr4-Not complex: the control freak of eukaryotic cells. Critical Reviews in Biochemistry and Molecular Biology *47*, 315-333.

112. Mishima, Y., and Tomari, Y. (2016). Codon usage and 3' UTR length determine maternal mRNA stability in zebrafish. Molecular cell *61*, 874–885.

113. Mittal, S., Aslam, A., Doidge, R., Medica, R., and Winkler, G.S. (2011). The Ccr4a (CNOT6) and Ccr4b (CNOT6L) deadenylase subunits of the human Ccr4–Not complex contribute to the prevention of cell death and senescence. Molecular Biology of the Cell *22*, 748-758.

114. Miyazaki, J., Araki, K., Yamato, E., Ikegami, H., Asano, T., Shibasaki, Y., Oka, Y., and Yamamura, K. (1990). Establishment of a pancreatic beta cell line that retains glucose-inducible insulin secretion: special reference to expression of glucose transporter isoforms. Endocrinology *127*, 126-132.

115. Momose, K., Nunomiya, S., Nakata, M., Yada, T., Kikuchi, M., and Yashiro, T. (2006). Immunohistochemical and electron-microscopic observation of beta-cells in pancreatic islets of spontaneously diabetic Goto-Kakizaki rats. Medical molecular morphology *39*, 146-153.

116. Morel, A.P., Sentis, S., Bianchin, C., Le Romancer, M., Jonard, L., Rostan, M.C., Rimokh, R., and Corbo, L. (2003). BTG2 antiproliferative protein interacts with the human CCR4 complex existing in vivo in three cell-cycle-regulated forms. Journal of Cell Science *116*, 2929-2936.

117. Morita, M., Oike, Y., Nagashima, T., Kadomatsu, T., Tabata, M., Suzuki, T., Nakamura, T., Yoshida, N., Okada, M., and Yamamoto, T. (2011). Obesity resistance and increased hepatic expression of catabolism-related mRNAs in Cnot3+/- mice. The EMBO journal *30*, 4678-4691.

118. Morita, M., Siddiqui, N., Katsumura, S., Rouya, C., Larsson, O., Nagashima, T., Hekmatnejad, B., Takahashi, A., Kiyonari, H., Zang, M.*, et al.* (2019). Hepatic posttranscriptional network comprised of CCR4–NOT deadenylase and FGF21 maintains systemic metabolic homeostasis. Proceedings of the National Academy of Sciences *116,* 7973-7981.

119. Morita, M., Suzuki, T., Nakamura, T., Yokoyama, K., Miyasaka, T., and Yamamoto, T. (2007). Depletion of Mammalian CCR4b Deadenylase Triggers Elevation of the *p27Kip1*mRNA Level and Impairs Cell Growth. Molecular and Cellular Biology *27*, 4980-4990.

120. Mostafa, D., Takahashi, A., Yanagiya, A., Yamaguchi, T., Abe, T., Kureha, T., Kuba, K., Kanegae, Y., Furuta, Y., and Yamamoto, T. (2020). Essential functions of the CNOT7/8 catalytic subunits of the CCR4-NOT complex in mRNA regulation and cell viability. *RNA Biology 17*, 403-416.

121. Murakawa, Y., Hinz, M., Mothes, J., Schuetz, A., Uhl, M., Wyler, E., Yasuda, T., Mastrobuoni, G., Friedel, C.C., Dölken, L.*, et al.* (2015). RC3H1 post-transcriptionally regulates A20 mRNA and modulates the activity of the IKK/NF-κB pathway. Nature Communications *6*, 7367.

122.   Muzumdar, M.D., Tasic, B., Miyamichi, K., Li, L., and Luo, L. (2007). A global double-fluorescent Cre reporter mouse. Genesis *45*, 593-605.

123.   Nakamura, T., Yao, R., Ogawa, T., Suzuki, T., Ito, C., Tsunekawa, N., Inoue, K., Ajima, R., Miyasaka, T., Yoshida, Y.*, et al.* (2004). Oligo-astheno-teratozoospermia in mice lacking Cnot7, a regulator of retinoid X receptor beta. Nature Genetics *36*, 528-533.

124.   Nathan, G., Kredo-Russo, S., Geiger, T., Lenz, A., Kaspi, H., Hornstein, E., and Efrat, S. (2015). MiR-375 promotes redifferentiation of adult human β cells expanded in vitro. PLOS ONE *10*, e0122108-e0122108.

125.   Neelankal John, A., Ram, R., and Jiang, F.X. (2018). RNA-Seq analysis of islets to characterise the dedifferentiation in type 2 diabetes model mice db/db. Endocrine Pathology *29*, 207-221.

126.   Neely, G.G., Kuba, K., Cammarato, A., Isobe, K., Amann, S., Zhang, L., Murata, M., Elmén, L., Gupta, V., Arora, S.*, et al.* (2010). A global in vivo Drosophila RNAi screen identifies NOT3 as a conserved regulator of heart function. Cell *141*, 142-153.

127.   Nesca, V., Guay, C., Jacovetti, C., Menoud, V., Peyot, M.-L., Laybutt, D.R., Prentki, M., and Regazzi, R. (2013). Identification of particular groups of microRNAs that positively or negatively impact on beta cell function in obese models of type 2 diabetes. Diabetologia *56*, 2203-2212.

128.   Ni, Q., Gu, Y., Xie, Y., Yin, Q., Zhang, H., Nie, A., Li, W., Wang, Y., Ning, G., Wang, W.*, et al.* (2017). Raptor regulates functional maturation of murine beta cells. Nature communications *8*, 15755-15755.

129.   Nishimura, W., Takahashi, S., and Yasuda, K. (2015). MafA is critical for maintenance of the mature beta cell phenotype in mice. Diabetologia *58*, 566-574.

130.   Norbury, C.J. (2013). Cytoplasmic RNA: a case of the tail wagging the dog. Nature Reviews Molecular Cell Biology *14*, 643-653.

131.   Nousch, M., Techritz, N., Hampel, D., Millonigg, S., and Eckmann, C.R. (2013). The Ccr4–Not deadenylase complex constitutes the main poly(A) removal activity in *C. elegans*. Journal of Cell Science *126*, 4274-4285.

132.   Olofsson, C.S., Göpel, S.O., Barg, S., Galvanovskis, J., Ma, X., Salehi, A., Rorsman, P., and Eliasson, L. (2002). Fast insulin secretion reflects exocytosis of docked granules in mouse pancreatic B-cells. Pflügers Archiv *444*, 43-51.

133.   Ozcan, S. (2015). microRNAs in pancreatic beta-cell physiology. Advances in Experimental Medicine and Biology *887*, 101-117.

134.   Parker, R. (2012). RNA Degradation in Saccharomyces cerevisae. Genetics *191*, 671-702.

135.   Parker, R., and Song, H. (2004). The enzymes and control of eukaryotic mRNA turnover. Nature Structural & Molecular Biology *11*, 121-127.

136.   Petit, A.-P., Wohlbold, L., Bawankar, P., Huntzinger, E., Schmidt, S., Izaurralde, E., and Weichenrieder, O. (2012). The structural basis for the interaction between the CAF1 nuclease and the NOT1 scaffold of the human CCR4–NOT deadenylase complex. Nucleic Acids Research *40*, 11058-11072.

137.   Piao, X., Zhang, X., Wu, L., and Belasco, J.G. (2010). CCR4-NOT deadenylates mRNA associated with rna-induced silencing complexes in human cells. Molecular and Cellular Biology *30*, 1486-1494.

138.   Piccand, J., Strasser, P., Hodson, D.J., Meunier, A., Ye, T., Keime, C., Birling, M.C., Rutter, G.A., and Gradwohl, G. (2014). Rfx6 maintains the functional identity of adult pancreatic beta cells. Cell Reports *9*, 2219-2232.

139.   Poitout, V., Hagman, D., Stein, R., Artner, I., Robertson, R.P., and Harmon, J.S. (2006). Regulation of the insulin gene by glucose and fatty acids. The Journal of Nutrition *136*, 873-876.

140.   Poy, M.N., Eliasson, L., Krutzfeldt, J., Kuwajima, S., Ma, X., MacDonald, P.E., Pfeffer, S., Tuschl, T., Rajewsky, N., Rorsman, P.*, et al.* (2004). A pancreatic islet-specific microRNA regulates insulin secretion. Nature *432*, 226-230.

141.   Prentki, M., Matschinsky, F.M., and Madiraju, S.R. (2013). Metabolic signaling in fuel-induced insulin secretion. Cell Metabolism *18*, 162-185.

142.   Prevot, D., Morel, A.P., Voeltzel, T., Rostan, M.C., Rimokh, R., Magaud, J.P., and Corbo, L. (2001). Relationships of the antiproliferative proteins BTG1 and BTG2 with CAF1, the human homolog of a component of the yeast CCR4 transcriptional complex: involvement in estrogen receptor alpha signaling pathway. Journal of Biological Chemistry *276*, 9640-9648.

143.   Pullen, T.J., da Silva Xavier, G., Kelsey, G., and Rutter, G.A. (2011). miR-29a and miR-29b contribute to pancreatic beta-cell-specific silencing of monocarboxylate transporter 1 (Mct1). Molecular Cell Biology *31*, 3182-3194.

144.   Pullen, T.J., Huising, M.O., and Rutter, G.A. (2017). Analysis of Purified Pancreatic Islet Beta and Alpha Cell Transcriptomes Reveals 11β-Hydroxysteroid Dehydrogenase (Hsd11b1) as a Novel Disallowed Gene. Frontiers in Genetics *8*.

145. Pullen, T.J., Khan, A.M., Barton, G., Butcher, S.A., Sun, G., and Rutter, G.A. (2010). Identification of genes selectively disallowed in the pancreatic islet. Islets *2*, 89-95.

146. Pullen, T.J., and Rutter, G.A. (2013). When less is more: the forbidden fruits of gene repression in the adult β-cell. Diabetes, Obesity and Metabolism *15*, 503-512.

147. Pullen, T.J., Sylow, L., Sun, G., Halestrap, A.P., Richter, E.A., and Rutter, G.A. (2012). Overexpression of monocarboxylate transporter-1 (SLC16A1) in mouse pancreatic beta-cells leads to relative hyperinsulinism during exercise. Diabetes *61*, 1719-1725.

148. Raisch, T., Chang, C.-T., Levdansky, Y., Muthukumar, S., Raunser, S., and Valkov, E. (2019). Reconstitution of recombinant human CCR4-NOT reveals molecular insights into regulated deadenylation. Nature Communications *10*, 3173.

149. Reiter, L., Rinner, O., Picotti, P., Hüttenhain, R., Beck, M., Brusniak, M.-Y., Hengartner, M.O., and Aebersold, R. (2011). mProphet: automated data processing and statistical validation for large-scale SRM experiments. Nature Methods *8*, 430-435.

150. Robinson, M.D., McCarthy, D.J., and Smyth, G.K. (2010). edgeR: a Bioconductor package for differential expression analysis of digital gene expression data. Bioinformatics (Oxford, England) *26*, 139-140.

151. Rorsman, P., and Renström, E. (2003). Insulin granule dynamics in pancreatic beta cells. Diabetologia *46*, 1029-1045.

152. Rosenberger, G., Bludau, I., Schmitt, U., Heusel, M., Hunter, C.L., Liu, Y., MacCoss, M.J., MacLean, B.X., Nesvizhskii, A.I., Pedrioli, P.G.A.*, et al.* (2017). Statistical control of peptide and protein error rates in large-scale targeted data-independent acquisition analyses. Nature Methods *14*, 921-927.

153. Rosengren, A.H., Braun, M., Mahdi, T., Andersson, S.A., Travers, M.E., Shigeto, M., Zhang, E., Almgren, P., Ladenvall, C., Axelsson, A.S.*, et al.* (2012). Reduced insulin exocytosis in human pancreatic β-cells with gene variants linked to type 2 diabetes. Diabetes *61*, 1726-1733.

154. Rouya, C., Siddiqui, N., Morita, M., Duchaine, T.F., Fabian, M.R., and Sonenberg, N. (2014). Human DDX6 effects miRNA-mediated gene silencing via direct binding to CNOT1. RNA *20*, 1398-1409.

155. Ruan, Q., Wang, T., Kameswaran, V., Wei, Q., Johnson, D.S., Matschinsky, F., Shi, W., and Chen, Y.H. (2011). The microRNA-21−PDCD4 axis prevents type 1 diabetes by blocking pancreatic β cell death. Proceedings of the National Academy of Sciences of the United States of America *108*, 12030-12035.

156. Russ, H.A., Bar, Y., Ravassard, P., and Efrat, S. (2008). In vitro proliferation of cells derived from adult human β-cells revealed by cell-lineage tracing. Diabetes *57*, 1575-1583.

157. Rutter, G.A. (2004). Visualising insulin secretion. The Minkowski Lecture 2004. Diabetologia *47*, 1861-1872.

158. Rutter, Guy A., Pullen, Timothy J., Hodson, David J., and Martinez-Sanchez, A. (2015). Pancreatic β-cell identity, glucose sensing and the control of insulin secretion. Biochemical Journal *466*, 203-218.

159. Sandler, H., Kreth, J., Timmers, H.T.M., and Stoecklin, G. (2011). Not1 mediates recruitment of the deadenylase Caf1 to mRNAs targeted for degradation by tristetraprolin. Nucleic Acids Research *39*, 4373-4386.

160. Schrimpe-Rutledge, A.C., Fontes, G., Gritsenko, M.A., Norbeck, A.D., Anderson, D.J., Waters, K.M., Adkins, J.N., Smith, R.D., Poitout, V., and Metz, T.O. (2012). Discovery of novel glucose-regulated proteins in isolated human pancreatic islets using LC-MS/MS-based proteomics. Journal of proteome research *11*, 3520-3532.

161. Schuit, F., Flamez, D., De Vos, A., and Pipeleers, D. (2002). Glucose-Regulated Gene Expression Maintaining the Glucose-Responsive State of β-Cells. Diabetes *51*, S326-S332.

162. Schwede, A., Ellis, L., Luther, J., Carrington, M., Stoecklin, G., and Clayton, C. (2008). A role for Caf1 in mRNA deadenylation and decay in trypanosomes and human cells. Nucleic Acids Research *36*, 3374-3388.

163. Seino, S., Shibasaki, T., and Minami, K. (2011). Dynamics of insulin secretion and the clinical implications for obesity and diabetes. The Journal of Clinical Investigation *121*, 2118-2125.

164. Semotok, J.L., Cooperstock, R.L., Pinder, B.D., Vari, H.K., Lipshitz, H.D., and Smibert, C.A. (2005). Smaug recruits the CCR4/POP2/NOT deadenylase complex to trigger maternal transcript localization in the early drosophila embryo. Current Biology *15*, 284-294.

165. Setyowati Karolina, D., Sepramaniam, S., Tan, H.Z., Armugam, A., and Jeyaseelan, K. (2013). miR-25 and miR-92a regulate insulin I biosynthesis in rats. RNA Biology *10*, 1365-1378.

166. Sgromo, A., Raisch, T., Bawankar, P., Bhandari, D., Chen, Y., Kuzuoğlu-Öztürk, D., Weichenrieder, O., and Izaurralde, E. (2017). A CAF40-binding motif facilitates recruitment of the CCR4-NOT complex to mRNAs targeted by Drosophila Roquin. Nature Communications *8*, 14307.

167. Sherman, B.T., Huang, D.W., and Lempicki, R.A. (2008). Bioinformatics enrichment tools: paths toward the comprehensive functional analysis of large gene lists. Nucleic Acids Research *37*, 1-13.

168. Shi, J., and Nelson, M.A. (2005). The cyclin-dependent kinase 11 interacts with NOT2. Biochemical and Biophysical Research Communications *334*, 1310-1316.

169. Shih, H.P., Wang, A., and Sander, M. (2013). Pancreas Organogenesis: From Lineage Determination to Morphogenesis. Annual Review of Cell and Developmental Biology *29*, 81-105.

170. Shirai, Y.T., Suzuki, T., Morita, M., Takahashi, A., and Yamamoto, T. (2014). Multifunctional roles of the mammalian CCR4-NOT complex in physiological phenomena. Frontiers in Genetics *5*, 286.

171. Shoelson, S.E., Lee, J., and Goldfine, A.B. (2006). Inflammation and insulin resistance. Journal of Clinical Investigation *116*, 1793-1801.

172. Solimena, M., Schulte, A.M., Marselli, L., Ehehalt, F., Richter, D., Kleeberg, M., Mziaut, H., Knoch, K.-P., Parnis, J., Bugliani, M.*, et al.* (2018). Systems biology of the IMIDIA biobank from organ donors and pancreatectomised patients defines a novel transcriptomic signature of islets from individuals with type 2 diabetes. Diabetologia *61*, 641-657.

173. Spijker, H.S., Ravelli, R.B.G., Mommaas-Kienhuis, A.M., van Apeldoorn, A.A., Engelse, M.A., Zaldumbide, A., Bonner-Weir, S., Rabelink, T.J., Hoeben, R.C., Clevers, H.*, et al.* (2013). Conversion of mature human β-cells into glucagon-producing α-cells. Diabetes *62*, 2471-2480.

174. Stolovich-Rain, M., Enk, J., Vikesa, J., Nielsen, Finn C., Saada, A., Glaser, B., and Dor, Y. (2015). Weaning triggers a maturation step of pancreatic β cells. Developmental Cell *32*, 535-545.

175. Suzuki, A., Igarashi, K., Aisaki, K.-i., Kanno, J., and Saga, Y. (2010). NANOS2 interacts with the CCR4-NOT deadenylation complex and leads to suppression of specific RNAs. Proceedings of the National Academy of Sciences *107*, 3594-3599.

176. Suzuki, T., K-Tsuzuku, J., Ajima, R., Nakamura, T., Yoshida, Y., and Yamamoto, T. (2002). Phosphorylation of three regulatory serines of Tob by Erk1 and Erk2 is required for Ras-mediated cell proliferation and transformation. Genes & Development *16*, 1356-1370.

177. Suzuki, T., Kikuguchi, C., Nishijima, S., Nagashima, T., Takahashi, A., Okada, M., and Yamamoto, T. (2019). Postnatal liver functional maturation requires Cnot complex-

mediated decay of mRNAs encoding cell cycle and immature liver genes. Development *146*, dev168146.

178.   Suzuki, T., Kikuguchi, C., Sharma, S., Sasaki, T., Tokumasu, M., Adachi, S., Natsume, T., Kanegae, Y., and Yamamoto, T. (2015). CNOT3 suppression promotes necroptosis by stabilizing mRNAs for cell death-inducing proteins. Scientific Reports *5*, 14779.

179.   Swisa, A., Avrahami, D., Eden, N., Zhang, J., Feleke, E., Dahan, T., Cohen-Tayar, Y., Stolovich-Rain, M., Kaestner, K.H., Glaser, B.*, et al.* (2017). PAX6 maintains β cell identity by repressing genes of alternative islet cell types. The Journal of Clinical Investigation *127*, 230-243.

180.   Takahashi, A., Adachi, S., Morita, M., Tokumasu, M., Natsume, T., Suzuki, T., and Yamamoto, T. (2015). Post-transcriptional stabilization of Ucp1 mRNA protects mice from Diet-Induced obesity. Cell Reports *13*, 2756-2767.

181.   Takahashi, A., Takaoka, S., Kobori, S., Yamaguchi, T., Ferwati, S., Kuba, K., Yamamoto, T., and Suzuki, T. (2019). The CCR4–NOT deadenylase complex maintains adipocyte identity. International Journal of Molecular Sciences *20*, 5274.

182.   Talchai, C., Xuan, S., Lin, Hua V., Sussel, L., and Accili, D. (2012). Pancreatic β Cell dedifferentiation as a mechanism of diabetic β cell failure. Cell *150*, 1223-1234.

183.   Tanaka, T., Takeno, T., Watanabe, Y., Uchiyama, Y., Murakami, T., Yamashita, H., Suzuki, A., Aoi, R., Iwanari, H., Jiang, S.-Y.*, et al.* (2002). The generation of monoclonal antibodies against human peroxisome proliferator-activated receptors (PPARs). Journal of Atherosclerosis and Thrombosis *9*, 233-242.

184.   Tattikota, S.G., Rathjen, T., Hausser, J., Khedkar, A., Kabra, U.D., Pandey, V., Sury, M., Wessels, H.H., Mollet, I.G., Eliasson, L.*, et al.* (2015). miR-184 regulates pancreatic beta-cell function according to glucose metabolism. Journal of Biological Chemistry *290*, 20284-20294.

185.   Tattikota, Sudhir G., Rathjen, T., McAnulty, Sarah J., Wessels, H.-H., Akerman, I., van de Bunt, M., Hausser, J., Esguerra, Jonathan L., Musahl, A., Pandey, Amit K.*, et al.* (2014). Argonaute2 mediates compensatory expansion of the pancreatic β cell. Cell Metabolism *19*, 122-134.

186.   Tattikota, S.G., Sury, M.D., Rathjen, T., Wessels, H.-H., Pandey, A.K., You, X., Becker, C., Chen, W., Selbach, M., and Poy, M.N. (2013). Argonaute2 regulates the pancreatic β-cell secretome. Molecular & Cellular Proteomics: MCP *12*, 1214-1225.

187. Temme, C., Zaessinger, S., Meyer, S., Simonelig, M., and Wahle, E. (2004). A complex containing the CCR4 and CAF1 proteins is involved in mRNA deadenylation in Drosophila. The EMBO Journal *23*, 2862-2871.

188. Thorel, F., Népote, V., Avril, I., Kohno, K., Desgraz, R., Chera, S., and Herrera, P.L. (2010). Conversion of adult pancreatic α-cells to β-cells after extreme β-cell loss. Nature *464*, 1149-1154.

189. Thorens, B., Tarussio, D., Maestro, M.A., Rovira, M., Heikkila, E., and Ferrer, J. (2015). Ins1(Cre) knock-in mice for beta cell-specific gene recombination. Diabetologia *58*, 558-565.

190. Thorrez, L., Laudadio, I., Van Deun, K., Quintens, R., Hendrickx, N., Granvik, M., Lemaire, K., Schraenen, A., Van Lommel, L., Lehnert, S.*, et al.* (2011). Tissue-specific disallowance of housekeeping genes: The other face of cell differentiation. Genome Research *21*, 95-105.

191. Tucker, M., Staples, R.R., Valencia‐Sanchez, M.A., Muhlrad, D., and Parker, R. (2002). Ccr4p is the catalytic subunit of a Ccr4p/Pop2p/Notp mRNA deadenylase complex in *Saccharomyces cerevisiae*. The EMBO Journal *21*, 1427-1436.

192. Tucker, M., Valencia-Sanchez, M.A., Staples, R.R., Chen, J., Denis, C.L., and Parker, R. (2001). The transcription factor associated Ccr4 and Caf1 proteins are components of the major cytoplasmic mRNA deadenylase in Saccharomyces cerevisiae. Cell *104*, 377-386.

193. van Arensbergen, J., García-Hurtado, J., Moran, I., Maestro, M.A., Xu, X., Van de Casteele, M., Skoudy, A.L., Palassini, M., Heimberg, H., and Ferrer, J. (2010). Derepression of Polycomb targets during pancreatic organogenesis allows insulin-producing beta-cells to adopt a neural gene activity program. Genome Research *20*, 722-732.

194. van de Bunt, M., Gaulton, K.J., Parts, L., Moran, I., Johnson, P.R., Lindgren, C.M., Ferrer, J., Gloyn, A.L., and McCarthy, M.I. (2013). The miRNA profile of human pancreatic islets and beta-cells and relationship to type 2 diabetes pathogenesis. PLOS ONE *8*, e55272.

195. van der Meulen, T., and Huising, M.O. (2014). Maturation of stem cell-derived beta-cells guided by the expression of urocortin 3. The Review of Diabetic Studies: RDS *11*, 115-132.

196.   van der Meulen, T., Xie, R., Kelly, O.G., Vale, W.W., Sander, M., and Huising, M.O. (2012). Urocortin 3 marks mature human primary and embryonic stem cell-derived pancreatic alpha and beta cells. PLOS ONE *7*, e52181.

197.   Van Etten, J., Schagat, T.L., Hrit, J., Weidmann, C.A., Brumbaugh, J., Coon, J.J., and Goldstrohm, A.C. (2012). Human pumilio proteins recruit multiple deadenylases to efficiently repress messenger RNAs. Journal of Biological Chemistry *287*, 36370-36383.

198.   Villanyi, Z., and Collart, Martine A. (2015). Ccr4–Not is at the core of the eukaryotic gene expression circuitry. Biochemical Society Transactions *43*, 1253-1258.

199.   Wahle, E., and Winkler, G.S. (2013). RNA decay machines: Deadenylation by the Ccr4–Not and Pan2–Pan3 complexes. Biochimica et Biophysica Acta (BBA) - Gene Regulatory Mechanisms *1829*, 561-570.

200.   Wang, H., Brun, T., Kataoka, K., Sharma, A.J., and Wollheim, C.B. (2007). MAFA controls genes implicated in insulin biosynthesis and secretion. Diabetologia *50*, 348-358.

201.   Wang, H., Morita, M., Yang, X., Suzuki, T., Yang, W., Wang, J., Ito, K., Wang, Q., Zhao, C., Bartlam, M.*, et al.* (2010). Crystal structure of the human CNOT6L nuclease domain reveals strict poly(A) substrate specificity. The EMBO Journal *29*, 2566-2576.

202.   Wang, Z., York, Nathaniel W., Nichols, Colin G., and Remedi, Maria S. (2014). Pancreatic β cell dedifferentiation in diabetes and redifferentiation following insulin therapy. Cell Metabolism *19*, 872-882.

203.   Watanabe, C., Morita, M., Hayata, T., Nakamoto, T., Kikuguchi, C., Li, X., Kobayashi, Y., Takahashi, N., Notomi, T., Moriyama, K.*, et al.* (2014). Stability of mRNA influences osteoporotic bone mass via CNOT3. Proceedings of the National Academy of Sciences *111*, 2692-2697.

204.   Webster, M.W., Chen, Y.-H., Stowell, J.A.W., Alhusaini, N., Sweet, T., Graveley, B.R., Coller, J., and Passmore, L.A. (2018). mRNA deadenylation is coupled to translation rates by the differential activities of Ccr4-Not nucleases. Molecular Cell *70*, 1089-1100.e1088.

205.   Weir, G.C., and Bonner-Weir, S. (2004). Five stages of evolving beta-cell dysfunction during progression to diabetes. Diabetes *53*, S16-S21.

206.   Wells, S.E., Hillner, P.E., Vale, R.D., and Sachs, A.B. (1998). Circularization of mRNA by eukaryotic translation initiation factors. Molecular Cell *2*, 135-140.

207.   Wicksteed, B., Alarcon, C., Briaud, I., Lingohr, M.K., and Rhodes, C.J. (2003). Glucose-induced translational control of proinsulin biosynthesis is proportional to preproinsulin mRNA levels in islet beta-cells but not regulated via a positive feedback of secreted insulin. The Journal of Biological Chemistry *278*, 42080-42090.

208.   Winkler, G.S., Mulder, K.W., Bardwell, V.J., Kalkhoven, E., and Timmers, H.T.M. (2006). Human Ccr4‐Not complex is a ligand‐dependent repressor of nuclear receptor‐mediated transcription. The EMBO Journal *25*, 3089-3099.

209.   Xu, X., D'Hoker, J., Stangé, G., Bonné, S., De Leu, N., Xiao, X., Van De Casteele, M., Mellitzer, G., Ling, Z., Pipeleers, D.*, et al.* (2008). β cells can be generated from endogenous progenitors in injured adult mouse pancreas. Cell *132*, 197-207.

210.   Yamaguchi, T., Suzuki, T., Sato, T., Takahashi, A., Watanabe, H., Kadowaki, A., Natsui, M., Inagaki, H., Arakawa, S., Nakaoka, S.*, et al.* (2018). The CCR4-NOT deadenylase complex controls Atg7-dependent cell death and heart function. Science Signaling *11*.

211.   Yamashita, A., Chang, T.-C., Yamashita, Y., Zhu, W., Zhong, Z., Chen, C.-Y.A., and Shyu, A.-B. (2005). Concerted action of poly(A) nucleases and decapping enzyme in mammalian mRNA turnover. Nature Structural &Amp; Molecular Biology *12*, 1054-1063.

212.   Yi, H., Park, J., Ha, M., Lim, J., Chang, H., and Kim, V.N. (2018). PABP cooperates with the CCR4-NOT complex to promote mRNA deadenylation and block precocious decay. Molecular Cell *70*, 1081-1088.

213.   Zekri, L., Kuzuoğlu-Öztürk, D., and Izaurralde, E. (2013). GW182 proteins cause PABP dissociation from silenced miRNA targets in the absence of deadenylation. The EMBO Journal *32*, 1052-1065.

214.   Zhang, C., Moriguchi, T., Kajihara, M., Esaki, R., Harada, A., Shimohata, H., Oishi, H., Hamada, M., Morito, N., Hasegawa, K.*, et al.* (2005). MafA is a key regulator of glucose-stimulated insulin secretion. Molecular and Cellular biology *25*, 4969-4976.

215.   Zhang, Z.-W., Zhang, L.-Q., Ding, L., Wang, F., Sun, Y.-J., An, Y., Zhao, Y., Li, Y.-H., and Teng, C.-B. (2011). MicroRNA-19b downregulates insulin 1 through targeting transcription factor NeuroD1. FEBS Letters *585*, 2592-2598.

216.   Zhao, C., and Rutter, G.A. (1998). Overexpression of lactate dehydrogenase A attenuates glucose-induced insulin secretion in stable MIN-6 β-cell lines. FEBS Letters *430*, 213-216.

217.   Zito, E., Chin, K.-T., Blais, J., Harding, H.P., and Ron, D. (2010). ERO1-β, a pancreas-specific disulfide oxidase, promotes insulin biogenesis and glucose homeostasis. The Journal of Cell Biology *188*, 821-832.

218.   Ziv, O., Glaser, B., and Dor, Y. (2013). The Plastic Pancreas. Developmental Cell *26*, 3-7.

6   Appendix

Table 3: Primers used for genotyping

Gene	Primers
Cnot3-conditional	
N3 FW	CCAGTCTATCTGATGTGGAATTCCTCCATG
N3 RV	AGGCTGGCAGCTCCTGGAAAGGCTAAGAGG
Cre	
Cre FW	TCGATGCAACGAGTGATGAG
Cre RV	TTCGGCTATACGTAACAGGG
Il-2 (internal control for Cre)	
Il-2 FW	CTAGGCCACAGAATTGAAAGATCT
Il-2 RV	GTAGGTGGAAATTCTAGCATCATCC
mTmG	
mTmG FW	CTCTGCTGCCTCCTGGCTTCT
mTmG RV	CGAGGCGGATCACAAGCAATA
mTmG Mut RV	TCAATGGGCGGGGGTCGTT
Cnot8-conditional	
N8C FW	GACCCTCTCCTACAGACACACATGCCACC
N8C RV	GCAAACAGTGGTGCTCAGCAACCCATGAGC
Cnot7-null	
N7 FW	CCAGCCCAGTTTTATAATTCACATTCATGATATTGG TG
N7 RV	CATCTCTTCATCCAGGTTACAAGCC

LacZ2	TGCGCAACTGTTGGGAAGGGCGATC
Cnot6-null	
N6 FW	GTGTGGTCCTTGTTCCATCAGCTCTAAGACATG
N6 RV	CTGGGATTGCATTCACCGTGCATGTTAGGCAG
N6 flox arm RV	GCTAGTTCTTTACAGTCTAGATAGATGGCTCAG
Cnot6l-null	
N6L WT FW	AATGATCCTTTTCCCCCCACAGACTAATAG
N6L WT RV	TATTTTAAAAGATCTAAAAAGAAGTGCCTC
N6L KO RV	TTTCTGCATCCCGGGGATCTGATATCATCG

Table 4: Primary antibodies used for immunoblot analysis

Antibody	dilution	Manufacturer (Cat#)
CNOT1	1:1000	Proteintech (14276-1-AP)
CNOT2	1:1000	Proteintech (34214)
CNOT3	1:1000	Bio Matrix Research Incorporation
CNOT6	1:1000	In-house (generated as previously described in (Tanaka et al., 2002))
CNOT6L	1:1000	Produced in collaboration with Bio Matrix Research Incorporation
CNOT7	1:1000	Abnova (H00029883-M01)
CNOT8	1:1000	Produced in collaboration with Bio Matrix Research Incorporation
CNOT9	1:1000	Proteintech (22503-1-AP)
CNOT10	1:1000	Bethyl Laboratories (A304-899A)
GAPDH	1:2000	Cell Signaling (2118L)
α-tubulin	1:1000	Sigma (T9026)
ALDH1A3	1:1000	Novus biologicals (NBP2-15339)
MCT1	1:30	Novus biologicals (NBP1-59656)
LDHA	1:30	Cell Signaling (2012)

ALDOB	1:1000	Proteintech (18065-1-1AP)
Roquin	1:1000	Bethyl Laboratories (A300-514A)
HuR	1:1000	Cell Signaling (12582)

Table 5: Secondary antibodies used for immunoblot analysis

Antibody	dilution	Manufacturer (Cat#)
Anti-Rabbit HRP	1:3000	GE healthcare (NA934V)
Anti- mouse HRP	1:3000	GE healthcare (NA931V)
Anti-mouse HRP (light chain specific)	1:6000	Jackson immunoresearch laboratories (115-035-174)

Table 6: Primary antibodies used for immunofluorescence analysis

Antibody	dilution	Manufacturer (Cat#)
CNOT3	1:100	Bio Matrix Research Incorporation
EGFP	1:100	Clontech (632569)
Insulin	No dilution	Agilent (IR00261)
GLUC	1:500	Phoenix pharmaceuticals (H-028-05)
SST	1:100	Sigma-Aldrich (SAB4502861)
PPT	$3\mu g/ml$ (no antigen retrieval)	Sigma-Aldrich (SAB2500747)
SYP	1:500	Abcam (ab32127)
MAFA	1:500	Bethyl Laboratories (IHC-00352)
GLUT2	$5\mu g/ml$	Abcam (ab54460)

Table 7: Secondary antibodies used for immunofluorescence analysis

Antibody	dilution	Manufacturer
Goat-anti-mouse-Alexa-488	1:500	Thermofisher (A-21424)
Goat-anti-rabbit-Alexa-488	1:500	Thermofisher (A-11008)
Goat- anti-guinea pig-647	1:500	Thermofisher (A-21450)
Goat-anti-rabbit-Alexa-555	1:500	Thermofisher (A-21429)
Donkey-anti-goat-568	1:500	Thermofisher (A-11057)

Table 8: Primers used for qPCR reactions

Gene	Forward (5'-3')	Reverse (5'-3')
Ins1	GAAGTGGAGGACCCACAAGTG	CTGAAGGTCCCCGGGGCT
Ins2	ATGGCCCTGTGGATGCGCTT	CTAGTTGCAGTAGTTCTCCAGCTGG
Ngn3	GTCGGGAGAACTAGGATGGC	AGTCACCCACTTCTGCTTCG
Aldh1a3	GGGCCTCAGATCGACCAAAA	CTAGCTTGGCCCCTTCCTTC
Myt1	TATGCTTGCCCCAAAGATTC	GGCTTTGTGCTGAGGTTCTC
Dcx	GCTGACTCAGGTAACGACCA	ACAGGTCTACCTTGTGCTTCC
Nes	CCCTTAGTCTGGAAGTGGCT	CTTCAGCTTGGGGGTCAGGAAAG
Tnfrsf11b	GTTTCCCGAGGACCACAAT	CCATTCAATGATGTCCAGGAG
Mafa	CAAGGAGGAGGTCATCCGAC	TCTCCAGAATGTGCCGCTG
Nkx2.2	CGCTACAAGATGAAACGTGCC	CACCTTGCGGACACTATGGG
Nkx6.1	GAGAGTCAGGTCAAGGTCTGGT	TCCGAGTCCTGCTTCTTCTTG
NeuroD1	TCCCTACTCCTACCAGTCCC	CTGGTGCAGTCAGTTAGGGG
Pdx1	CAGTGGGCAGGAGGTGCTTA	GGGCCGGGAGATGTATTTGTT
Slc2a2	ATTACCGACAGCCCATCCTC	AGCACAGAGACAGCCGTGAA
Pcx	GGGCGGAGCTAACATCTACC	TATACTCCAGACGCCGGACA
Gck	CTGTTAGCAGGATGGCAGCTT	TTTCCTGGAGAGATGCTGTGG
Cpe	GGTACTGCTCACGAATACAGTTCC	CTGCTCAGGTAATTGAAGTCTTGC
Pcsk1	GACCTGCACAATGACTGCAC	GGTCCAGACAACCAGATGCT
Pcsk2	GTTTTTGCGTCTGCCGAGAG	CAAAGGGGAGCTTTCGGACT
Abcc8	TCAACTTGTCTGGTGGTCAGC	GAGCTGAGAAAGGGTCATCCA
Ucn3	GCTGTGCCCCTCGACCT	TGGGCATCAGCATCGCT
Slc30a8	CAGAGAACTTCGACAGAAGCC	CTTGCTTGCTCGACCTGTT

Cacna1c	ATGAAAACACGAGGATGTACGTT	ACTGACGGTAGAGATGGTTGC
Cacna1d	GAAGCTGCTTGACCAAGTTGT	AACTTCCCCACGGTTACCTC
Cacnb2	GCAGGAGAGCCAGATGGA	TCCTGGCTCCTTTTCCATAG
Slc16a1	GCTTGGTGACCATTGTGGAAT	CCCAGTACGTGTATTTGTAGTCTCCAT
Ldha	ATGAAGGACTTGGCGGATGA	ATCTCGCCCTTGAGTTTGTCTT
Hk1	GTGGACGGGACGCTCTAC	TTCACTGTTTGGTGCATGATT
Hk2	GCCTCGGTTTCTCTATTTGGC	ATACTGGTCAACCTTCTGCACT
Rest	GCGCACAGTTCAGAGGAGT	CATGTTGGCACTGTTGTTGA
Pdgfra	GCGAGTTTAATGTTTATGCCTTG	GGCACAGGTCACCACGAT
Aldob	AGAAGGACAGCCAGGGAAAT	GTTCAGAGAGGCCATCAAGC
Slc5a10	ACCTACACTGTGTGTCCCT	CGGCCACATTCAAGGCAAAAT
Wnt5b	AGCACCGTGGACAACACAT	AAGGCAGTCTCTCGGCTACC
Cat	TGCCCCCAACTATTACCCCA	TCCGCACCTGAGTGACATTG
Abtb2	CGCTGAGCACGGTTACCT	CAGCTTCCAGGGAACACC
Fgf1	TTATACGGCTCGCAGACACC	TCTGGCCATAGTGAGTCCGA
Yap1	AAATGCTCCAAAATGTCAGGA	CATTCGGAGTCCCTCCATC
Igfbp4	AAGATCGTGGGGACACCTC	GTGGGTACGGCTCTGTGAG
Acot7	AGGTGCCTCCCATTGTGTAT	TTCTGGGCTTCATAGCGTTT
Cxcl12	CCCTGCCGGTTCTTCGA	CAGCCGTGCAACAATCTGAA
Foxo3	GCTAAGCAGGCCTCATCTCA	TTCCGTCAGTTTGAGGGTCT
Txnip1	ATCCCAGATACCCCAGAAGC	TGAGAGTCGTCCACATCGTC
Gapdh	CTGCACCACCAACTGCTTAG	GTCTTCTGGGTGGCAGTGAT

Table 9: Primers used for 3'UTR cloning

mRNA	Forward (5'-3')	Reverse (5'-3')
Slc16a1 cloned as two fragments		
Slc16a1-A	AATCTAGACCTGTGAAGCCTGGAGAGAG	AATCTAGACACCCTGTCAATTACAATGG

Slc16a1-B	AATCTAGAGGGTGAATATA GATTTAAAACC	AATCTAGAGGACCAAGAAG ATTGTTTTTTA
Ldha	AATCTAGAAGTCTTCCCCG TGTCCTAGC	AATCTAGACACTGTTCAAGG TTTTATTTGG
Wnt5b	AATCTAGACTGCACCACAC GGGCCTTCAGG	AATCTAGACCTCAGTAAAAA GATATTTAATGTCAAAGGGA CGCTGTACATGTGG
Abtb2	AATCTAGAGGCAGGATGGA GGGGGACTGTTATC	AATCTAGACAATGTTAATGA GTGTTTATTGTTGATAAAAC CATAGC

Solutions and buffers used for SDS-PAGE:

For poly-acrylamide gel preparation:

30% Acrylamide stock

146 g Acrylamide

 4 g Bis-acrylamide

Dissolved and brought to 500 mL with ddH$_2$O then filtered

Lower gel buffer

90.85 g Tris

2 g SDS

Dissolved in 400 mL in ddH$_2$O and adjusted to pH 8.8 with HCl then brought to 500 mL with ddH$_2$O and filtered

Upper gel buffer

30.3 g Tris

2 g SDS

Dissolved in 400 mL in ddH$_2$O and adjusted to pH 6.8 with HCl then brought to 500 mL with ddH$_2$O and filtered

For running electrophoresis:

10x SDS running buffer

30.0 g Tris

144.1 g Glycine

10 g SDS

Dissolved in ddH$_2$O and adjusted to the volume 1000 mL.

For immunoblotting:

10x Transfer buffer

30.3 g Tris

144.1 g Glycine

Dissolved in ddH$_2$O and adjusted to the volume 1000 mL.

10x TBS

1M (2M) Tris-HCl (pH 7.5) 200 mL (100 mL)

87.66 g NaCl

Dissolved in ddH$_2$O and adjusted to the volume 1000 mL.

1M Tris-HCL (pH 7.5, 8)

Dissolved 121.14 g of Tris in ~ 850 mL ddH$_2$O

Adjusted to pH (7.5 or 8) with HCl then brought to the volume 1000 mL

TBST

100 mL 10x TBS

0.5 mL Tween 20

Dissolved in ddH$_2$O and brought to the volume 1000 mL

<u>3x Sample buffer</u>

15.6 mL Upper gel buffer

3.6 g SDS

12 mL Glycerol

6 mL 2-mercaptoethanol

Dissolve with ddH_2O and adjust to volume to 40 mL